thermal scale modeling of the mariner IV spacecraft

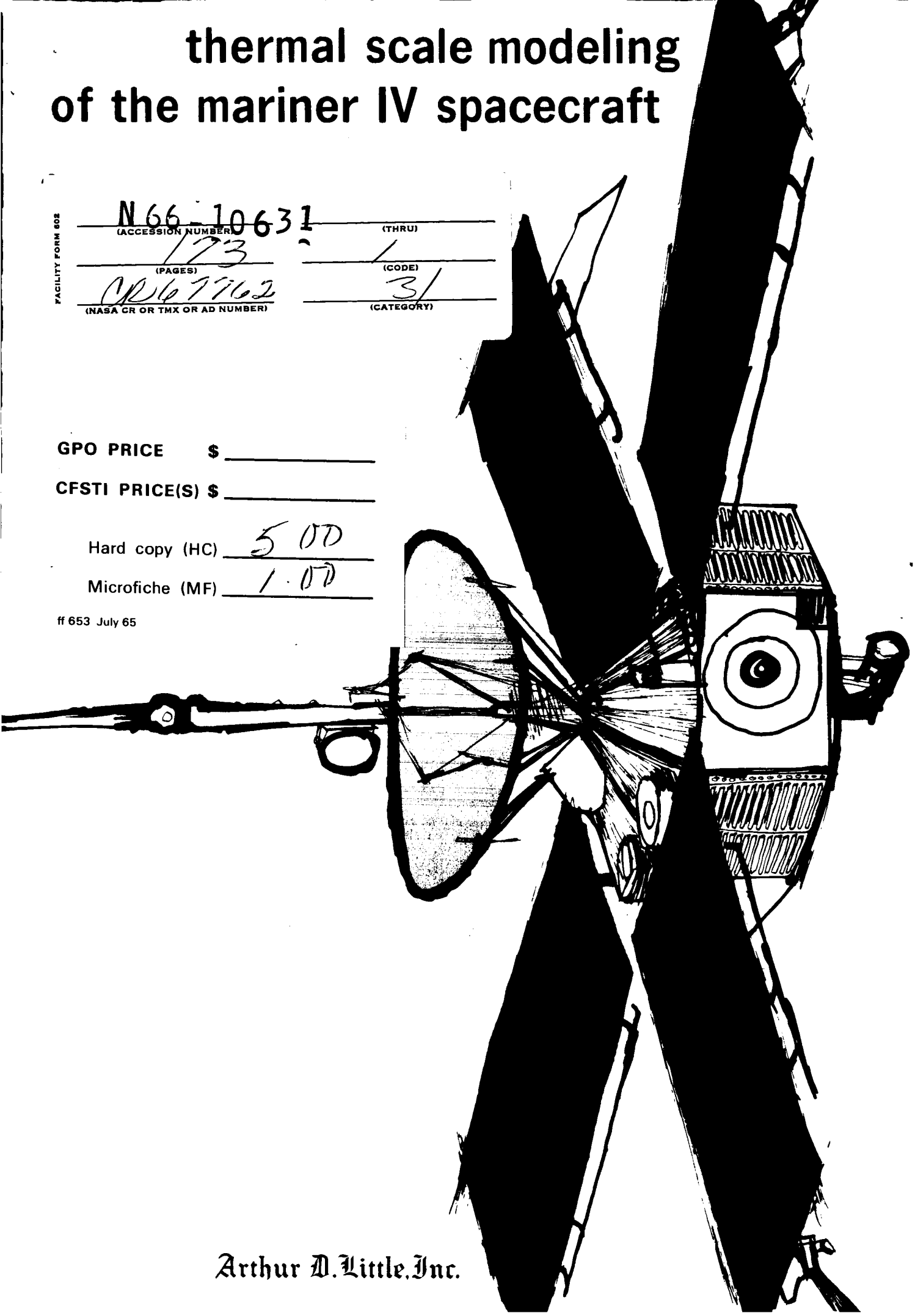

Arthur D. Little, Inc.

THERMAL SCALE MODELING OF THE MARINER IV SPACECRAFT

Final Report

to

Jet Propulsion Laboratory
Contract 950789

This work was performed for the Jet Propulsion Laboratory, California Institute of Technology, sponsored by the National Aeronautics and Space Administration under Contract NAS7-100.

by

Frank Gabron
Robert W. Johnson

Arthur D. Little, Inc.
Cambridge, Massachusetts

August 20, 1965

C-66326

Acknowledgments

During the design, fabrication and testing of the Thermal Scale Model, it was necessary to obtain a large amount of information and complete sets of drawings of Mariner IV from Jet Propulsion Laboratory. Arthur D. Little, Inc., wishes to acknowledge the efforts of Dr. J. M. F. Vickers and Dr. J. W. Lucas of Jet Propulsion Laboratory in organizing and transmitting this data.

During the course of the program, Messrs. D. Lewis, L. Dumas and D. Miller of Jet Propulsion Laboratory provided us valuable assistance in interpreting the details of the drawings with respect to the thermal behavior of the spacecraft.

The Phase III tests of the Thermal Scale Model were undertaken in NASA Lewis Research Center Solar Simulator. The efforts of Dr. Herman Mark, Mr. Ralph Sommers and other Lewis personnel who were responsible for the planning and execution of the tests are greatly appreciated.

Table of Contents

	Page
Acknowledgments	ii
List of Tables	v
List of Figures	vi
Introduction	viii
Summary and Conclusions	xi
PHASE II PROGRAM	1
A. Description of Phase II Model	1
1. Introduction	1
2. Scaling Procedures	4
3. Octagonal Bus Structure	6
4. Packaging Assembly	8
5. Scaling of Bolted Joints	11
6. Thermal Control Louvers	16
7. Post Injection Propulsion System	20
8. Insulation and Paint Treatments	21
B. Phase II Test Procedures	23
1. Description of Tests	23
2. Test Equipment and Measurements	25
C. Test Results	27
D. Discussion of Test Results	28
PHASE III PROGRAM	33
A. Description of Phase III Thermal Scale Model	33
1. Introduction	33
2. Octagonal Bus	37
3. Magnetometer	39
4. Ion Chamber	40
5. Low-Gain Antenna	41
6. High-Gain Antenna	42
7. Cosmic Dust Detector	43
8. Sun Sensors	43
9. Trapped Radiation Detector	45
10. Absorptivity Standard and Plasma Probe	46

Table of Contents (continued)

	Page
11. Insulation and Shielding	46
12. Solar Panels	48
13. Planetary Science	49
14. Canopus Tracker	49
15. Surface Finishes	50
B. Test Facility	51
C. Test Procedures	54
1. Description of Tests	54
2. Test Measurements	55
D. Test Results	58
E. Discussion of Temperature Predictions	61
1. Sunlit Appendages	61
2. Internal Bus Locations	62
3. Shaded Appendages	65
APPENDIX I - TSM POWER BREAKDOWN-PHASE II CONFIGURATION	91
APPENDIX II - JOINT CONDUCTANCE TEST RESULTS	100
APPENDIX III - TSM POWER BREAKDOWN-PHASE III CONFIGURATION	103
APPENDIX IV - CALCULATION OF ANTENNA HEAT LOSS	110
APPENDIX V - TEMPERATURE CONTROL SURFACES SCIENCE & APPENDAGES	112
APPENDIX VI - ERROR ANALYSIS-SUNLIT APPENDAGES	114
APPENDIX VII - DISCUSSION OF CANOPUS TRACKER TESTS	117

List of Tables

Table		Page
1	SUMMARY OF PHASE II TEST CONDITIONS	68
2	COMPARISON OF TEMPERATURE RESULTS--TEST 1, PHASE II	69
3	COMPARISON OF TEMPERATURE RESULTS--TEST 2, PHASE II	70
4	COMPARISON OF TEMPERATURE RESULTS--TEST 3, PHASE II	71
5	COMPARISON OF AVERAGE BAY TEMPERATURES, PHASE II	72
6	COMPARISON OF TEMPERATURE DIFFERENCE ACROSS BOLTED JOINTS--PHASE II	75
7	COMPARISON OF CHASSIS TEMPERATURE RESULTS--TEST 1, PHASE II	76
8	COMPARISON OF TSM TEMPERATURES--TESTS 3 AND 3A, PHASE II	77
9	COMPARISON OF TSM TEMPERATURES--TESTS 3 AND 4, PHASE II	78
10	COMPARISON OF TSM AND MARINER IV TEMPERATURES, EARTH CRUISE	79
11	COMPARISON OF TSM AND MARINER IV TEMPERATURES, MARS CRUISE	80
12	COMPARISON OF TSM AND MARINER IV TEMPERATURES, MARS PLAYBACK	81
13	EFFECT OF SOLAR PANEL TEMPERATURE ON INTERNAL TEMPERATURES	82
14	THERMAL SCALE MODEL TEMPERATURE DATA, EARTH CRUISE	83
15	THERMAL SCALE MODEL TEMPERATURE DATA, MARS CRUISE	85
16	THERMAL SCALE MODEL TEMPERATURE DATA, MARS PLAYBACK	87
17	THERMAL SCALE MODEL TEMPERATURE DATA, MARS PLAYBACK, HIGH SOLAR PANEL TEMPERATURE	89

List of Figures

Figure		Page
1	TEMPERATURE CONTROL MODEL - PHASE II CONFIGURATION	120
2	THERMAL SCALE MODEL - PHASE II CONFIGURATION	121
3	THERMAL SCALE MODEL (BAYS 5, 6, 7)	122
4	TOP VIEW - TSM BUS	123
5	BOTTOM VIEW - TSM BUS	124
6	BOTTOM VIEW - TCM BUS	125
7	INTERIOR VIEW - TSM	126
8	INTERIOR VIEW - TCM	127
9	TOP OCTAGONAL FRAME	128
10	CHASSIS ASSEMBLY	129
11	LONGERON	130
12	PACKAGING ASSEMBLY BAY 1	131
13	PACKAGING ASSEMBLY BAY 3	132
14	PACKAGING ASSEMBLY BAY 4	133
15	PACKAGING ASSEMBLY BAY 5	134
16	PACKAGING ASSEMBLY BAY 6	135
17	PACKAGING ASSEMBLY BAY 7	136
18	PACKAGING ASSEMBLY BAY 8	137
19	THERMAL CONTROL LOUVER BLADE ASSEMBLY	138
20	THERMAL CONTROL LOUVER ASSEMBLY	139
21	THERMAL CONTROL LOUVER PERFORMANCE	140
22	POST INJECTION PROPULSION SYSTEM	141
23	BAY 6 CONFIGURATION - TEST 3	142

List of Figures (continued)

Figure		Page
24	MODIFIED BAY 6 CONFIGURATION - TEST 4	143
25	CONFIGURATION - MARINER IV SPACECRAFT	144
26	BOTTOM VIEW - MARINER IV SPACECRAFT	145
27	MARINER TEMPERATURE CONTROL MODEL	146
28	THERMAL SCALE MODEL - TOP VIEW	147
29	CONFIGURATION, MARINER-C SPACECRAFT AS OF 10-16-64	148
30	THERMAL SCALE MODEL	149
31	THERMAL SCALE MODEL	150
32	THERMAL SCALE MODEL - BOTTOM VIEW	151
33	THERMAL SCALE MODEL (LOUVERS AND UPPER SHIELD REMOVED)	152
34	THERMAL SCALE MODEL, BAYS 1, 2, 3	153
35	THERMAL SCALE MODEL, BAYS 4, 5, 6	154
36	THERMAL SCALE MODEL, BAYS 7, 8	155
37	SCHEMATIC OF NASA LEWIS SPACE SIMULATOR	156
38	SOLAR ILLUMINATION PATTERN	157
39	SOLAR INTENSITY VARIATION	158
40	TSM CANOPUS TRACKER	159

Introduction

The interest in using thermal modeling techniques as a development tool in producing a flight spacecraft is mainly derived from the high costs of fabricating and testing full-scale prototype hardware. The use of small, simplified thermal models will also, in many instances, reduce the development time required to establish a workable thermal control design. Furthermore, temperature predictions made with thermal scale models may be inherently more accurate than predictions made with full-scale prototypes of very large spacecraft due to the size and performance limitations of presently available solar simulators.

The concept of using thermal scale modeling techniques for predicting the temperatures of full-scale flight spacecraft from environmental simulation tests of reduced-scale models has recently received attention in the literature. The theoretical basis for the design of thermal scale models has been established, and preliminary experiments with extremely simple prototypes and models have been undertaken.

The work to be described herein comprises the first known attempt to predict the temperatures in an actual spacecraft, of considerable complexity, by use of thermal modeling techniques.

In a one-year research and development program, a one-half scale (approximately) thermal model of the Mariner IV spacecraft was designed, fabricated and tested in a simulated solar environment. The over-all objective of the program was to determine the feasibility of predicting equilibrium temperatures in a complex flight spacecraft from environmental simulation tests of a small-scale thermal model. The basis for

determining the feasibility of the technique was a comparison of scale model temperatures, measured in solar simulation tests, with temperature data obtained during the recent Mariner IV flight to Mars.

The aim of the contract was to develop a one-half scale thermal model whose temperatures, at thermal equilibrium, would correspond to those measured in a full-scale prototype within 5 degrees Fahrenheit. Furthermore, the design, fabrication and testing of the Thermal Scale Model (TSM) was to be completed without prior knowledge of the temperatures that were measured by Jet Propulsion Laboratory in prototype tests.

The program was divided into three separate phases. Phase I, a nine week effort, was an analysis and preliminary design effort. The problems associated with detailed design and fabrication of the TSM were studied, and a preliminary layout design for a 0.43 scale thermal model of a Mariner Spacecraft was completed. This design was based on a set of thermal scaling laws which predict identical temperatures at homologous locations in model and prototype.

During Phase II, which was a 24 week effort, a 0.43 scale model of the basic octagonal bus of a modified JPL Mariner Temperature Control Model (TCM) was fabricated and tested in a thermal-vacuum chamber. The tests were made in a cold-wall (LN_2 temperature) vacuum chamber without solar simulation. The TSM tests were made at Arthur D. Little, Inc., in a five foot diameter chamber. Independent tests of the TCM were made under conditions of thermal similitude by Jet Propulsion Laboratory. Temperature measurements at 48 locations (identical thermocouple locations were used in the TSM and TCM) were

made at thermal equilibrium conditions.

Phase III, a 19 week effort, involved the design and fabrication of thermally scaled versions of the superstructure, solar panels, scientific experiments and other appendages on the Mariner IV spacecraft. The Phase III TSM configuration, which was essentially a complete thermal scale model of the Mariner IV, was tested in the NASA Lewis Research Center Solar Simulator.

Temperature predictions made by use of the TSM were compared with Mariner IV "cruise" flight data for the 98th and 180th flight day measured from launch to determine the influence of solar intensity on the accuracy of scale model predictions. (The solar intensity decreases by approximately 30 percent during this interval of 82 days.) Comparisons of temperature predictions were also made for the "Mars Playback" mode in which the internal power dissipation in the spacecraft is significantly reduced.

The equilibrium temperatures at 75 locations within the thermal model were measured in the solar simulation chamber for each of the three tests. Twenty of the temperature measurements were made at homologous locations in the model and Mariner IV, and these measurements constitute the basis for comparing the scale model temperature predictions with flight temperature data telemetered to Earth from Mariner IV.

Summary and Conclusions

The results of this program have shown that thermal scale modeling techniques can be successfully applied to the prediction of flight temperatures of a complex spacecraft. Temperature predictions made from measurements with a small-scale thermal model in an environmental chamber are sufficiently accurate to presently warrant the use of these techniques in preliminary design and development of large, complex spacecraft.

The thermal behavior of temperature-actuated, thermal control louvers was successfully modeled at one-half scale, and the accuracy of the thermal scale model was independent of the magnitude of the temperature gradients within the structure.

The temperature differences across bolted joints, typical of those used in power-dissipating, electronic subchassis, were measured in model and prototype. In all tests, the thermal modeling of the joint conductances was within the experimental accuracy of the measurements.

Temperature predictions of both solar dependent and independent spacecraft appendages were successful.

The accuracy of temperature predictions made for the Mariner IV spacecraft by use of the half-scale thermal model tested in a simulated solar environment is summarized below. (The comparisons are based on measurements at twenty homologous locations in the model and Mariner IV. The basis for the comparison was temperature data telemetered to Earth from the Mariner IV spacecraft.)

	Number of Model Temperature Measurements With Indicated Error			
	< 5F	< 10F	< 15F	< 25F
Test 1 Earth Cruise Mode	14	15	16	19
Test 2 Mars Cruise Mode	3	11	16	17
Test 3 Mars Playback Mode	1	3	13	15

For the three tests, 48 percent of all measurements corresponded within 10F and 85 percent within 25F.

Subsequent analyses of the temperature predictions have shown that significant improvements in the accuracy of the temperature predictions would be expected in testing future models of similar complexity.

The results have also shown that large temperature errors can be introduced in scale model temperature predictions by simplifications in the details of construction. The treatment of details will be a governing factor in establishing a confidence level on the application of the technique to larger and more complicated spacecraft. However, the reduction in ground handling problems and in testing time and costs, plus the possibility for increasing the accuracy of temperature predictions of very large spacecraft make the technique attractive.

The design and fabrication of the half-scale thermal model was based on a group of thermal similitude relationships which, in theory, produce identical temperatures at homologous locations in model and prototype. The use of this "temperature preservation" scaling technique requires that materials having different thermal conductivities be used in model and prototype and that the surface properties (emittances and solar absorptances) be identical in model and prototype. It is important

to note that no difficulty was encountered in finding materials with the proper thermal characteristics.

Further work is needed to correlate and compare the accuracy of scale-model temperature predictions for a flight spacecraft with temperature predictions made by use of full-scale thermal test prototypes or the actual flight spacecraft in ground testing with large solar simulators.

This program was entirely devoted to the prediction of spacecraft temperatures at thermal equilibrium. Additional work is needed to explore the feasibility of applying thermal modeling techniques to spacecraft where transient effects are important.

The thermal scale model of the Mariner IV was designed, fabricated and tested in a one-year program. A considerable fraction of this period was devoted to preliminary tests of only a portion of the spacecraft. The results of the present program indicate that intermediate testing could be by-passed in fabricating another thermal model of a spacecraft of similar complexity. With the knowledge gained in this program, a similar model could now be tested in solar simulation within approximately seven months after design initiation. Improvements in the accuracy of the temperature predictions and a significant cost reduction would be anticipated.

PHASE II PROGRAM

A. Description of Phase II Model

1. Introduction

The objective of the Phase II test program was to compare temperatures measured in a one-half scale model of the basic octagonal bus of the Mariner IV spacecraft with temperatures measured independently by Jet Propulsion Laboratory with a similar full-scale configuration. These tests were made in cold-wall environmental chambers without solar simulation since the temperatures of the octagonal bus of the Mariner IV spacecraft are primarily governed by internal power dissipation.

For purposes of these special tests, a full-scale Mariner Temperature Control Model (TCM) was modified and tested by Jet Propulsion Laboratory. (A TCM is identical to a flight spacecraft with the exception that the power dissipated in electronic subchassis is simulated by heaters instead of the actual electronics and the various propellant and pressurant containers are not filled. Jet Propulsion Laboratory has determined that these differences are not important to the determination of temperature distributions in an actual Mariner-type spacecraft.)

Views of the modified full-scale TCM and the half-scale TSM, as used in the Phase II test program, are shown in Figures 1 and 2. The modified TCM shown in Figure 1 consists of the octagonal bus structure. The complete Mariner TCM was modified to this configuration by removing all of the appendages including the solar panels. Thermal shields, consisting of layers of "super-insulation" were attached to the top and

bottom surfaces. By thermally shielding the top and bottom surfaces the total internal power dissipated within the spacecraft was emitted from the eight bays of the octagonal bus.

In previous solar simulation tests of the TCM (conducted by JPL), it was found that the uppermost thermal shield did not act as an adiabatic surface and the internal temperature of the bus was affected by the heat leaks through the thermal shield. Therefore, for the special tests conducted in the Phase II program, a heated "hat" section was installed on the top of the bus to increase the total internal power dissipation and thereby set the bus temperature within a normal operating temperature range.

The scale model was geometrically similar to the prototype TCM except reduced in size. Many of the construction details in the TCM were simplified in the TSM. These simplifications will be discussed in following sections of this report.

The diameter of the prototype TCM was approximately 48 inches and the height of the bus was 16 inches. The diameter of the scale model was 21 inches and the height approximately 7 inches. The nominal internal power dissipation of the prototype TCM was 170 watts; the nominal power dissipated in the scale model was 32 watts.

Five of the eight bays (Bays 1, 3, 4, 7, and 8) were equipped with temperature actuated thermal control louvers. These assemblies are variable emittance devices which increase the effective emittance of the bus with an increase in bus temperature. The louver assemblies used on the TSM were thermally scaled versions of those used on the TCM.

An over-all view of Bay 2, which contains the Post Injection Propulsion System, is also shown in Figure 2.

Figure 3 shows the exterior of Bays 5, 6 and 7 (right to left) of the TSM. Bay 5 was completely shielded and Bay 6 was partially shielded. The exposed area of Bay 6 in the TSM was scaled from the exposed area of the TCM.

Top and bottom views, showing the interior of the TSM, are shown in Figures 4 and 5. These photographs were taken prior to final assembly and do not show the thermal control louvers or thermal shields. For comparison, a bottom view of the JPL TCM (attached to a mounting ring) is shown in Figure 6. It can be seen that much of the detail has been reproduced in the TSM with the exception of some additional wiring.

The similarity of the mounting of the power dissipating electronic subchassis in the TSM and TCM is shown in Figures 7 and 8. These interior views show some of the details in Bays 6, 7 and 8.

In the following sections, we will discuss the procedures used in designing the TSM and the details of construction of the components.

2. Scaling Procedures

The TSM was designed in accordance with a set of thermal scaling laws which predict identical temperatures in model and prototype at homologous locations. The use of this "temperature preservation" technique was specified by Jet Propulsion Laboratory. In addition, it was desired to make model and prototype geometrically similar.

As it was desired to compare model and prototype temperatures at thermal equilibrium conditions, no consideration was given to the similitude parameters which govern transient scale modeling.

The theoretical basis for the design of thermal scale models of spacecraft has been established and the results of successful experiments with simplified thermal scale models--using the temperature preservation technique--have been presented in the literature [1].

The following relationships were used as a basis for the design of the TSM:

$$\frac{\epsilon_m}{\epsilon_p} = 1 \tag{1}$$

$$\frac{\alpha_m}{\alpha_p} = 1 \tag{2}$$

$$\frac{k_m}{k_p} = \frac{L_m}{L_p} = R \tag{3}$$

$$\frac{C_m}{C_p} = 1 \tag{4}$$

1. Fowle, A. A., et. al., Thermal Scale Modeling of Spacecraft: An Experimental Investigation, paper presented at AIAA Space Simulation Testing Conference, Pasadena, California, Nov. 16-18, 1964.

$$\frac{q_m}{q_p} = \left(\frac{L_m}{L_p}\right)^2 \tag{5}$$

where

ϵ - emittance
α - absorptance
k - thermal conductivity
L - characteristic length
R - geometric scale ratio
C - thermal joint conductance
q - rate of heat flow
m - model
p - prototype

Equations (1) and (2) require that identical emittances and absorptances be used in model and prototype. Equation (3) requires that the ratio of thermal conductivities be equal to the geometric scale ratio. Equations (4) and (5) require that the thermal conductances across bolted joints be identical and that the ratio of the rates of heat flow be proportional to the square of the geometric scale ratio.

In the design of the TSM, the emittances were made equal to those in the TCM by using the same surface finishes and paints. The materials of construction of the TSM were chosen to have thermal conductivities approximately 0.43 of those used in the TCM. The choice of a geometric scale ratio of 0.43, rather than, say, 0.5, was based on the availability of the particular materials which were used to fabricate the TSM. The joint conductances were made equal by design and test procedures to be discussed in a following section. Finally, the rates of heat flow in the

model were designed to be 0.1849 times the rates that existed in the prototype. In the Phase II configuration no external power was applied to the prototype and, therefore, Equation (5) was satisfied by simply scaling the internal power dissipation.

A further discussion of the details of the application of the scaling parameters to the components that comprise the TSM is given in the following sections.

3. Octagonal Bus Structure

The basic structural assembly consists of two octagonal frames bolted together with longerons. To this assembly are bolted the eight chassis plates (shear webs) which in turn support the electronic sub-chassis.

During the preliminary design phase of our work, several analyses were made to determine the relative effects of conduction and radiation in determining the temperature gradients within the entire structure. The results showed that the azimuthal temperature distribution in the bus is mainly determined by radiative effects, whereas conductive effects are important in determining the axial temperature distributions in the chassis plates and the temperature patterns in the regions where power dissipating sub-chassis are bolted to the chassis.

The shear webs were thus important with respect to conductive effects, and we chose to use SAE 1015 steel for fabricating the shear webs in the TSM.

The thermal conductivity of the ZK 60A magnesium TCM shear webs was estimated to be 1.21 watts/cm-K and SAE 1015 steel has a conductivity

of approximately 0.519 watts/cm-K. The geometric scale ratio was then set to be

$$\frac{L_m}{L_p} = \frac{k_m}{k_p} = \frac{0.519}{1.21} = 0.43$$

This geometric scale factor was then applied to all of the dimensions of the TCM to arrive at the proper dimensions of the TSM.

The octagonal frames were machined from an Alloy 9B aluminum bronze casting. This composition is reported [1] to have a conductivity of 0.63 watts/cm-K which is 52% of the conductivity of the magnesium used in the TCM. A drawing of the top frame section is shown in Figure 9. The webs that were cast in this frame structure were not required from the thermal standpoint but were provided for the attachment of equipment to be used in the Phase III program.

The details of the shear webs are shown in Figure 10. These plates were geometrically scaled in thickness from those used in the TCM and were fabricated from SAE 1015 steel. As shown in Figure 10, several of the shear webs were designed with varying thicknesses. Because of the importance of conductance effects in determining the temperature distributions within the shear webs, a scaled geometry was used in the TSM, although some changes in the radii of the machined patterns were made for ease of fabrication.

The magnesium longerons in the TCM were also thermally scaled by using 1015 steel and scaled wall thicknesses in the TSM. Instead of

---

1. Metals Handbook, Volume 1, Properties and Selection of Metals, 1961.

fabricating the longerons from a single casting, the TSM longerons were made from weldments as shown in Figure 11.

4. Packaging Assembly

There are seven bays that dissipate power in the TCM--Bay 2 houses the PIPS and does not have any internal power. Of those that dissipate power, Bays 6, 8 and 1 dissipate 39, 20 and 14 percent of the total internal power, respectively. Because of the wide variation in internal power between bays, we simplified the electronic packaging in those bays or modules that have small power dissipations. Since each bay was treated in a slightly different manner, we will discuss the layout of each bay in turn in the following paragraphs.

The individual modules are radiatively coupled to one another and are conductively coupled to the shear web through bolted joints. The emittance of the TSM modules is approximately the same as the corresponding TCM modules. Gold plated boxes were used where required and the emittance of the Dow 7 used on the TCM was reproduced by a black oxide finish.

The modules that dissipate more than 1 watt (in the TCM) have scaled radiating areas and conduction paths. For these TSM modules, the number of shear web bolted connections were identical to the number used in the TCM. The only geometrical difference between these TSM modules and those used in the TCM was the location of the horizontal divider to which the heater was attached. In the TSM the divider was located at the bottom of the module instead of on a central plane. These modules were made from SAE 1015 steel with scaled wall thicknesses.

The modules in the TCM which dissipate less than one watt or have no power dissipation were not exactly scaled in the TSM. The maximum temperature rise of these modules if they are conductively decoupled will be only 3 to 4 degrees C per watt of power dissipation. Therefore, certain liberties were taken in modeling these modules. In these cases, the modules were bolted to the shear web face but did not have the bolted tab connections. These modules were fabricated from SAE 1015 steel and had scaled wall thicknesses. These modules were similar in shape to the higher power modules except that two of the vertical sides were omitted. This change did not appreciably affect the radiative coupling between bays or modules, and did represent a considerable simplification with respect to manufacturing.

Heaters and thermistors were affixed to each module in the same relative locations as on the TCM. Each module was equipped with a disconnect to facilitate the removal of a complete chassis assembly.

We will now discuss the characteristics of each chassis in turn.

A packaging assembly drawing for Bay 1 is shown in Figure 12. This bay contains scaled versions of modules that dissipate more than and less than one watt in the TCM. In Figure 12 the scaled powers for each component are identified with the JPL identification as noted on the JPL drawing J 4901042. The powers were obtained from the appropriate scaling ratio of $(0.43)^2$ which is 0.185. (A listing of the TSM powers and the thermocouple list used is presented in Appendix I.) An example of the module construction we used for those TCM modules that dissipate more than one watt is module 4A13. Examples of the simulation of

modules that dissipate less than one watt in the TCM are modules 8A1/8A2. One of these is shown in section A-A of Figure 12.

In Figures 13 and 14 are shown the layouts of Bays 3 and 4. The layout of Bay 3 is similar to the TCM with the exceptions previously noted. In order to simulate the gap between boxes 3A1 and 6A8 on the TCM, we combined the powers of modules 3A1 and 3A5, and modules 6A8 and 6A10. This change is noted in Figure 14.

The assembly of Bay 5 is shown in Figure 15. The bay contains two low emittance boxes, viz., 2RA2 and 2RA1 which dissipate rather large amounts of power. Module 16A1--which does not dissipate power--was simulated by use of a single plate bolted to the vertical members of the shear web. In the TCM this module was not bolted to the shear web face and we are merely representing the radiation blockage between the interior of the shear web face and the interior of the bus.

The assembly of Bay 6 is shown in Figure 16. This bay has a larger amount of power than any other bay, and also contains component 2PA1 which singly dissipates more power than any other module or component.

The assembly layout of Bay 7 is shown in Figure 17. In the TCM, the attitude control electronics are attached to the left side of Bay 7. We have simulated this component by a single module having the same approximate shape. This representation is shown in Figure 17 as module 7A1. The remaining modules were reasonable thermal versions of those used in the TCM except that the area occuped by the gyro control (7A2) in the TCM was simulated by two smaller modules.

The layout of Bay 8 is shown in Figure 18. In this bay the heaters were directly attached to the dividers and the shear web face as in the TCM. The locations of the heaters are noted. In this particular drawing we have not shown the cover that blocks the Bay 8 shear web from viewing the interior of the bus.

5. Scaling of Bolted Joints

In our studies [1] of the problems associated with the thermal design of scaled bolted joints, it was shown that the bolt load in the model should be equal to the bolt load in the prototype multiplied by the scaling ratio--which in this case is 0.43. This conclusion is based on the assumption that the mating surfaces are thermally scaled, and that the hardness and surface roughness are nearly identical in model and prototype. However, our studies also showed that the temperature differences between the sub-chassis and the chassis plates were in large part controlled by the "constriction resistance" in the chassis plate. This constriction resistance is due to the fact that the heat flow patterns in the chassis are governed by the conductance of the chassis. In this case the temperature differences across the bolted joints are more strongly influenced by the area of contact and the thermal conductance of the chassis than by the actual temperature difference across the metal-to-metal interface.

The basic approach used to scale the bolted joint thermal performance involved the use of reduced size bolts, torqued to a scaled

---

1. Thermal Scale Modeling of the Mariner Mars 64 Spacecraft, Phase IB Preliminary Report to Jet Propulsion Laboratory, Arthur D. Little, Inc., Cambridge, Massachusetts, July 2, 1964.

load. For example, the #8-32 titanium bolts (35 inch-lb torque) used to join the chassis to frame were modeled by use of #6-32 stainless bolts torqued to approximately 7 inch-pounds. The #6-32 stainless bolts (18 inch-lb torque) used to attach the power dissipating sub-chassis to the chassis plates were modeled by use of #4-40 stainless steel bolts torqued to 5.5 inch-pounds. The bolt sizes and torques used in the TSM were selected to have a scaled bolt load of approximately 43% of the load that existed in the corresponding bolts of the TCM. The loads were estimated from the friction torque characteristics of bolts presented in the literature [1].

In recognizing the uncertainties involved in basing the joint designs on limited theory and approximate calculations of friction coefficients, etc., we completed a series of ancillary tests to determine whether the basic approach stated above would be applicable to the thermal scaling of the joints between the power dissipating modules (sub-chassis) and the chassis.

A TCM sub-chassis was bolted (in accordance with JPL specifications) to a 10 inch diameter magnesium plate of approximately the same thickness as the TCM chassis. A 25 watt heater was installed in the sub-chassis, and the sub-chassis and back of the 10 inch plate were "super-insulated". The assembly was placed in a small vacuum chamber with a liquid nitrogen cooled interior shroud and temperature differences across the bolted joint were measured. The 10 inch plate was used to radiate the 25 watts to the cooled vacuum chamber shroud. A 0.43 scale

1. Belford, R. B., et. al., Joint Design, Machine Design, March 21, 1963.

TSM sub-chassis and a scaled radiating plate (both were fabricated from 1015 steel) were assembled in accordance with the scaling methods discussed previously. The power input to the TSM chassis was scaled to be 4.6 watts. This assembly was also used to make temperature difference measurements in the vacuum chamber.

The full scale assembly was used to investigate the effects of bolt torque, bolt material and the conductance of the radiating plate on the temperature differences from the sub-chassis to the radiating plate.

The basis of comparison for the tests was the temperature difference measured with the TCM sub-chassis attached to the magnesium plate with three #6-32 stainless steel bolts torqued to 18 inch-pounds. The measured temperature difference for this configuration was 83.5 F with 25 watts of internal power dissipation. (The mean fourth power temperature of the radiating plate was used to arrive at the temperature differences.) Reducing the bolt torque to 9 inch-pounds increased the temperature difference to 107.3 F. Changing the bolt material from stainless to titanium (at the same torque) did not affect the temperature difference. Increasing the thermal conductance of the radiating plate by substituting a copper plate of the same thickness as the magnesium plate--thereby increasing the conductance by a factor of about three--decreased the temperature difference from 83.5 F to 41 F. This result shows the importance of scaling the conductive paths around the bolted regions. The results of these tests are tabulated in Appendix II.

From the results of these tests with the full-scale bolted joint assembly, we concluded that the scaling of the conductive paths (i.e., the constriction resistance) and the bolt torque would be important in determining the temperature patterns in the scaled sub-chassis.

Next, the TSM sub-chassis assembly was tested to determine whether or not the temperature differences would correspond with those measured in the full-scale assembly. It was desired to have the temperature differences in the TSM assembly correspond with those measured in the TCM assembly with the magnesium radiating plate and the bolts torqued to 18 inch-pounds as this configuration is typical of the fully assembled TCM.

The scaled TSM sub-chassis was bolted to the scaled radiating plate with three #4-40 stainless screws torqued to 5.5 inch-pounds. The measured temperature difference was 69.8 F which was lower than the 83.5 F difference measured with the TCM sub-chassis. Reducing the torque to 2.7 inch-pounds increased the difference to 88.9 F. At this point, we could have chosen to set the bolt torques at about 4.7 inch-pounds and this presumably would have set the temperature difference to correspond with the TCM sub-chassis assembly at 83.5 F. However, we decided to investigate one additional variable, viz., the size of the clearance hole in the radiating plate since we had rather arbitrarily used a clearance hole diameter of 0.125 inches in this test setup. The clearance hole was enlarged to 0.149 inches and the temperature difference increased from 69.8 F to 93.4 F (at 5.5 inch-pounds of torque). This surprising result showed that the geometry of

the hole pattern was influential in determining the temperature distribution for these sub-chassis. If the temperature difference is assumed to be linear with clearance hole diameter, a 0.136 inch clearance hole diameter in the TSM assembly (with a bolt torque of 5.5 inch-pounds) would make the temperature differences in model and prototype correspond.

The holes for the sub-chassis bolts in the TSM chassis plates were drilled to this diameter and the bolt torques set at 5.5 inch-pounds.

We anticipated that the thermally scaled joint problem would be most critical for the bolted modules that dissipated relatively large amounts of power in the TCM. Therefore, we did not complete any experiments with the joints between the frame and chassis plates. In this case, we believed that only small amounts of power would be transferred between the frame and chassis and that the temperature differences would be small.

In conclusion, we thermally scaled the bolted joints by use of a limited amount of theory and the results of ancillary tests with a full-scale JPL sub-chassis and a 0.43 thermal scale model of the sub-chassis. The results of these tests were used to determine bolt torques and clearance hole diameters which would provide temperature difference correspondence in model and prototype.

6. Thermal Control Louvers

The five sets of thermal control louvers used on the TCM are used to regulate the bus temperatures. The normal operating temperature range is from 55 to 80 F. The louver blades are fabricated from polished aluminum which has a low infrared emittance. In the closed position the blades shield the spacecraft bus. As the blades open, the chassis--which is painted to have a high emittance--is exposed, thereby increasing the effective emittance of the assembly. At temperatures below 55 F, the louver blades are closed and the assembly has an effective emittance of 0.12. At temperatures above 80 F, the louver blades are wide open and the effective emittance of each assembly is 0.76. At 55 F a typical set of louvers will radiate 6.9 watts of power and at 80 F the power dissipation will be 52.6 watts. These results were obtained from JPL tests [1].

Each pair of louver blades on a TCM assembly is driven by a bi-metallic spring which will rotate approximately 90 degrees with a temperature change of 25 F. The bi-metallic actuating springs are radiatively coupled to the chassis of the spacecraft so that the angular position of the blades is a function of the chassis temperature. Each set of blades can be adjusted within a small range to set the temperature at which the blades open.

In the tests completed by JPL with the modified TCM, the louver blades on the assemblies mounted on Bays 7 and 8 were set to open at 55 F and on Bays 1, 3 and 4, the blades were set to open at 63 F.

1. Mariner Louver Performance, Interoffice Memo by M. Gram, January 15, 1964.

In designing the louver assemblies for the TSM, it was decided to utilize the same method for controlling the blade angles and to retain, as closely as possible, the geometrical characteristics of the TCM assemblies. The design of the TSM louvers was thus based on a requirement to have eleven pairs of individually actuated blades in each assembly. The scaling laws (c.f. Eq. 1) require that the emittances be identical in model and prototype, and that the ratio of conductivities be equal to the scaling ratio. However, in the case of the louvers, the power dissipated is controlled by radiative rather than conductive effects. Therefore, the TSM louvers were made from the same material, polished aluminum, to have essentially the same emittance as the prototype TCM assembly.

An exploded view of a typical blade assembly for the 0.43 scale TSM louvers is shown in Figure 19. This figure shows the bi-metallic actuating spring, the micarta axle and nylon bushings used to support the assembly. A view of a partially assembled set of blades is shown in Figure 20. A fully assembled set of louvers, complete with center section housing, is shown in Figure 3.

In designing the TSM louver assemblies at 0.43 scale, two problems were encountered. First, bi-metallic springs less than half the size of those used in the TCM were not readily available. Therefore, the dimensions of the center section housing the springs were larger than a scaled dimension thus reducing the effective radiating area of the exposed chassis with the blades in the open position. Second, in small bi-metal spring sizes, the maximum available rotation was

3 degrees of rotation per degree F temperature change. The TCM springs produced 3.6 degrees of rotation per degree F of temperature change. Therefore, the temperature span associated with the fully closed to fully open blade position was 5 F greater in the TSM.

To examine the thermal performance of a typical "scaled" TSM louver assembly, an extra assembly was fabricated for testing. The power dissipation vs. temperature characteristics of a TCM louver assembly were known from JPL tests and it was desired to compare these results--on a scaled basis--with the measured performance of a TSM louver assembly.

The power dissipation vs. temperature characteristics of a TSM louver assembly were measured in a vacuum bell jar with a liquid nitrogen cooled "black" inner shroud. The louver assembly was mounted on an aluminum plate to which was affixed a heating element. The aluminum plate was painted with PV 100[1] paint (also used on the TCM) on the side facing the louver assembly and insulated with multi-foil super-insulation on the other side. By measuring the temperature of the aluminum plate and measuring the input power to the heater, the thermal performance of the louver was obtained over a wide range of temperatures. For this particular setup, the opening temperature of the louver blades was set at approximately 55 F. A comparison of the TCM louver and TSM louver performance is shown in Figure 21. The upper curve is based on JPL data scaled by Equation 5 (page 7) which requires that the power be scaled in proportion to the geometric scale ratio

1. Vita-Var Paint Co., Orange, N. J., #15966.

(0.43) squared. The experimental data obtained with the scaled TSM louver indicate that the effective radiating area was low. Between the fully closed and open blade positions, the differences can be attributed in part to spring characteristics and the problems associated with "sticking" blades. The effective radiating area of the TSM louvers was known to be approximately 10% low because of the additional non-scaled area of the center housing. Therefore, to increase the effective radiating area of the assemblies used on the TSM, the chassis were painted with 3-M Optical Black Velvet paint instead of PV 100 paint. The emittance of PV 100 was measured to approximately 0.85. The emittance of 3-M paint was approximately 0.95. The substitution of this paint thus increased the effective radiating area by 10%. No additional experiments were made on the louver assembly with the 3-M painted surface since this correction was relatively straightforward. The temperature correspondence between model and prototype at a given power level was estimated to be of the order of 5 F which was of the same order as the experimental error. On the basis of this limited test program, it was decided to use the TSM configuration without further refinements to produce exact temperature correspondence. The reasons for making this decision were twofold. Tests of each of the five TCM and TSM louvers would be required to make precise comparisons, and the use of five assemblies on the spacecraft tends to "smear out" differences in the temperatures of individual bays.

It should be noted that in the assembly of the five sets of louvers used on the TSM, the angular position of the blades was

adjusted by setting the blades in the fully open position corresponding to the "fully open" temperature of the TCM assemblies. This approach was taken since the internal temperature of the spacecraft is more sensitive to changes in effective emittance when the louvers are at or near the fully open position.

7. Post Injection Propulsion System

The PIPS consists of a group of propellant and pressurant tanks, a rocket engine and associated controls. The entire bay containing the PIPS system--as installed on the TCM--is thermally isolated from the external environment by low emittance surfaces except for the "black cavity" produced by the rocket exhaust nozzle. Since no power is dissipated within the bay and the power radiated from the bay is small due to the low effective emittance of the exterior surfaces, errors associated with thermally modeling the system will have little influence on the temperatures of the other seven bays. For this reason, the TSM design was based on an approach which would simulate the gross thermal behavior and, therefore, many simplifications were made in designing a thermal mockup of the PIPS.

A drawing illustrating the TSM PIPS configuration is shown in Figure 22. The geometry of the system was retained, however, much of the detail used on the TCM such as piping, rocket motor insulation, etc., was omitted from the TCM. The conductive paths in the exhaust nozzle and jet vane support were approximately scaled from the thermal standpoint, however, it was recognized that the temperatures within the system would tend to "float". That is, because of the use of low

conductivity materials and low emittances, the temperatures within the nozzle, for example, are extremely sensitive to small changes in heat flux. In the following discussion of the comparison of temperatures measured for the TCM and TSM, it will be shown that the temperature correspondence between model and prototype in this particular bay was poorer than in any other location.

8. Insulation and Paint Treatments

The top and bottom of the spacecraft bus were insulated by use of multi-foil superinsulation. Approximately 12 layers of aluminized Mylar separated by silk netting were used as an insulation package. A similar system of insulation--from the thermal standpoint--was used on the TCM. In this particular spacecraft configuration, small heat leaks associated with the superinsulation package have little influence on the internal temperatures because of the large amounts of power radiated from the large areas of high emittance on the sides.

The thermal shields mounted on the sides of the TCM were made of polished aluminum and were thermally "shorted" to the bus by aluminum standoffs with bolts. Polished aluminum shields of approximately the same thickness were used on the TSM. They were also thermally short-circuited to the bus. Again, because of the large amounts of power dissipated by the unshielded bays, the influence of differences in the thermal coupling and emittances of the shields is small from the standpoint of predicting interior temperatures.

Three types of paint were used on the interior of the TCM and the same paint treatments were applied to the interior portions of the TSM.

The interior surfaces of the bus and the longerons were painted with Cat-A-Lac[1] Flat Black 463-3-8. The exterior portions of the longerons were painted with Cat-A-Lac Gloss White 443-1-500. The exterior surfaces of the chassis were painted with PV 100 White[2]. To insure that the emittances in model and prototype were equivalent, the emittances of several samples of each surface--painted by JPL to flight specifications--were compared with samples of the same paint prepared by ADL. The relative emittances were determined by calorimetric techniques using the ADL Emissometer. The results showed that the maximum difference in the relative emittance was 1.2% for the three paints which have total hemispherical emittances at room temperature ranging from 0.847 to 0.886.

1. Finch Paint Co., Torrance, California.
2. Vita-Var Paint Co., Orange, New Jersey.

B. Phase II Test Procedures

1. Description of Tests

The Phase II test program consisted of the experimental determination of the TSM "bus" temperatures for three different test conditions. These TSM tests were performed in a thermal-vacuum chamber at Arthur D. Little, Inc. Solar simulation was not used in these tests. Three corresponding tests were performed by Jet Propulsion Laboratory using a modified TCM. The temperatures at 48 locations within the "bus" were measured at thermal equilibrium. The location of the temperature measurements was identical in TCM and TSM.

Jet Propulsion Laboratory provided information on the TCM internal power, the power supplied to the TCM "hat section" for each test, and the measured temperatures of the TCM "hat section". The measured TCM bus temperatures were supplied to ADL following the submission of the measured TSM temperatures to Jet Propulsion Laboratory.

The three tests undertaken in Phase II were designed to provide information on the accuracy of the thermal scale model in three different situations. In each of the three tests, the amount of power dissipated in the "bus" was maintained constant at the "Earth Cruise" condition.

In Test 1, the power supplied to the "hat section" was made relatively small with respect to the power dissipated in the "bus" in order to set the average bus temperature within the normal operating temperatures of the thermal control louver assemblies. The purpose of this test was to compare the measured temperature distributions of the TCM and TSM when the louver assemblies were partially open.

In Test 2, the power supplied to the hat section was increased to set the average "bus" temperature at or above the "fully open" position of the thermal control louver assemblies. The purpose of this test was to compare the measured temperature distributions at elevated temperature levels when the thermal control function of the louver assemblies was removed.

In Test 3, two of the thermal control louver assemblies were caged in the fully-open position (Bays 1 and 3) and the remaining three assemblies were caged in the fully-closed position (Bays 4, 7, 8). The purpose of this test was to compare temperature distributions in the TCM and TSM when the bus temperature gradients were intentionally made large by forcing most of the internal power to be emitted by the two bays with caged open louver assemblies.

In addition to the three aforementioned tests, two additional tests were performed with the TSM. The first of these supplementary tests, Test 3A, was performed to evaluate the influence of "heat leaks" associated with gaps between the "flight-type" thermal shields on the temperatures of the TSM. During the installation of the thermal shields on the TSM, it was recognized that differences in the relative gap dimensions between the TSM and TCM could exist because of tolerance limits in the manufacture and final assembly of the shields. The gaps between the thermal shields, which act as "black-body" cavities, were covered with a low emittance aluminized tape and Test 3 was repeated in order to assess the influence of these "heat leak" paths on the TSM temperatures.

The second additional test of the TSM, Test 4, was performed to determine the influence of substituting a simplified version of Bay 6 for the complicated assemblage of simulated electronic sub-chassis. Test 4 was performed under the same conditions as Test 3, viz., with two louver assemblies caged fully open and the remaining assemblies caged closed. A view of the interior assembly of Bay 6, as used in Test 3, is shown in Figure 23. The modified Bay 6 configuration used in Test 4 is shown in Figure 24. This single heater dissipated the same amount of power as the total amount dissipated in the five sub-chassis used in the Test 3 configuration.

The internal powers that were dissipated in each test of the modified TCM and the TSM and the positions of the thermal control louver assemblies are presented in Table 1.

2. Test Equipment and Measurements

The TSM tests were conducted in a five foot diameter thermal-vacuum chamber with an interior shroud cooled to liquid nitrogen temperatures. The interior surface of the shroud was coated with an optical black paint to produce a high infrared emittance. During the TSM tests the internal pressure in the chamber was maintained in the 10^{-6} torr range.

Power was supplied to the TSM by use of a 300 volt DC power supply with 0.007 percent regulation. The individual heaters used within the TSM were precision wire-wound power resistors. Power measurements were made by current and resistance measurements. It was estimated that the total power measurements were accurate to within 0.09 percent.

The temperatures were measured by use of calibrated, matched thermistors. The entire lot of thermistors had resistance vs. temperature characteristics such that any single thermistor would have an error of less than $\pm$ 1/2 F over the temperature range of 32 to 212 F when a single resistance vs. temperature curve was used. Calibrations were made by the vendor to establish the resistance vs. temperature curve and three point calibrations of each thermistor were made by Arthur D. Little, Inc., as acceptance tests. These calibrations showed that the maximum error was less than $\pm$ 1/2 F.

A constant current of 30 microamps was supplied to the thermistors. The voltages were read on a digital voltmeter. The voltages were translated to temperature by use of a digital computer data reduction program. It was estimated that the total system error in measuring the temperatures was of the order of $\pm$ 1/2 F.

Temperature measurements of the TSM were recorded at approximately one hour time intervals. The final steady-state temperature measurements were made when the change in any temperature between three successive readings was less than 0.1 F. The time required for the TSM to reach thermal equilibrium varied with the test condition, however, the average time was approximately 12 hours.

C. Test Results

The measured temperatures for the three tests of the modified TCM and the TSM are presented in Tables 2, 3, and 4. In each table, the temperature differences between the TSM and the TCM measured at homologous locations are tabulated.*

Comparisons of the average temperatures in each bay for the three tests are presented in Table 5. Comparisons of the temperature levels of each bay in the TCM and TSM were made by computing the average of all of the temperature measurements within a given bay. The percentage errors in the average temperatures of the TSM bays were based on the average absolute temperatures of the TCM bays.

In Table 6, data are presented for the temperature differences between four electronic sub-chassis and the shear webs to which they are mounted. Comparisons of the measured temperature differences for each of the three TCM and TSM tests are presented.

Comparisons of measured chassis temperatures in Test 1 of the TSM and TCM are made in Table 7.

Tables 8 and 9 contain data on the two tests made only with the TSM. A comparison of Tests 3 and 3A--which were used to determine the influence of heat leakage paths in the thermal shields--is made in Table 8.

The effect of making a simplified version of the Bay 6 heater arrangement is shown in Table 9. In this table, the TSM temperatures measured in Tests 3 and 4 are compared.

* Thermocouple #324 was not recorded in the JPL tests of the TCM. The temperatures at the same location measured in the TSM are listed for reference.

D. Discussion of Test Results

This discussion of the test results must be prefaced by the remark that the prediction of the spacecraft bus temperatures by use of the one-half scale thermal model was remarkably good. Generally speaking, the results show that the temperatures within a spacecraft structure, typical of the Mariner Mars 64, could be predicted by thermal modeling techniques to within 5 degrees Fahrenheit.

In reviewing the data obtained in all of the tests, there were only three temperature measurements that fell outside of the limits of accuracy generally required for thermal design purposes. These three temperature measurements were made within the Post Injection Propulsion System and the umbilical connector. A simplified thermal model of the PIPS was used in the TSM, and the umbilical connector was "mocked-up" rather than scaled from the thermal standpoint.

The approach used in designing and fabricating the Thermal Scale Model was based on the objective of accurately predicting the temperatures of bus structure and the electronic sub-chassis, particularly those having a high internal power dissipation. For this reason, considerable emphasis was placed on the scaling of the thermal control louver assemblies and the bolted joints through which large amounts of power are being transferred.

The data indicate that this objective was met with considerable success.

The detailed temperature comparisons for the Phase II test program will be discussed in the following paragraphs.

The results of Test 1--a test in which all louvers were free to operate normally--indicate that the average absolute error in the TSM temperatures was 5.2 F, or one percent of the absolute temperature. (The absolute values of all differences were summed and averaged over the 44 bus temperature measurements.) Four temperatures were in error by 10 F or greater and only ten were in error by more than 6 F. In particular, the largest errors were encountered in Bay 2. The maximum error was 31.5 F as measured in the rocket nozzle. The errors associated with Bay 2 measurements are due to the relatively poor thermal coupling between these elements and the remainder of the spacecraft, and the fact that no internal power is dissipated in Bay 2. Furthermore, because of the large temperature gradients in these areas the temperature correspondence between TCM and TSM is subject to larger errors.

In Test 1, the temperature correspondence in the Bays with high internal power, such as Bays 6 and 8, is extremely good although in general the model ran slightly lower in temperature than the TCM. In a following discussion of Tests 3 and 3A, it will be shown that the presence of non-scaled gaps between the thermal shields--which act as "black-body" cavities--caused the model temperatures to be slightly low.

The results of Test 2 show that the temperature errors follow the same pattern as in Test 1; however, as expected the errors are slightly larger because of the higher temperature level and the fact that the thermal control function of the louver assemblies was deleted by driving the louvers wide open at these high temperature levels. The average absolute error between the TCM and TSM for Test 2 was 7.7 F, or

about 1.4 percent of the absolute temperature level. The "hat" temperature measurements showed that the "hat section" in the model was nearly 30 degrees F colder than the TCM. The power to the "hat section" was appropriately scaled and small heat leaks in the super-insulation on the top of the hat would not result in a difference of this magnitude. An examination of the details of the TSM and TCM indicated that the TCM had proportionately more radiative blockage between the hat and the bus. The blockage is due to the presence of wiring, connections, and the cable troughs. This effect would tend to decrease the hat temperatures of the TSM for a properly scaled power dissipation in the hat itself.

Test 3 forms the basis of a temperature comparison with increased temperature gradients in the bus and with the louvers on three bays caged closed. The average absolute error between the TCM and TSM was 4.7 F in Test 3. This is slightly less than the error in Test 1. The test results showed that the temperature differences across the octagonal bus were significantly altered. The temperature difference between Bays 3 and 7--on opposing sides of the octagonal structure--was less than 5 F in Test 1 and over 40 F in Test 3. A conclusion that can be drawn from the comparisons of Tests 1 and 3 is that the accuracy of the temperature predictions is preserved when the temperature differences between bays are increased by an order of magnitude. This result is appropriate to considerations of the application of thermal modeling techniques to other spacecraft designs where temperature gradients within the structure are significant.

The comparison of average bay temperatures as presented in Table 5 summarizes the errors in average temperature correspondence. The average bay temperatures correspond to within one percent for Tests 1 and 3 and the maximum error is less than 1.5 percent.

The comparison of the temperature differences across four electronic sub-chassis, as presented in Table 6, indicates that the modeling of the joint conductances was within the experimental accuracy of the measurements.* The temperature drop across the bolted joint in sub-chassis 2PA1--which has a large power dissipation--corresponded to within two degrees. Similar correspondence was obtained for sub-chassis 2PS1 which had a joint temperature drop of nearly 30 degrees F.

The temperatures of the chassis, i.e., the shear webs, are compared in Table 7 for Test 1. The average absolute error of the 16 measurements was 3.3 degrees F. The results indicate that the accuracy of temperature predictions was of the same order as the accuracy of the experimental measurements.

The influence of the heat leakage paths between the gaps in the thermal shields is shown in the data presented in Table 8 for Tests 3 and 3A. These test results were obtained in two similar tests of the TSM. The data indicate that covering the gaps in the thermal shields with low emittance aluminized tape increased the average temperature level of the model by about 5 degrees F. However, in Bay 3 the temperature level was increased by about 10 degrees F. It was noted that the measured temperatures in Bay 3 of the TSM were disproportionately lower

* The accuracy of the TCM measurements was estimated to be $\pm$ 1 F by JPL. The accuracy of the TSM measurements was estimated to be $\pm$ 1/2 F.

than the other bays when compared to the TCM results. The results of Test 3A indicate that part of the error was due to "non-scaled" gaps between the thermal shields used on Bay 3. It should be noted that dimensional tolerances associated with these gaps are significant from the thermal standpoint. Deviations in the "gap areas" of two full-scale spacecraft or a model of the full-scale spacecraft can result in appreciable temperature differences.

The results of Test 4, which was made with a simplified version of Bay 6, point out the fact that a complicated bay can be simplified without appreciable error in the temperatures. The chassis temperatures in Bay 6 were within a few degrees of the Test 3 results with either the TSM or TCM. This change did not appreciably alter the temperatures of the remainder of the bus. Therefore, in future thermal modeling studies, one should consider the possibilities of using simplified heating arrangements to determine structural temperatures.

PHASE III PROGRAM

A. Description of Phase III Thermal Scale Model

1. Introduction

The purpose of the Phase II program was to fabricate a model of the spacecraft bus, which is sun-independent, and to compare model temperatures with temperatures measured in a modified prototype of Mariner IV. Since the full-scale prototype used in the Phase II tests was based on an early development model of Mariner IV, it was necessary to modify and update the TSM bus to correspond to the Mariner IV flight spacecraft.

Since the purpose of the Phase III program was to investigate the accuracy of applying thermal modeling techniques to a complete spacecraft with appendages whose temperatures are sun-dependent, it was necessary to add thermally scaled versions of many of the appendages on Mariner IV.

The TSM configuration used in the Phase III test program was essentially a thermally scaled version of the Mariner IV flight spacecraft. Two views of the Mariner IV illustrating the over-all configuration and the appendages are presented in Figures 25 and 26.

The orientation of the Mariner IV is maintained during flight such that the roll axis as shown in Figure 25 is colinear with the spacecraft sun vector. Therefore, during the cruise portion of the flight from Earth to Mars, the solar panels, upper thermal shield and appendages above the upper thermal shield are in direct sunlight. The sides of the octagonal bus, the lower thermal shield and the appendages below the lower thermal shield are shaded from sunlight.

During the flight, the solar intensity decreases by approximately 58 percent as the spacecraft travels from Earth to Mars and moves away

from the sun. The total flight period from Earth to Mars encounter is approximately 230 days. The upper thermal shield is used to insulate the octagonal structure from solar energy. The internal temperatures of the octagonal bus and the electronics packages are maintained at a relatively constant level by the internal power dissipation and the action of the six sets of thermal control louvers. The temperatures of the appendages above the upper thermal shield and the solar panels are determined by the solar intensity, their internal power dissipation and the degree to which they are thermally coupled to the octagonal bus structure. Thus, the temperatures of the appendages above the upper thermal shield and the solar panels are solar-dependent, whereas the temperatures of the appendages below the lower thermal shield are basically independent of the solar intensity.

The change in solar intensity with respect to time is quite small (of the order of 1/2 percent per day) and, therefore, the temperatures of even solar-dependent appendages change very slowly. (A typical value for the ion chamber which is a solar-dependent appendage with a small thermal time constant is 1/2 ^{o}F per day.) Because transient effects are not important to the general temperature level of the Mariner IV spacecraft, the thermal scale model was not designed for predicting transient temperatures and the tests of the model were made at thermal equilibrium.

The geometric scaling ratio of 0.43, which was used in designing the octagonal bus structure during Phase II, was also used in obtaining the dimensions of the appendages used on the Phase III configuration. The relative sizes of the 0.43 scale TSM and the full scale prototype

are clearly shown in Figures 27 and 28.

The full-scale prototype shown in Figure 27 is an early version of a JPL temperature control model equipped with dummy solar panels which are considerably shorter than the actual flight versions.

The solar panels used on the TSM were electrically heated mock-ups designed to provide the proper thermal boundary conditions on the TSM bus and external equipment. The panels were electrically heated since the solar beam used in the Phase III simulation tests was not large enough to illuminate an entire panel.

Figures 30 through 33 also show some of the details of construction of the appendages used on the TSM. Many of the appendages on the TSM were mocked-up or eliminated rather than thermally scaled. The primary objective of the program was to predict temperatures of several solar-dependent appendages and several appendages attached to the spacecraft below the lower thermal shield. In addition to the temperatures within the bus, effort was concentrated on thermally scaling the magnetometer, ion chamber, and trapped radiation detector whose temperatures are solar-dependent and the Canopus tracker, television camera and science platform thermal simulator (SPITS) whose temperatures are essentially solar-independent. However, the thermal characteristics of other appendages were scaled in situations where the temperatures of the appendages were believed to influence the bus temperature.

The following table lists and classifies the external appendages depending on whether they were scaled, mocked-up or not used on the TSM. The locations of the appendages are identified in Figure 29.

	Thermally Scaled	Mock-up	Not Used
Low-gain antenna	x		
Low-gain antenna ground plane		x	
Low-gain antenna damper	x		
Magnetometer	x		
Ion chamber	x		
High-gain antenna	x		
High-gain antenna support truss	x		
Solar panel damper	x		
Solar panels		x	
Solar pressure vane and gas jets			x
Solar panel latch, switch, pin			x
Cosmic dust detector	x		
Plasma probe		x	
Absorptivity standard		x	
Upper thermal shield	x		
Primary sun sensor	x		
Sun gate detector		x	
Earth detector	x		
Trapped radiation detector	x		
Superstructure	x		
Cable trough		x	
Scan actuator		x	
Canopus sensor and shutter	x		
TV camera	x		
Science cover	x		
Acquisition sensor	x		
Mars gate	x		
Science platform inertial thermal simulator (SPITS)	x		
Separation initiated timer		x	
Separation spring pad		x	

	Thermally Scaled	Mock-up	Not Used
Sun sensors - secondary		x	
Pyrotechnic arming switch		x	
In-flight disconnect		x	
Cosmic ray telescope	x		
Lower thermal shield	x		

A discussion of the details of construction of the TSM and the changes made in the octagonal bus structure to update the bus to simulate flight configuration will be presented in the following sections.

2. Octagonal Bus

The octagonal bus was modified during the Phase III program to account for changes which had been made in the design of Mariner IV. The changes in the TSM Phase II configuration were associated with a new internal power distribution, changing the peripheral thermal shields and increasing the number of louver assemblies from five to six.

The heaters used in the TSM subchassis to simulate the power dissipated by the electronics in the spacecraft were wired so that the internal power could be changed to simulate a "cruise mode" of the spacecraft or a "Mars playback" mode where the internal power is reduced. The detailed power breakdown for the bus for both operational modes is presented in Appendix III.

Figure 33 illustrates the basic bus configuration and the superstructure ring supporting the high gain antenna.

Six of the eight bays (1, 3, 5, 6, 7, and 8) were equipped with scaled thermal control louvers (c.f. Figures 34, 35 and 36). The tem-

peratures at which the louver blades were fully open were adjusted in accordance with Mariner IV specifications. The "full-open" temperature was set at 80F for Bays 7 and 8 and 85F for the remaining bays. Four louver blades were removed from the Bay 6 assembly to simulate the flight assembly. These details are shown in Figure 35. Three blades were removed from the lower right corner and one from the upper left corner.

3. Magnetometer

The flight configuration of the Mariner IV magnetometer comprised a sensor ball, electronic chassis located above and below the sensor ball, and a thermal shield. The hollow sensor ball was 4.350 inches in diameter, and was made from fiberglas, gold plated to have a low emittance. The electronic chassis attached to the top and bottom of the sensor ball were made of 6061-T6 aluminum polished to have a low emittance. The thermal shield consisted of a single aluminum foil to which were attached 10 layers of 1/4 mil aluminized mylar and a single layer of 5 mil aluminized teflon. The teflon layer faced the sun and the entire assembly was thermally isolated from the upper electronics chassis. The shield assembly shaded the upper electronics chassis and a portion of the sensor ball from direct sunlight.

The TSM version of the magnetometer was a 2 inch diameter, 0.032 in. wall thickness, stainless steel ball, which was gold plated to have a low emittance. The electronic chassis, located above and below the sensor ball, were made from 6061-T6 aluminum, chemically polished to obtain a low emittance surface. Instead of using a multi-layered insulation shield, the TSM thermal shield consisted of a single polished aluminum plate thermally isolated from the chassis. A thin teflon sheet was cemented to this shield to provide the same surface emittance as the outer layer of the flight magnetometer shield.

The TSM magnetometer was attached to the low-gain antenna by 1100 aluminum brackets. The magnetometer was isolated from the brackets by use of micarta stand-offs. Four #2-56 screws held the magnetometer.

The magnetometer mounting brackets were attached to the antenna by four aluminum rivets. This construction, from a thermal standpoint, was similar to the method used in supporting the magnetometer to the antenna on the flight configuration.

The magnetometer assembly used on the TSM was not designed by exactly scaling all of the conductive paths on the full-scale version. The approach taken here was to provide a scaled amount of power dissipation, scale the effective radiating area and isolate the magnetometer from the antenna, and use a thermal shield to shadow part of the magnetometer. The effective radiating area was scaled by using the same surface finishes, retaining over-all geometric similarity and scaling down the dimensions by the scaling ratio of 0.43. Similar materials in model and prototype were, in fact, used to fabricate the electronic subchassis. The reasons for this approach stem from the fact that the internal power was small and, therefore, gradients within the structure were judged to be small.

4. Ion Chamber

The ion chamber experiment consists of an electronic chassis, an ion sensor ball, a detector tube and a thermal shield which partially shadows the electronic chassis from direct sunlight. The ion chamber was attached to the low-gain antenna by use of thermal standoffs.

The 5 inch diameter ball of the prototype ion sensor was fabricated from stainless steel and had a wall thickness of 0.010 inches. A black oxide coating was applied to the exterior surface. The temperatures within the ball were judged to be governed by radiative effects rather than conductive effects. Therefore, the ion chamber used on the TSM

was also made from stainless steel (because of availability) with a wall thickness of 0.032 inches.

The prototype GM detector was made from a thin wall stainless tube. A nylon rod with the same paint pattern was used on the TSM.

The gold plated prototype electronics chassis was made from ZK 60 T-5 magnesium (k = 1.21 watts/cm-K), while the model chassis was fabricated from 1015 steel (k = 0.64 watts/cm-K). The wall thicknesses were 0.062 in. and 0.031 in. for the prototype and model. In this case, the thermal scaling laws were not strictly adhered to since the wall thickness was reduced by 0.5 rather than 0.43 and the ratio of conductivities was 0.53 instead of 0.43. It was believed that these differences would not appreciably change the temperature distributions.

The prototype thermal shield consisted of a 1/4-inch thick, aluminum honeycomb. The top surface was painted and the bottom surface polished to have a low emittance. A 1/8-inch micarta shield, painted in the same fashion, was used on the TSM. A 1/4-mil aluminized mylar sheet was cemented to the bottom to produce a low emittance surface.

5. Low-Gain Antenna

The prototype low-gain antenna was a 3.875 inch ID, 6061-T6 aluminum alloy tube, with a .025 inch wall thickness. The ground plane, magnetometer and ion chamber were attached to the antenna. The external surface of the antenna was highly polished (mirror-like finish) in order to obtain a low emittance surface. The lower end of the antenna was riveted to a ring and bolted to the bus. Two support rods were used to stabilize the antenna. One of these support rods was attached to the

bus and the other to the superstructure ring. These support rods are identified as the short and long dampers for the low-gain antenna. One damper was black anodized, the other was painted. The prototype ground plane was a 1/4-inch aluminun honeycomb ring, 7 inches in diameter. The top and sides were painted, the bottom surface was polished aluminum.

Due to the fact that the ion chamber and magnetometer assemblies were thermally isolated from the antenna, their temperatures are not significantly influenced by the antenna temperature. In addition, the heat loss from the bus via the shaded antenna was conservatively calculated to be small with respect to the total internal power dissipated within the spacecraft. This calculation is presented in Appendix IV. Therefore, the TSM antenna was designed to simulate rather than exactly scale the temperature distributions in the prototype.

The TSM antenna was fabricated from a 1.75 inch OD aluminum tube having a wall thickness of 0.022 inch. The exterior surface was polished to have essentially the same emittance as the prototype. The TSM ground plane was made from 1/8-inch thick micarta, and painted with the same paints as used on the prototype. The two dampers used to support the antenna on the TSM were made from 1/4-inch diameter fiberglas rod. They were also painted to have the same surface characteristics as the prototype.

6. High-Gain Antenna

The temperature of the high-gain antenna does not significantly influence other temperatures within the spacecraft since it is supported by a structure of low conductance. Of more importance was the shadow

pattern cast by the antenna on the spacecraft bus. Therefore, the over-all shape of the prototype antenna was scaled so that the shadow patterns would be similar in model and prototype. The TSM antenna was made from 1/8-inch thick aluminum, the prototype antenna was fabricated from aluminum honeycomb. Identical surface finishes were used in model and prototype.

The antenna feed was more or less mocked-up from the prototype. Conductive paths were not scaled, but the surface finishes and over-all geometry were made similar.

7. Cosmic Dust Detector

The prototype cosmic dust detector consisted of a rectangular, magnesium sensing plate (with a vacuum deposited aluminum outer surface) which protruded from the upper thermal shield. An electronic subchassis was attached to the sensing plate below the thermal shield. The entire assembly was supported by the superstructure.

The TSM sensing plate for the detector was fabricated from aluminum, polished to have a low emittance, with a wall thickness of 0.032 inches. Calculations showed that the temperature gradients in the sensing plate would be small and that the total heat leak from the plate would be small because of its low surface emittance. For these reasons, the conductive paths were not scaled exactly; however, the proper area and a low surface emittance were used on the modeled version of the detector.

8. Sun Sensors

The sun sensors on the prototype are mounted to pedestals which, in turn, are attached to the spacecraft bus by three #6-32 bolts. No provisions were made for thermally isolating the sensors or pedestals. The

sensor pedestals were made from ZK 60 magnesium, gold plated on the outside to have a low emittance.

The design of the TSM sun sensor assembly was based on the fact that the heat flow through the pedestal walls would influence the temperature of the sensor and the heat flow into or out of the bus. The same paint patterns and surface finishes were used in model and prototype and the conductive paths in pedestal were scaled as follows.

The heat flow paths in the pedestal were two-dimensional and, therefore, the wall thicknesses can be distorted to obtain the proper scaled conductive paths. Equation 3 requires that the ratio of conductivities of model and prototype be equal to the geometric scaling ratio. However, for one or two-dimensional heat flow patterns, it is only necessary to make the conductances scale in model and prototype for identical temperature distributions. The relationship is

$$k_m \delta_m = k_p \delta_p R^2 \qquad (3a)$$

where

k - thermal conductivity
δ - wall thickness
R - geometric scale factor
p - prototype
m - model

Thus, the product of conductivity and wall thickness must be scaled for thermal similitude. It was desired to use a reasonably thick wall section (for fabrication purposes) of low conductivity such as 410 stainless steel.

The required wall thickness of the model pedestal is given by:

$$\delta_m = \delta_p \frac{k_p}{k_m} R^2$$

Inserting the following numerical values

$R = 0.43$ - the scale ratio

$k_p = 1.20$ watts/cm-K (ZK 60 mag.)

$k_m = 0.27$ watts/cm-K (410 S.S.)

$\delta_p = 0.040$ in.

we find that

$$\delta_m = 0.032 \text{ inches.}$$

The actual fabrication was made with 20 gauge material with a thickness of 0.036 inches.

The previous calculation illustrates the fact that where the heat flow patterns are not three-dimensional, a combination of selecting a material and convenient wall thickness can be used to produce modeled sections of approximately the right conductance.

The sensors which were mounted on the pedestals were machined from aluminum in the TSM. Because of their small size and short path lengths for heat flow, it was judged that only a small temperature gradient could exist. The surface finishes and over-all geometry were made similar in model and prototype.

9. Trapped Radiation Detector

The chassis of the prototype detector was fabricated from AZ31B magnesium alloy with a thickness of approximately 0.030 inches. Four

detector tubes mounted on the chassis were thermally coupled to the chassis by use of indium foil washers. The chassis was thermally isolated from the frame of the spacecraft by insulating washers at the four bolting points.

The TSM chassis was fabricated from 0.030 inch thick 304 stainless steel and micarta washers were used to thermally isolate the chassis from the bus. Indium foil gaskets were used at the joint between the detector tubes and chassis. Identical paint and surface finishes were used in model and prototype.

10. Absorptivity Standard and Plasma Probe

These instruments were both conductively isolated from the spacecraft bus by use of insulating washers and the upper thermal shield prevented radiation transfer from these instruments to the spacecraft bus. Thus, their temperatures were not important to the over-all temperature level of the spacecraft.

The absorptivity standard used on the TSM was a mock-up. The over-all geometry was scaled; however, no attempt was made to scale the conductive paths within the instrument. The plasma probe used on the TSM was geometrically scaled and similar paint patterns were used on model and prototype.

11. Insulation and Shielding

The lower thermal shield of the prototype consisted of 20 layers of 1/4-mil thick aluminized mylar and two layers of 1-mil aluminized teflon. The 20 layers of aluminized mylar were placed between the two layers of aluminized teflon. In both cases, the teflon sheets faced outward.

Lightweight aluminum angles were sewn to the insulation and bolted to the spacecraft frame to support the assembly.

It was estimated that the heat flow through the lower shield was small with respect to that dissipated by the louver assemblies. On the reduced scale TSM version, only five layers of aluminized mylar were used. The reduction in the number of layers was based on previous experience which has shown that it is possible to increase the heat leak in small packages because the proportions of exposed edges and seams increase with respect to the total area as the size is reduced.

The upper thermal shield used on the prototype was composed of 30 layers of 1/4-mil thick aluminized mylar, a layer of 1-mil aluminized teflon, and a layer of 5-mil thick black dacron. The outer surface of the upper thermal shield was black dacron, and to this was sewn 30 layers of aluminized mylar and a layer of aluminized teflon.

The TSM upper thermal shield was composed of one layer of 5-mil black dacron and five layers of 1/4-mil aluminized mylar. This assembly was sewn together with the black dacron material facing outward.

Portions of the eight bays on the bus were shielded by use of thin (0.010 inch) polished aluminum shields having a low emittance. These peripheral shields were used at the edges of the louver assemblies and on the corners of the octagonal bus. Bay 4 was entirely shielded with a peripheral shield (c.f. Figure 35). The prototype thermal shields were thermally shorted at the attachment points. The TSM peripheral shields were also made of polished aluminum approximately 0.010 inches thick and they were thermally shorted to the bus structure. The louver

assemblies have a high effective radiating area by comparison to the effective radiating area of the shields; and, therefore, the degree to which conductive paths in the shields or emittances are scaled is relatively unimportant as long as the emittance is reasonably low. In order to preserve the low emittance in model and prototype, it was decided to use similar materials in both.

12. Solar Panels

In the solar simulation tests of the TSM, the solar beam was not large enough to completely illuminate the four solar panels. Therefore, the incident solar flux which would normally be absorbed was simulated by use of heaters attached to the bottom of each solar panel.

As shown in Figures 25 and 28, the geometry of the TSM solar panels was distorted. In the flight spacecraft, the temperatures of the outboard sections of the solar panels do not influence the spacecraft temperatures because the radiant interchange view factor becomes extremely small. The widths of the TSM panels were geometrically scaled from the prototype. The length was chosen on the basis of radiant interchange. At the extreme outboard edge of the TSM panel, the view factor to the spacecraft bus was calculated to be of the order of 2 percent, whereas the view factor at the inboard edge is approximately 50 percent.

The conductive paths in the TSM solar panels were not scaled from the prototype except that similar mounting arrangements, reduced in scale, were used to support the panels at the spacecraft bus. The reason that conductive paths were not scaled is that the solar flux which is uniformly absorbed on the panels is large with respect to the flux emanating from the spacecraft. The temperature gradients in the panels are, therefore, small.

The heaters used to provide the proper boundary temperatures on the TSM solar panels were designed to have a uniform spatial power dissipation. Data on the effective solar absorptance of a prototype panel was used to calculate the power to be dissipated in each of the four solar panel heaters for the TSM tests in which the solar panels were not illuminated.

13. Planetary Science

The planetary science instruments consist of a TV camera, Mars gate, acquisition sensor, SPITS, and a movable science cover. This equipment is extremely complex and the design of the TSM version was primarily based on an attempt to reproduce, in scaled fashion, the effective radiating area of the entire system. Thus, the heat leak from the spacecraft bus would be scaled.

The science equipment, being on the shaded side of the bus, radiates to the outer space environment and is radiatively coupled by high emittance surfaces to the interior of the bus above the lower thermal shield. Some conductive coupling to the bus is made via the rotating support structure.

The TSM version of these instruments was considerably simplified in detail; however, the over-all dimensions and surface emittances were properly scaled.

14. Canopus Tracker

The prototype canopus tracker consisted of an internal chassis to which the electronics, light baffles, and detector were attached. The structure was made of 6061 aluminum approximately 0.050 inches thick

and was bolted to the lower frame of the bus without any thermal isolation by four #8-32 screws. An 0.020 inch thick polished aluminum thermal shield was bolted to the chassis. Electrical connections between the canopus tracker and the interior of the bus were made by an electrical connector and cable assembly.

A view of the interior of the scaled TSM canopus tracker and thermal shield is shown in Figure 40. The chassis was scaled (c.f. Equation 3a) by use of 0.029 inch thick 1018 steel. Four #6-32 screws were used for mounting. The thermal shield was not conductively scaled. It was fabricated from 0.020 inch thick polished aluminum, and bolted directly to the chassis. The aperture size was scaled and the interior surface finishes were identical in model and prototype.

15. Surface Finishes

Since it was desired to have identical surface properties in model and prototype, the various paint patterns used on the flight version were reproduced in the model. Because space does not permit listing all of the paint patterns in detail, the characteristics of the thermal control surfaces are summarized in Appendix V for each of the appendages.

B. Test Facility

The solar simulation tests of the Phase III TSM configuration were conducted in the NASA Lewis Research Center Solar Simulator. A schematic drawing of this facility is shown in Figure 37.

The working space is approximately 6 feet in diameter and 10 feet in length. The inner shroud is coated to have a high infrared emittance and solar absorptance and was cooled to liquid nitrogen temperature for the TSM tests. (The facility does have provisions for cooling the shroud to near liquid helium temperatures; however, this feature was not used in the TSM tests.) During all tests of the TSM the pressures with the test chamber were maintained below 10^{-6} torr.

A modified Genarco ME-6, 28 KW, Carbon Arc Lamp is used as an energy source. Various diaphragms and a set of fused quartz absorbing plates are used to control the intensity of the simulated solar radiation at the test plane.

The radiation enters the optical tower via a system of condenser lenses, a flat mirror and a small field lens mounted in the side of the optical tower. A spherical collimator of 15 foot focal length is used to direct the radiation through a 36 inch diameter fused quartz lens, which is mounted approximately 12 feet above the test plane. The optical tower is evacuated during operation to minimize the required thickness of the large quartz window, to minimize the absorption in the optical path and to keep the large optical elements clean.

The intensity of the simulated beam is measured and continuously monitored during testing by use of three water-cooled Hy-Cal Engineering

Co. calorimeters mounted on a 20 inch diameter circle in a plane approximately six feet above the test plane. The Hy-Cal detectors were calibrated before and after the TSM tests by NASA Lewis personnel. The stated[1] accuracy of the solar intensity measurements was ± 5 percent.

The collimation of the solar simulator beam in the NASA Lewis Simulator is reported[2] to be less than 2 degrees. The uniformity of the beam varies over the test plane. In three of the four quadrants, the uniformity of illumination is reported[3] to be within approximately ± 5 percent over a 22 inch diameter. The intensity in one quadrant falls off by approximately 20 percent at a diameter of 20 inches due to the "tail flame" formation in the arc lamp source.

A diagram showing the solar illumination pattern of the TSM during the tests at NASA Lewis is presented in Figure 38. The location of the circle of illumination with respect to the model is shown in Figure 13 with the shadow pattern of the intensity sensors. It can be seen that the illumination pattern was slightly de-centered with respect to the spacecraft and that the shadow of one of the intensity sensors (viz., sensor #1) fell on the exposed area of the Trapped Radiation Detector. This situation was unavoidable since it was desired to have the low-gain antenna located between sensors #1 and #2--where the intensity of the beam was most uniform--and major modifications to the support system were required to relocate the sensors.

---

1. Sommers, R., NASA Lewis Research Center, Personal Communication, June 15, 1965.
2. Uguccini, Orlando W., and Pollack, John L., "A Carbon-Arc Solar Simulator," Paper 62-WA-241, ASME, 1962.
3. Mark, H., NASA Lewis Research Center, Personal Communication, April 27, 1965.

During the test program, the desired solar intensity was set by taking the average readings of the solar intensities as measured by the #1 and #2 Hy-Cal sensors. The simulated solar intensities were varied by inserting various numbers of fused quartz absorbing plates in the beam at the carbon arc lamp. During the TSM tests, the simulated solar intensity was varied from a maximum of 0.091 watts/cm^2 (65.5 percent of one solar constant) to a minimum of approximately 0.059 watts/cm^2 (42 percent of one solar constant) to simulate a range of flight intensities.

C. Test Procedures

1. Description of Tests

The basic objective of the Phase III test program was to compare the measured TSM temperatures with flight data obtained from the Mariner IV at two solar intensity levels with a constant internal power dissipation. These two tests were chosen to simulate the "cruise" conditions of the spacecraft where the internal power dissipation is relatively high. A third test was chosen to simulate a "Mars Playback" mode where the internal power dissipation in the spacecraft is relatively low.

The first test of the TSM was completed with a simulated solar intensity equal to 65.5 percent of one solar constant (0.091 watts/cm^2 or 288.3 Btu/hr-ft^2). This test is identified with an "Earth Cruise" operating mode. This simulated solar intensity corresponds to the solar intensity incident upon the Mariner IV, 98 flight days from launch. The power dissipation in the TSM was adjusted to simulate the cruise mode of the Mariner IV with the cruise science and TWT "on", and the cavity amplifier and battery charger "off."

The second test of the TSM was completed at a simulated solar intensity equal to 45.5 percent of one solar constant (0.063 watts/cm^2 or 199.6 Btu/hr-ft^2). This test is identified with a "Mars Cruise" operating mode. The simulated solar intensity corresponds to 180 flight days. Both the "Earch Cruise" and "Mars Cruise" TSM tests were completed with the same internal power dissipation.

The third test of the TSM was completed at a simulated solar intensity equal to 42 percent of one solar constant (0.059 watts/cm^2 or

186.9 Btu/hr-ft^2). This test is identified with a "Mars Playback" operating mode. The simulated solar intensity corresponds to the actual intensity at 234 flight days. In the Mars Playback simulation, the internal power dissipated within the TSM was adjusted to simulate the changes that occur in the Mariner power dissipation. The total internal power dissipation in the bus of the Mariner decreases from approximately 149 watts to 137.5 watts in switching from the "Cruise" to "Playback" modes. In addition, in the "Playback" mode no power is dissipated in the magnetometer, ion chamber, cosmic dust and trapped radiation detectors, the cosmic ray telescope and television assembly.

A fourth test of the TSM was completed to determine the influence of the temperatures of the simulated solar panels on the bus temperatures of the TSM. With the TSM operating in a "Mars Playback" mode, the input power to the mocked-up solar panels was increased to arbitrarily raise their temperature by approximately 20F.

The four tests of the TSM were completed in succession without removing the TSM from the simulator. The time required to complete the four tests (from pre-cooling of the chamber to removal of the model) was approximately 72 hours; however, a considerable fraction of this time was used in obtaining the proper simulated solar intensity. During the tests, it was found that the TSM would reach thermal equilibrium within a maximum time of approximately 5 hours provided that the solar simulator could be held at a constant intensity for this period.

2. Test Measurements

Power was supplied to the TSM by use of a 300 volt DC power supply with 0.007 percent regulation. The individual heaters used within the

TSM were precision wire-wound power resistors. Power measurements were made by current and resistance measurements. It was estimated that the total power measurements were accurate to within 0.09 percent. An auxiliary 36 volt DC, voltage regulated power supply was used to supply power to the solar panel mock-ups.

The total power dissipated in the TSM was 27.616 watts for the Earth and Mars cruise modes and 25.269 watts for the Mars Playback mode. The total power dissipated within the mocked-up solar panels was as follows:

Earth Cruise	329.06 watts
Mars Cruise	199.08 watts
Mars Playback	183.25 watts

Temperature measurements were made at 75 locations within the TSM. Twenty of the 75 temperature sensors in the TSM were located at points corresponding to the locations of the temperature sensors used in the Mariner IV spacecraft for data transmission.

The TSM temperatures were measured by use of calibrated, matched thermistors. The entire lot of thermistors had resistance vs. temperature characteristics such that any single thermistor would have an error of less than $\pm$ 1/2 F over the temperature range of 32 to 200 F when a single resistance vs. temperature curve was used. Calibrations were made by the vendor to establish the resistance vs. temperature curve and three point calibrations of each thermistor were made by Arthur D. Little, Inc., as acceptance tests.

A constant current of 30 microamps was supplied to the thermistors. The voltages were read on a digital voltmeter. The voltages were trans-

lated to temperature by use of a digital computer data reduction program. It was estimated that the total system error in measuring the temperatures was of the order of $\pm$ 1/2 F in the range of 32 to 200 F. Below 32 F the accuracy of the measurements decreases. At temperatures in the range of -20 F the accuracy is estimated to be $\pm$ 5F.

The temperatures of the TSM were recorded at approximately half-hour intervals until the TSM approached thermal equilibrium. Readings were then taken at 15 minute intervals until the largest temperature change over several consecutive readings was of the order of 1/2 F, and the changes in temperature were random.

D. Test Results

Tables 10, 11 and 12 list the measured TSM temperatures and the flight temperatures of Mariner IV as recorded by Jet Propulsion Laboratory.

The "Earth Cruise" temperatures measured for the TSM are in remarkably good agreement with flight data with several exceptions. The trapped radiation detector temperature was over 20F lower than the flight measurement. The temperature predictions for the bus were also in good agreement with flight results with the exception of the lower ring at the Canopus mount on Bay 8 and the bottom of the attitude control N_2 tank also located in the vicinity of Bay 8. The TSM temperature predictions for the Canopus tracker showed poor agreement with flight results while the TV camera and SPITS (Science Platform Inertial Thermal Simulator) showed good agreement.

The data for the "Mars Cruise" mode are presented in Table 11. A comparison of the data for the Earth and Mars Cruise modes shows that the entire temperature level of the spacecraft decreases appreciably with a decrease in the solar intensity. The temperature drop of the isolated sunlit appendages is approximately 30F. The thermal control action of the louver assemblies and the relatively high internal power dissipated within the bus reduces the temperature drop in the bus to less than 10F.

The largest errors in the temperature predictions for both the Earth Cruise and Mars Cruise modes occur at the same locations; and, in general, the TSM operated at a lower temperature level than Mariner IV.

The temperature comparisons for the "Mars Playback" mode are presented in Table 12. The data in Table 12 show that the temperature level of the spacecraft decreases from the Mars Cruise mode due to the internal power reduction and the decrease in solar intensity. The temperature changes of the magnetometer and ion chamber, as observed in the TSM tests, are seen to be -21 and -12.6F, respectively. The remainder of the TSM changes by 10 to 20F. The accuracy of these predicted Mariner temperatures was estimated by JPL[1] to be ± 10F for the magnetometer, ± 5F for the ion chamber, and ± 3F for the remainder. The predictions for the magnetometer in the Playback mode are in poorer agreement with the flight results than in the Earth or Mars Cruise modes. The error in the Canopus Tracker remains essentially constant. The accuracy of the bus temperature predictions are also poorer in the Playback mode.

A comparison of the measured solar panel temperatures for the Mariner and the TSM is presented below for the three tests.

	Earth Cruise	Mars Cruise	Mars Playback
Average TSM Solar Panel Temperature	96F	43	29
Mariner Solar Panel Temperature	69F	22	9

The differences between the predicted and measured temperatures occur because of the uncertainties involved in calculating the power which should have been dissipated in the mocked-up solar panels of the TSM, and the spillover of the simulated solar beam on the TSM panels during the tests.

1. Lucas, J. W., Jet Propulsion Laboratory, Personal Communication, 2 July 1965.

Table 13 summarizes the results of two tests made with the TSM to determine the influence of solar panel temperature on the internal temperatures of the bus. In both tests, the TSM power dissipation in the bus was maintained constant. The data indicate that a 20F temperature change in the solar panel temperature changes the average internal bus temperatures by approximately 2F.

Complete sets of temperature data for the four tests completed with the TSM are presented in Tables 14, 15, 16, and 17. The first five columns are channel identifications for the TSM, the full-scale TCM and the MC-3 (Mariner IV) spacecraft thermocouple and telemetry channels. The measured TSM temperatures are listed in columns 6 and 7.

E. Discussion of Temperature Predictions

1. Sunlit Appendages

The temperature predictions for the ion chamber and magnetometer for the "Earth Cruise" and "Mars Cruise" modes were extremely good. The error was less than 6F at "Earth Cruise" and less than 13F at "Mars Cruise." For these appendages whose temperatures are to a large extent controlled by the solar intensity, the predictions are close to the limit of experimental accuracy.

Temperature comparisons for the "Mars Playback" mode--where the internal power dissipated in the magnetometer and ion chamber is switched off--show that both TSM appendages were considerably higher in temperature than the predicted flight temperature. The errors were approximately 8F for the ion chamber and 27F for the magnetometer. An error analysis of these sunlit appendages is presented in Appendix VI. The results of this analysis show that an uncertainty of $\pm$ 5 percent in the simulated solar intensity would alone account for errors of $\pm$ 5F in the temperatures of these components. Other factors which must be considered are the uncertainty intervals in the measured flight and test temperatures.

The TSM temperature predictions for the Trapped Radiation Detector were of questionable value. The TSM was installed in the NASA Lewis Space Simulator in such a location that the area of the solar beam with the best uniformity would fall upon the ion chamber and magnetometer which were the two sunlit items of most importance to this modeling study. Unfortunately, a shadow of one of the Hy-Cal intensity sensors

(mounted above the model) was cast on the exposed area and on the shield covering the trapped radiation detector. This shadow pattern, shown in Figure 38, could not be rearranged without major modifications to the support ring and Hy-Cal water cooling lines and it was decided to accent the errors which would be introduced by the shadow. In each of the three tests, the detector temperature was 20 to 30F below the flight temperature. Although it is anticipated that a significant fraction of the error was introduced by the shadow pattern, further tests would be required to determine the magnitude of the uncertainty.

2. Internal Bus Locations

In general, the TSM predictions for the bus temperatures were sufficiently accurate for engineering purposes with the exception of the Bay 8 lower ring above the Canopus tracker, and the bottom of the N_2 sphere also located in the vicinity of Bay 8. Comparing the three tests, it can be seen that the bus temperature prediction errors tend to increase as the absolute temperature level of the spacecraft decreases, and the TSM bus is lower in temperature than the flight spacecraft. At the Mars Cruise and Mars Playback modes, all of the bays except 6 and 8 are at a sufficiently low temperature to force the thermal control louvers closed. In this situation, the interior bus temperatures are highly dependent upon the heat leakage in the louvers and the gaps around the peripheral thermal shields. Small differences in the power dissipated by the louver assemblies in the closed position produce rather large uncertainties in temperature. For example, in a typical set of fully-closed TSM louvers, a heat leak of 100 milliwatts will produce a temperature change of 10F.

The temperature comparisons of flight and TSM data also show that the Bay 6 TSM temperature was approximately 12F higher than the corresponding flight data at "Earth Cruise." This difference is attributed to errors in the thermal performance of the scaled TSM louver assemblies. In this particular bay, four of the louver blades are removed so that approximately 20 percent of the effective reradiating area of the shear web is unaffected by the position of the louver blades. In previous tests of the TSM louver assemblies (c.f. Figure 21), it was shown that the thermal performance of the half-scale louver assemblies did not exactly correlate, on a scaled basis, the measured performance of a full-scale assembly. The test results showed that an error of 5 percent in the effective reradiating area of the louver assemblies would produce an error of approximately 7F in the average bay temperature with the louver blades wide open. Non-scaled areas and differences in the emittances of the shear web between model and prototype could easily account for an error of 5 to 10 percent in the reradiating area.

The uncertainty in the average bus temperature due to the errors in simulating the thermal boundary conditions for the solar panels is less than 2F.

The TSM lower ring and N_2 tank temperatures were 30F below the temperatures measured for the flight spacecraft (c.f. channels 430 and 218 in Table 10). Also the complete temperature results of the TSM listed in Table 14 show that the temperature difference between the top and bottom (near the lower ring) of Bay 8 was approximately 20F. Previous Phase II thermal tests of the bus, with the same internal power dissipation, showed that the temperature difference was less than 5F.

The N_2 tank is radiatively coupled to the lower thermal shield and, therefore, its temperature is sensitive to changes in the heat flux through the lower thermal shield. Previous Phase II tests of the bus with a similar lower thermal shield showed that the temperature of the same N_2 tank was approximately equal to the average Bay 8 temperature. In these Phase III tests, its temperature was considerably below the average Bay 8 temperature.

The temperature prediction errors associated with the lower ring (frame) and the bottom of the N_2 bottle, both in Bay 8, are traceable, in part, to heat leaks in the lower thermal shield. During transportation of the model to NASA Lewis, a large electrical connector worked loose within the model and completely punctured the lower thermal shield in the vicinity of Bay 8. Due to scheduling problems, a new thermal shield could not be fitted, and it was necessary to repair the damaged shield by interleaving additional layers of aluminized mylar between the torn segments. Thermal short circuits resulting from these repairs undoubtedly affected the efficiency of the super-insulation blanket.

In addition, it is noted that the temperature predictions for the Canopus tracker were in error. It will be shown in a following section that the power radiated from the Canopus tracker was excessive and, therefore, this additional heat leak influenced the frame (lower ring) and Bay 8 temperature predictions. Unfortunately, it is difficult analytically to compute the relative importance of the damaged lower thermal shield or the increased heat leak from the Canopus tracker on the internal bus temperatures. However, the results of a simplified

error analysis of the TSM Canopus tracker thermal performance show that the error in the average TSM bus temperature was of the order of 6F due to the increased heat leak from the Canopus tracker.

3. Shaded Appendages

The TSM temperature predictions for the TV camera and SPITS were accurate to within approximately 10F for all tests. The predictions for the Canopus tracker were, however, in error by 50 to 60F.

The temperature of the Canopus tracker (c.f. Figure 40) is controlled by its internal power dissipation, the rate of heat flow through the joint where four bolts are used to attach the appendage to the lower frame, and its effective radiating area.

The temperature difference across the bolted joint can be obtained by comparing the measurement channels 430 and 410 in Table 10. For the TSM, the temperature difference across the joint was approximately 30F whereas the measured temperature difference across the joint in Mariner IV was only 5F. Several effects could produce this situation. If the internal power dissipation in the TSM Canopus tracker was incorrectly scaled, the temperature could be in error. A check of the heater circuit showed that the power was correctly modeled and that the power was dissipated during the testing. An improperly scaled joint with a high thermal resistance would increase the temperature difference across the joint. Finally, if the TSM version of the Canopus tracker were to have an effective radiating area larger than that predicted by the scaling laws, the temperature difference across the joint would increase due to the increased heat flow rate and the temperature of the Canopus would be too low. An error in the effective

radiating area could be caused by differences in the emittance or effective shielding factor of the thermal shield between the TSM and Mariner IV. Furthermore, a non-scaled power dissipation would influence the temperatures of the lower ring of the bus.

After completing the solar simulation tests, the TSM Canopus tracker was removed from the bus and a number of tests were completed to determine the cause of the error in the TSM temperature predictions. The tracker was mounted on a heated plate whose temperature could be varied to simulate the lower ring temperature. Super-insulation was placed between the Canopus tracker and the plate (except for the mounting bolt penetrations) to simulate the effect of the lower thermal shield. The unit was tested in a small, cold-wall, vacuum chamber. The test results are presented in Appendix VII.

The first two tests were run with the Canopus tracker in its original test condition to verify that the temperatures measured in the solar simulation tests could be reproduced in the small test chamber. The third test was made to determine the influence of bolt torque, and, therefore, the joint conductance, on the temperature difference across the joint. The results of this test showed that increasing the bolt torque by a factor of three decreased the temperature difference by approximately 8F. However, the temperature difference was still in error by 20 to 25F. A fourth test was run to determine the influence of adding additional light baffles in the aperture of the Canopus tracker since in the design of the scaled version four baffles used in the prototype configuration were eliminated. This change did not influence the temperatures. A final test was conducted

to determine whether or not the shielding on the Canopus tracker was effective. Two layers of 1/4-mil aluminized mylar super-insulation were applied to the exterior surface except for the aperture. The results of this test showed that the addition of the insulation decreased the temperature drop to 2F which was approximately the temperature difference as measured in Mariner IV.

The test results showed that the errors in the Canopus tracker temperature predictions were caused by a combination of errors in modeling the joint conductance and the effective radiating area of the thermal shield surrounding the chassis. The non-scaled radiating area effect was dominant. The error in the effective radiating area could have been produced by scaling errors in: 1) the emittance of the thermal shield; 2) the conductive paths in the shield; and 3) the areas of exposed gaps between the edges of the thermal shields. Because of time limitations the actual source of this error was not determined by further tests. However, it is anticipated that Jet Propulsion Laboratory will make further tests to determine the source of the uncertainty.

A summary of the test data on the Canopus tracker and an analysis of the uncertainties is presented in Appendix VII.

TABLE 1

SUMMARY OF PHASE II TEST CONDITIONS

	Test 1	Test 2	Test 3	Test 3A	Test 4
Power (watts)					
TCM Bus	147.37	147.37	147.37	-	-
TCM Hat	23.6	264.0	50.2	-	-
TCM TOTAL	170.97	411.37	197.57		
TSM Bus	27.21	27.21	27.21	27.21	27.21
TSM Hat	4.36	48.81	9.28	9.28	9.28
TSM TOTAL	31.57	76.02	36.49	36.49	36.49
Louver Positions					
Bay 1	Free	Free	Caged Open	Caged Open	Caged Open
Bay 3	Free	Free	Caged Open	Caged Open	Caged Open
Bay 4	Free	Free	Caged Closed	Caged Closed	Caged Closed
Bay 7	Free	Free	Caged Closed	Caged Closed	Caged Closed
Bay 8	Free	Free	Caged Closed	Caged Closed	Caged Closed

TABLE 2

COMPARISON OF TEMPERATURE RESULTS--TEST 1, PHASE II

JPL TC NO.	BAY NO.	LOCATION	TSM (ADL) T_m (°F)	TCM (JPL) T_p (°F)	$T_m - T_p$
242	-	Bus Tube, Bottom	72.8	78.0	- 5.2
243	-	Bus Tube, Top	73.0	78.0	- 5.0
245	4	N_2 Bottle, Top	73.2	79.0	- 5.8
246	8	N_2 Bottle, Bottom	73.1	77.0	- 3.9
248	1	4A15	83.6	84.0	- 0.4
249	1	Chassis, 4A15	73.5	77.0	- 3.5
250	1	4A13	83.6	81.0	2.6
303	1	4A17	67.7	68.0	- 0.3
305	2	Nozzle Throat	49.5	18.0	31.5
306	2	Jet Vane Ring	40.0	57.0	-17.0
307	2	Prop. Tank	65.5	71.0	- 5.5
309	2	Umbilical	15.4	3.0	12.4
310	2	Shear Plate	58.1	59.0	- 0.9
311	3	33A2	70.7	80.0	- 9.3
316	3	32A4	70.2	81.0	-10.8
322	3	Chassis C/L Top	65.2	71.0	- 5.8
323	3	Chassis C/L Center	63.8	70.0	- 6.2
324	3	Chassis C/L Bottom	61.9	-	-
329	4	6A13	82.2	77.0	5.2
330	4	Chassis, 6A13	75.1	74.0	1.1
332	4	6A9	68.1	63.0	5.1
333	4	Flight	70.8	76.0	- 5.2
336	5	2TR1	80.3	86.0	- 5.7
337	5	2RA1	83.7	86.0	2.3
340	5	Chassis C/L Top	76.6	81.5	- 4.9
341	5	Chassis C/L Center	77.9	82.0	- 4.1
342	5	Chassis C/L Bottom	77.0	81.5	- 4.5
345	6	2PA1 Case	101.0	110.5	- 9.5
347	6	Chassis, 2PA1	84.4	93.0	- 8.6
348	6	2PS1	108.0	108.5	- 0.5
349	6	Chassis, 2PS1	82.1	80.0	2.1
350	6	2RE1	91.2	87.5	3.7
401	6	Chassis C/L Top	83.0	84.0	- 1.0
402	6	Chassis C/L Center	79.8	79.0	0.8
403	6	Chassis C/L Bottom	83.4	87.5	- 4.1
406	7	7A1	77.7	72.5	5.2
412	7	7A2	66.2	66.5	- 0.3
415	7	5A8	73.5	72.0	1.5
418	7	Flight	67.1	66.5	0.6
419	8	Diodes, Upper	73.1	66.5	6.6
420	8	Diodes, Lower	70.1	64.5	5.6
422	8	Booster, Upper	93.8	91.5	2.3
423	8	C/L Top	69.2	67.5	1.7
425	8	C/L Bottom	67.6	64.5	3.1
426	8	Battery Cover	72.1	71.5	0.6
451	-	Hat, Center	76.2	83.0	- 6.8

TABLE 3

COMPARISON OF TEMPERATURE RESULTS--TEST 2, PHASE II

JPL TC NO.	BAY NO.	LOCATION	TSM (ADL) T_m (°F)	TCM (JPL) T_p (°F)	$T_m - T_p$
242	-	Bus Tube, Bottom	145.1	160.0	- 14.9
243	-	Bus Tube, Top	139.1	151.0	- 11.9
245	4	N_2 Bottle, Top	147.8	159.0	- 11.2
246	8	N_2 Bottle, Bottom	126.7	143.0	- 16.3
248	1	4A15	104.2	111.0	- 6.8
249	1	Chassis, 4A15	96.1	102.5	- 6.4
250	1	4A13	103.4	117.0	- 13.6
303	1	4A17	91.5	97.5	- 6.0
305	2	Nozzle Throat	95.3	64.0	31.3
306	2	Jet Vane Ring	83.8	109.5	- 25.7
307	2	Prop. Tank	120.0	134.0	- 14.0
309	2	Umbilical	45.8	32.0	13.8
310	2	Shear Plate	108.2	100.0	8.2
311	3	33A2	107.6	118.0	- 10.4
316	3	32A4	96.1	111.0	- 14.9
322	3	Chassis C/L Top	95.8	101.0	- 5.2
323	3	Chassis C/L Center	85.3	90.0	- 4.7
324	3	Chassis C/L Bottom	85.0	-	-
329	4	6A13	119.7	109.0	10.7
330	4	Chassis, 6A13	110.8	102.5	8.3
332	4	6A9	95.5	84.0	11.5
333	4	Flight	99.2	103.0	- 3.8
336	5	2TR1	138.9	144.0	- 5.1
337	5	2RA1	134.3	138.0	- 3.7
340	5	Chassis C/L Top	133.8	136.0	- 2.2
341	5	Chassis C/L Center	130.1	134.0	- 3.9
342	5	Chassis C/L Bottom	126.3	131.0	- 4.7
345	6	2PA1 Case	144.7	157.0	- 12.3
347	6	Chassis, 2PA1	129.9	141.0	- 11.1
348	6	2PS1	152.6	155.0	- 2.4
349	6	Chassis, 2PS1	126.3	124.0	2.3
350	6	2RE1	133.1	132.0	1.1
401	6	Chassis C/L Top	134.3	135.5	- 1.2
402	6	Chassis C/L Center	123.7	123.5	0.2
403	6	Chassis C/L Bottom	127.9	134.0	- 6.1
406	7	7A1	114.0	112.0	2.0
412	7	7A2	95.0	102.0	- 7.0
415	7	5A8	112.2	112.0	0.2
418	7	Flight	95.4	99.0	- 3.6
419	8	Diodes, Upper	103.7	96.0	7.7
420	8	Diodes, Lower	95.0	93.0	2.0
422	8	Booster, Upper	122.2	118.0	4.2
423	8	C/L Top	99.4	95.0	4.4
425	8	C/L Bottom	89.9	90.5	- 0.6
426	8	Battery Cover	114.0	115.0	- 1.0
451	-	Hat, Center	185.2	214.0	- 28.8

TABLE 4

COMPARISON OF TEMPERATURE RESULTS--TEST 3, PHASE II

JPL TC NO.	BAY NO.	LOCATION	TSM (ADL) T_m (°F)	TCM (JPL) T_p (°F)	$T_m - T_p$
242	-	Bus Tube, Bottom	74.5	80.0	- 5.5
243	-	Bus Tube, Top	73.9	78.5	- 4.6
245	4	N_2 Bottle, Top	74.8	79.5	- 4.7
246	8	N_2 Bottle, Bottom	73.6	77.5	- 3.9
248	1	4A15	63.5	64.5	- 1.0
249	1	Chassis, 4A15	51.9	54.5	- 2.6
250	1	4A13	63.6	62.5	1.1
303	1	4A17	46.4	46.5	- 0.1
305	2	Nozzle Throat	38.1	9.0	29.1
306	2	Jet Vane Ring	29.8	45.5	- 15.7
307	2	Prop. Tank	55.3	60.5	- 5.2
309	2	Umbilical	-0.1	-10.5	10.4
310	2	Shear Plate	45.6	39.5	6.1
311	3	33A2	48.1	55.5	- 7.4
316	3	32A4	45.5	57.5	- 12.0
322	3	Chassis C/L Top	40.9	44.0	- 3.1
323	3	Chassis C/L Center	35.0	37.5	- 2.5
324	3	Chassis C/L Bottom	35.1	-	-
329	4	6A13	82.0	73.5	8.5
330	4	Chassis, 6A13	74.0	69.5	4.5
332	4	6A9	65.2	69.5	- 4.3
333	4	Flight	68.8	71.5	- 2.7
336	5	2TR1	82.9	87.5	- 4.6
337	5	2RA1	85.6	87.5	- 1.9
340	5	Chassis C/L Top	78.6	82.0	- 3.4
341	5	Chassis C/L Center	79.5	82.0	- 2.5
342	5	Chassis C/L Bottom	78.2	81.5	- 3.3
345	6	2PA1 Case	103.8	113.5	- 9.7
347	6	Chassis, 2PA1	87.5	95.5	- 8.0
348	6	2PS1	111.9	112.5	- 0.6
349	6	Chassis, 2PS1	86.9	85.0	1.9
350	6	2RE1	95.7	93.0	2.7
401	6	Chassis C/L Top	87.6	89.0	- 1.4
402	6	Chassis C/L Center	83.8	83.5	0.3
403	6	Chassis C/L Bottom	87.7	91.5	- 3.8
406	7	7A1	88.1	83.5	4.6
412	7	7A2	77.2	79.0	- 1.8
415	7	5A8	86.2	85.5	0.7
418	7	Flight	80.8	81.5	- 0.7
419	8	Diodes, Upper	85.9	80.5	5.4
420	8	Diodes, Lower	82.0	77.5	4.5
422	8	Booster, Upper	98.6	95.5	3.1
423	8	C/L Top	81.2	80.0	1.2
425	8	C/L Bottom	78.1	75.0	3.1
426	8	Battery Cover	77.9	75.5	2.4
451	-	Hat, Center	83.8	94.0	- 10.2

TABLE 5

COMPARISON OF AVERAGE BAY TEMPERATURES
PHASE II

BAY 1

LOUVERED

Internal Power (Earth Cruise) TCM 20.898 watts TSM 3.864 watts

	Test 1	Test 2	Test 3
TCM (JPL)	77.5F	107.0F	57.0F
TSM (ADL)	77.0F	98.8F	56.4F
Error in Model Temperature (%)	-0.093	-1.446	-0.116

BAY 2

POST INJECTION PROPULSION SYSTEM

Internal Power TCM 0.0 watts TSM 0.0 watts

	Test 1	Test 2	Test 3
TCM (JPL)	41.6F	87.9F	28.8F
TSM (ADL)	45.7F	90.6F	33.9F
Error in Model Temperature (%)	+0.817	+0.493	+1.044

BAY 3

LOUVERED

Internal Power (Earth Cruise) TCM 9.118 watts TSM 1.686 watts

	Test 1	Test 2	Test 3
TCM (JPL)	70.8F	96.6F	45.0F
TSM (ADL)	66.4F	93.9F	40.9F
Error in Model Temperature (%)	-0.829	-0.485	-0.811

TABLE 5 (Continued)

BAY 4

LOUVERED

Internal Power (Earth Cruise) TCM 15.036 watts TSM 2.779 watts

	Test 1	Test 2	Test 3
TCM (JPL)	72.5F	99.6F	71.0F
TSM (ADL)	74.1F	106.3F	72.5F
Error in Model Temperature (%)	+0.300	+1.197	+0.282

BAY 5

SHIELDED

Internal Power (Earth Cruise) TCM 6.500 watts TSM 1.202 watts

	Test 1	Test 2	Test 3
TCM (JPL)	83.4F	136.6F	84.1F
TSM (ADL)	79.1F	132.7F	80.9F
Error in Model Temperature (%)	-0.791	-0.654	-0.588

BAY 6

PARTIALLY SHIELDED

Internal Power (Earth Cruise) TCM 56.607 watts TSM 10.466 watts

	Test 1	Test 2	Test 3
TCM (JPL)	91.3F	137.8F	95.4F
TSM (ADL)	89.1F	134.1F	93.1F
Error in Model Temperature (%)	-0.399	-0.619	-0.414

TABLE 5 (Continued)

BAY 7

LOUVERED

Internal Power (Earth Cruise)	TCM 9.615 watts		TSM 1.775 watts
	Test 1	Test 2	Test 3
TCM (JPL)	69.4F	106.3F	82.4F
TSM (ADL)	71.1F	104.2F	83.1F
Error in Model Temperature (%)	+0.321	-0.370	+0.110

BAY 8

LOUVERED

Internal Power (Earth Cruise)	TCM 29.600 watts		TSM 5.473 watts
	Test 1	Test 2	Test 3
TCM (JPL)	71.0F	101.3F	80.7F
TSM (ADL)	74.3F	104.0F	83.9F
Error in Model Temperature (%)	+0.621	+0.481	+0.592

TABLE 6

COMPARISON OF TEMPERATURE DIFFERENCES ACROSS BOLTED JOINTS-PHASE II

Electronic Sub-chassis 4A15

Internal Power	TCM 8.26 watts		TSM 1.527 watts
	Test 1	Test 2	Test 3
Differential Temperature TCM (JPL)	7.0F	8.5F	10.0F
Differential Temperature TSM (ADL)	10.1F	8.1F	11.6F

Electronic Sub-chassis 6A13

Internal Power	TCM 6.70 watts		TSM 1.239 watts
	Test 1	Test 2	Test 3
Differential Temperature TCM (JPL)	3.0F	6.5F	4.0F
Differential Temperature TSM (ADL)	7.1F	8.9F	8.0F

Electronic Sub-chassis 2PA1

Internal Power	TCM 26.8 watts		TSM 4.955 watts
	Test 1	Test 2	Test 3
Differential Temperature TCM (JPL)	17.5F	16F	18F
Differential Temperature TSM (ADL)	16.6F	14.8F	16.3F

Electronic Sub-chassis 2PS1

Internal Power	TCM 20.1 watts		TSM 3.716 watts
	Test 1	Test 2	Test 3
Differential Temperature TCM (JPL)	28.5F	31F	27.5F
Differential Temperature TSM (ADL)	25.9F	26.3F	25.0F

TABLE 7

COMPARISON OF CHASSIS TEMPERATURE RESULTS--TEST 1, PHASE II

JPL TC NO.	BAY NO.	LOCATION	TSM (ADL) T_m (°F)	TCM (JPL) T_p (°F)	$T_m - T_p$
249	1	Chassis 4A15	73.5	77.0	- 3.5
310	2	Shear Plate	58.1	59.0	- 0.9
322	3	Chassis C/L Top	65.2	71.0	- 5.8
323	3	Chassis C/L Center	63.8	70.0	- 6.2
324	3	Chassis C/L Bottom	61.9	-	-
330	4	Chassis 6A13	75.1	74.0	+ 1.1
340	5	Chassis C/L Top	76.6	81.5	- 4.9
341	5	Chassis C/L Center	77.9	82.0	- 4.1
342	5	Chassis C/L Bottom	77.0	81.5	- 4.5
347	6	Chassis 2PA1	84.4	93.0	- 8.6
349	6	Chassis 2PS1	82.1	80.0	+ 2.1
401	6	Chassis C/L Top	83.0	84.0	- 1.0
402	6	Chassis C/L Center	79.8	79.0	+ 0.8
403	6	Chassis C/L Bottom	83.4	87.5	- 4.1
418	7	Flight (Chassis)	67.1	66.5	+ 0.6
423	8	C/L Top	69.2	67.5	+ 1.7
425	8	C/L Bottom	67.6	64.5	+ 3.1

TABLE 8

COMPARISON OF TSM TEMPERATURES--TESTS 3 AND 3A, PHASE II

(Gaps in thermal shields taped in Test 3A.)

JPL TC NO.	BAY NO.	LOCATION	TSM TEMPERATURES (^{o}F) Test 3A	Test 3	Difference
242	-	Bus Tube, Bottom	81.2	74.5	6.7
243	-	Bus Tube, Top	80.5	73.9	6.6
245	4	N_2 Bottle, Top	81.6	74.8	6.8
246	8	N_2 Bottle, Bottom	80.1	73.6	6.5
248	1	4A15	69.6	63.5	6.1
249	1	Chassis, 4A15	58.1	51.9	6.2
250	1	4A13	69.9	63.6	6.3
303	1	4A17	53.1	46.4	6.7
305	2	Nozzle Throat	45.3	38.1	7.2
306	2	Jet Vane Ring	36.6	29.8	6.8
307	2	Prop. Tank	63.2	55.3	7.9
309	2	Umbilical	10.7	- 0.1	10.8
310	2	Shear Plate	53.0	45.6	7.4
311	3	33A2	58.0	48.1	9.9
316	3	32A4	57.2	45.5	11.7
322	3	Chassis C/L Top	51.7	40.9	10.8
323	3	Chassis C/L Center	46.6	35.0	11.6
324	3	Chassis C/L Bottom	45.3	35.1	10.2
329	4	6A13	89.8	82.0	7.8
330	4	Chassis, 6A13	82.0	74.0	8.0
332	4	6A9	73.6	65.2	8.4
333	4	Flight	76.9	68.8	8.1
336	5	2TR1	89.2	82.9	6.3
337	5	2RA1	92.1	85.6	6.5
340	5	Chassis C/L Top	85.3	78.6	6.7
341	5	Chassis C/L Center	86.3	79.5	6.8
342	5	Chassis C/L Bottom	85.1	78.2	6.9
345	6	2PA1 Case	108.7	103.8	4.9
347	6	Chassis, 2PA1	92.8	87.5	5.3
348	6	2PS1	116.8	111.9	4.9
349	6	Chassis, 2PS1	91.9	86.9	5.0
350	6	2RE1	101.0	95.7	5.3
401	6	Chassis C/L Top	92.9	87.6	5.3
402	6	Chassis C/L Center	88.8	83.8	5.0
403	6	Chassis C/L Bottom	93.1	87.7	5.4
406	7	7A1	94.6	88.1	6.5
412	7	7A2	83.8	77.2	6.6
415	7	5A8	92.7	86.2	6.5
418	7	Flight	87.3	80.8	6.5
419	8	Diodes, Upper	92.0	85.9	6.1
420	8	Diodes, Lower	88.1	82.0	6.1
422	8	Booster, Upper	104.1	98.6	5.5
423	8	C/L Top	86.9	81.2	5.7
425	8	C/L Bottom	83.9	78.1	5.8
426	8	Battery Cover	84.1	77.9	6.2

TABLE 9

COMPARISON OF TSM TEMPERATURES--TESTS 3 AND 4, PHASE II
(Modified Bay 6 heater in Test 4.)

JPL TC NO.	BAY NO.	LOCATION	TSM TEMPERATURES (°F) Test 3	Test 4	Difference
242	-	Bus Tube, Bottom	74.5	72.9	1.6
243	-	Bus Tube, Top	73.9	72.3	1.6
245	4	N_2 Bottle, Top	74.8	73.2	1.6
246	8	N_2 Bottle, Bottom	73.6	72.0	1.6
248	1	4A15	63.5	61.9	1.6
249	1	Chassis, 4A15	51.9	50.3	1.6
250	1	4A13	63.6	61.9	1.7
303	1	4A17	46.4	44.6	1.8
305	2	Nozzle Throat	38.1	36.1	2.0
306	2	Jet Vane Ring	29.8	28.1	1.7
307	2	Prop. Tank	55.3	53.7	1.6
309	2	Umbilical	- 0.1	3.3	-3.4
310	2	Shear Plate	45.6	42.4	3.2
311	3	33A2	48.1	45.4	2.7
316	3	32A4	45.5	43.7	1.8
322	3	Chassis C/L Top	40.9	39.0	1.9
323	3	Chassis C/L Center	35.0	33.5	1.5
324	3	Chassis C/L Bottom	35.1	33.6	1.5
329	4	6A13	82.0	80.8	1.2
330	4	Chassis, 6A13	74.0	72.7	1.3
332	4	6A9	65.2	63.6	1.6
333	4	Flight	68.8	67.2	1.6
336	5	2TR1	82.9	82.9	0.0
337	5	2RA1	85.6	84.7	0.9
340	5	Chassis C/L Top	78.6	78.2	0.4
341	5	Chassis C/L Center	79.5	78.8	0.7
342	5	Chassis C/L Bottom	78.2	77.3	0.9
345	6	2PA1 Case	103.8	-	-
347	6	Chassis, 2PA1	87.5	-	-
348	6	2PS1	111.9	-	-
349	6	Chassis, 2PS1	86.9	87.7	-0.8
350	6	2RE1	95.7	-	-
401	6	Chassis C/L Top	87.6	91.1	-3.5
402	6	Chassis C/L Center	83.8	86.0	-2.2
403	6	Chassis C/L Bottom	87.7	87.5	0.2
406	7	7A1	88.1	86.9	1.2
412	7	7A2	77.2	75.4	1.8
415	7	5A8	86.2	84.2	2.0
418	7	Flight	80.8	79.1	1.7
419	8	Diodes, Upper	85.9	83.7	2.2
420	8	Diodes, Lower	82.0	79.9	2.1
422	8	Booster, Upper	98.6	96.7	1.9
423	8	C/L Top	81.2	78.8	2.4
425	8	C/L Bottom	78.1	75.9	2.2
426	8	Battery Cover	77.9	76.0	1.9
451	-	Hat, Center	83.8	82.1	1.7

TABLE 10

COMPARISON OF TSM AND MARINER IV TEMPERATURES

Operating mode: Earth Cruise
Day from launch: 98
Solar intensity: 0.091 watts/cm^2 (S/S_o = 0.655)

	Channel	Temperatures (F) Mariner 4	TSM	Difference
Sunlit Appendages				
Magnetometer	439	- 3	2.9	- 5.9
Ion Chamber	419	19	22.7	- 3.7
Trapped Radiation Detector	438	65	41.4	+23.6
Internal Bus Locations				
Bay 1	401	67	68.4	- 1.4
Bay 2	421	57	57.7	- 0.7
Bay 3	402	64	61.6	+ 2.4
Bay 4	423	64	65.2	- 1.2
Bay 5	404	64	65.6	- 1.6
Bay 6	405	74	85.4	-11.4
Bay 7	426	61	63.2	- 2.2
Power Regulator, Bay 8	407	88	90.1	- 2.1
Battery, Bay 8	428	67	63.1	+ 3.9
Lower Ring, Bay 8, at Canopus Mount	430	58	34.4	+23.6
Upper Ring, Bay 2	431	66	64.2	+ 1.8
M/C Fuel Tank	217	60	58.0	+ 2.0
N_2 Tank, Bottom	218	62	45.0	+17.0
N_2 Tank, Top	219	63	60.2	+ 2.8
Shaded Appendages				
Canopus Tracker	410	55	1.3	+53.7
Television Camera	418	21	19.2	+ 1.8
SPITS	437	21	22.0	- 1.0

TABLE 11

COMPARISON OF TSM AND MARINER IV TEMPERATURES

Operating mode: Mars Cruise
Day from launch: 180
Solar intensity: 0.063 watts/cm^2 (S/S_o = 0.455)

	Channel	Temperatures (F) Mariner 4	TSM	Difference
Sunlit Appendages				
Magnetometer	439	-29	-18.1	-10.9
Ion Chamber	419	-13	- 0.1	-12.9
Trapped Radiation Detector	438	52	20.3	+31.7
Internal Bus Locations				
Bay 1	401	62	55.7	+ 6.3
Bay 2	421	45	33.4	+11.6
Bay 3	402	54	42.2	+11.8
Bay 4	423	57	47.4	+ 9.6
Bay 5	404	61	54.1	+ 6.9
Bay 6	405	71	78.1	- 7.1
Bay 7	426	59	54.1	+ 4.9
Power Regulator, Bay 8	407	84	79.7	+ 4.3
Battery, Bay 8	428	62	51.7	+10.3
Lower Ring, Bay 8, at Canopus Mount	430	55	26.4	+28.6
Upper Ring, Bay 2	431	50	37.8	+12.2
M/C Fuel Tank	217	52	39.3	+12.7
N_2 Tank, Bottom	218	56	32.1	+23.9
N_2 Tank, Top	219	54	43.4	+10.6
Shaded Appendages				
Canopus Tracker	410	52	- 4.6	+56.6
Television Camera	418	17	7.0	+10.0
SPITS	437	15	9.3	+ 5.7

TABLE 12

COMPARISON OF TSM AND MARINER IV TEMPERATURES

Operating mode: Mars Playback
Day from launch: 234
Solar intensity: 0.059 watts/cm^2 (S/S_o = 0.42)

	Channel	Temperatures (F) Mariner 4	TSM	Difference
Sunlit Appendages				
Magnetometer	439	-66	-39	-27
Ion Chamber	419	-21*	-12.7	-8.3
Trapped Radiation Detector	438	39	6.4	+32.6
Internal Bus Locations				
Bay 1	401	54	43.5	+10.5
Bay 2	421	33	20.1	+12.9
Bay 3	402	34	20.3	+13.7
Bay 4	423	47	34.3	+12.7
Bay 5	404	59	46.7	+12.3
Bay 6	405	70	71.7	- 1.7
Bay 7	426	57	45.6	+11.4
Power Regulator, Bay 8	407	77	69.9	+ 7.1
Battery, Bay 8	428	57	41.8	+15.2
Lower Ring, Bay 8, at Canopus Mount	430	52	18.5	+33.5
Upper Ring, Bay 2	431	38	24.0	+14.0
M/C Fuel Tank	217	39	23.5	+15.5
N_2 Tank, Bottom	218	50	22.0	+28.0
N_2 Tank, Top	219	45	31.6	+13.4
Shaded Appendages				
Canopus Tracker	410	50	-10.7	+60.7
Television Camera	418	9	- 2.4	+11.4
SPITS	437	9	- 0.3	+ 9.3

* Ion chamber temperature is estimated by JPL to be less than -21F.

TABLE 13

EFFECT OF SOLAR PANEL TEMPERATURE ON INTERNAL TEMPERATURES

Location	Temperatures (F)			
	Test 3		Test 4	
	Solar Panel	Bay	Solar Panel	Bay
Bay 1	37.6	43.5	55.1	45.2
Bay 2	-	20.1	-	22.8
Bay 3	35.0	20.3	54.4	22.7
Bay 4	-	34.3		36.6
Bay 5	28.0	46.7	48.6	49.0
Bay 6	-	71.7	-	73.4
Bay 7	30.1	45.6	50.2	47.5
Bay 8	-	69.9	-	71.4

TABLE 14

THERMAL SCALE MODEL TEMPERATURE DATA

EARTH CRUISE S1=0.66 S2=0.65 S3=0.56
TEST 1 RDG 12 TIME0618 DATE JUNE 8 1965

ADL TH	TSM	TCM	MC3 TC	MC3 TEL	TEMPERATURE DEG K	DEG F	LOCATION
1	248	248	148		301.2	82.5	BOX 4A15
2	249	249		401	293.4	68.4	CHASSIS AT 4A15
3	250	250			291.8	65.6	BOX 4A13
4	303	303			288.5	59.7	BOX 4A17
5	305	305	146		280.0	44.3	NOZZLE
6	306	306			274.5	34.4	JET VANE RING
7	307	307		217	287.6	58.0	PROPELLANT TANK
8	309	309			260.0	8.3	UMIBILICAL CONNECTOR
9	310	310		421	287.4	57.7	BAY 2 SHEAR PLATE
10	311	311	143		302.7	85.3	BOX 33A2
11	316	316			295.2	71.7	BOX 32A4
12	322	322			292.0	65.8	BAY 3 CHASSIS TOP
13	323	323		402	289.6	61.6	BAY 3 CHASSIS CENTER
14	324	324			287.5	57.8	BAY 3 CHASSIS BOTTOM
15	245	245		219	288.8	60.2	N2 BOTTLE TOP
16	329	329	136		298.9	78.3	BOX 6A13
17	330	330			293.1	68.0	CHASSIS AT 6A13
18	332	332			288.8	60.2	BOX 6A9
19	333	333		423	291.6	65.2	BAY 4 FLIGHT
20	336	336			294.2	69.8	BOX 2TR1
21	337	337			295.0	71.3	BOX 2RA1
22	340	340			291.9	65.8	BAY 5 CHASSIS TOP
23	341	341		404	291.8	65.6	BAY 5 CHASSIS CENTER
24	342	342			291.0	64.1	BAY 5 CHASSIS BOTTOM
25	345	345	121		302.1	84.1	BOX 2PA1
26	347	347			296.2	73.5	CHASSIS AT 2PA1
27	348	348	122		299.5	79.5	BOX 2PS1
28	349	444	202		311.3	100.7	SOLAR PANEL 5 INBOARD
29	350	350			301.5	83.0	BOX 2RE1
30	401	401			301.2	82.4	BAY 6 CHASSIS TOP
31	402	402		405	302.8	85.4	BAY 6 CHASSIS CENTER
32	403	403			299.2	78.8	BAY 6 CHASSIS BOTTOM
33	406	406	124		294.7	70.8	BOX 7A1
34	412	412	125		286.7	56.3	BOX 7A2
35	415	415			295.3	71.8	BOX 5A8
36	418	418		426	290.5	63.2	FLIGHT
37	246	246		218	280.4	45.0	N2 BOTTLE BOTTOM
38	419	419			294.1	69.6	BAY 8 DIODES UPPER
39	420	420			286.9	56.7	BAY 8 DIODES LOWER
40	422	422	129	407	305.4	90.1	BAY 8 BOOSTER UPPER
41	423	423			292.8	67.4	BAY 8 C/L TOP
42	425	425			282.9	49.5	BAY 8 C/L BOTTOM
43	426	426	127	428	290.4	63.1	BAY 8 BATTERY COVER
44	242	242			285.0	53.4	BUS TUBE BOTTOM
45	243	243			283.0	49.7	BUS TUBE TOP
46	227	227	131	410	256.1	1.3	CANOPUS TRACKER
47	228	228		430	274.5	34.4	LOWER FRAME CANOPUS
48	139	142	140		307.4	93.6	HI GAIN ANTENNA 1/4

TABLE 14 (continued)

THERMAL SCALE MODEL TEMPERATURE DATA

EARTH CRUISE S1=0.66 S2=0.65 S3=0.56
TEST 1 RDG 12 TIME0618 DATE JUNE 8 1965

ADL TH	TSM	TCM	MC3 TC	MC3 TEL	TEMPERATURE DEG K	DEG F	LOCATION
-1	140	140	141		306.8	92.6	HI GAIN ANTENNA CENTER
-2	145	145	133		283.9	51.4	HI GAIN FEED
-3	147		134		288.2	59.1	SUPER STRUCTURE RING
-4	203	204	139		289.1	60.8	COS. DUST ELECTRONICS
-5	149	203	138		290.2	62.7	COS. DUST SENSOR
-6	208	208	145		291.2	64.4	BAY 2 UPPER SUN SENSOR
-7	211	211		431	291.0	64.2	BAY 2 UPPER FRAME SUN SENSOR
-8	213	213		438	278.4	41.4	RAD. DETECTOR CHASSIS
-9	236	214	137		279.6	43.7	RAD. DETECTOR TUBE D
-10	234	234	126	418	266.1	19.2	TV OPTICS
-11	235	235		437	267.6	22.0	S.P.I.T.S.
-12	127	129	116	439	257.0	2.9	MAGNETOMETER
-13	132	132	118	419	268.0	22.7	ION CHAMBER ELECTRONICS
-14	130		117		272.3	30.4	ION CHAMBER GM TUBE
-15	126		120		316.3	109.6	BOX 2PS3
-16	128		123		328.6	131.8	BOX 2PA2
-17	218	216	119		289.6	61.6	UPPER SUN SENSOR BAY 6
-18	217	217	135		281.0	46.2	EARTH DETECTOR BAY 6
-19	209			434	301.7	83.3	UPPER SHIELD BAY 2
-20	239	230		435	288.1	59.0	LOWER SHIELD BAY 5
-21	229	432	219		311.5	101.0	SOL. PANEL 1 INBOARD
-22	146	428	222		310.1	98.5	SOL. PANEL 1 OUTBOARD
-23	210	438	226		316.4	109.9	SOL. PANEL 3 INBOARD
-24	212	434	229		311.6	101.2	SOL. PANEL 3 OUTBOARD
-26	137	440	205		308.2	95.1	SOL. PANEL 5 OUTBOARD
-27	131	450	209		309.2	96.9	SOL. PANEL 7 INBOARD
-28	133	446	213		303.8	87.1	SOL. PANEL 7 OUTBOARD

TABLE 15

THERMAL SCALE MODEL TEMPERATURE DATA

MARS CRUISE S1=0.43 S2=0.48 S3=0.44
TEST 2 RDG 8 TIME0100 DATE JUNE 9 1965

ADL TH	TSM	TCM	MC3 TC	MC3 TEL	TEMPERATURE DEG K	DEG F	LOCATION
1	248	248	148		294.6	70.5	BOX 4A15
2	249	249		401	286.3	55.7	CHASSIS AT 4A15
3	250	250			284.8	52.9	BOX 4A13
4	303	303			280.7	45.6	BOX 4A17
5	305	305	146		270.1	26.4	NOZZLE
6	306	306			265.3	17.9	JET VANE RING
7	307	307		217	277.2	39.3	PROPELLANT TANK
8	309	309			252.1	-5.9	UMIBILICAL CONNECTOR
9	310	310		421	274.0	33.4	BAY 2 SHEAR PLATE
10	311	311	143		290.6	63.4	BOX 33A2
11	316	316			284.4	52.2	BOX 32A4
12	322	322			280.5	45.2	BAY 3 CHASSIS TOP
13	323	323		402	278.9	42.2	BAY 3 CHASSIS CENTER
14	324	324			277.0	38.8	BAY 3 CHASSIS BOTTOM
15	245	245		219	279.5	43.4	N2 BOTTLE TOP
16	329	329	136		289.1	60.7	BOX 6A13
17	330	330			282.9	49.5	CHASSIS AT 6A13
18	332	332			279.9	44.1	BOX 6A9
19	333	333		403	281.7	47.4	BAY 4 FLIGHT
20	336	336			287.2	57.2	BOX 2TR1
21	337	337			289.4	61.2	BOX 2RA1
22	340	340			284.7	52.7	BAY 5 CHASSIS TOP
23	341	341		404	285.4	54.1	BAY 5 CHASSIS CENTER
24	342	342			284.5	52.4	BAY 5 CHASSIS BOTTOM
25	345	345	121		298.1	76.8	BOX 2PA1
26	347	347			291.9	65.7	CHASSIS AT 2PA1
27	348	348	122		294.7	70.8	BOX 2PS1
28	349	444	202		282.7	49.1	SOLAR PANEL 5 INBOARD
29	350	350			298.2	77.0	BOX 2RE1
30	401	401			296.8	74.5	BAY 6 CHASSIS TOP
31	402	402		405	298.8	78.1	BAY 6 CHASSIS CENTER
32	403	403			294.9	71.1	BAY 6 CHASSIS BOTTOM
33	406	406	124		289.6	61.6	BOX 7A1
34	412	412	125		281.5	47.0	BOX 7A2
35	415	415			288.9	60.3	BOX 5A8
36	418	418		426	285.4	54.1	FLIGHT
37	246	246		218	273.2	32.1	N2 BOTTLE BOTTOM
38	419	419			288.4	59.5	BAY 8 DIODES UPPER
39	420	420			282.0	47.8	BAY 8 DIODES LOWER
40	422	422	129	407	299.6	79.7	BAY 8 BOOSTER UPPER
41	423	423			287.4	57.6	BAY 8 C/L TOP
42	425	425			278.2	41.0	BAY 8 C/L BOTTOM
43	426	426	127	428	284.1	51.7	BAY 8 BATTERY COVER
44	242	242			276.4	37.8	BUS TUBE BOTTOM
45	243	243			274.7	34.8	BUS TUBE TOP
46	227	227	131	410	252.8	-4.6	CANOPUS TRACKER
47	228	228		430	270.1	26.4	LOWER FRAME CANOPUS
48	139	142	140		280.4	45.0	HI GAIN ANTENNA 1/4

TABLE 15 (continued)

THERMAL SCALE MODEL TEMPERATURE DATA

MARS CRUISE S1=0.43 S2=0.48 S3=0.44
TEST 2 RDG 8 TIME0100 DATE JUNE 9 1965

ADL TH	TSM	TCM	MC3 TC	MC3 TEL	TEMPERATURE DEG K	DEG F	LOCATION
-1	140	140	141		280.0	44.3	HI GAIN ANTENNA CENTER
-2	145	145	133		260.7	9.6	HI GAIN FEED
-3	147		134		270.9	27.9	SUPER STRUCTURE RING
-4	203	204	139		275.2	35.7	COS. DUST ELECTRONICS
-5	149	203	138		275.3	35.9	COS. DUST SENSOR
-6	208	208	145		273.0	31.8	BAY 2 UPPER SUN SENSOR
-7	211	211		431	276.4	37.8	BAY 2 UPPER FRAME SUN SENSOR
-8	213	213		438	266.6	20.3	RAD. DETECTOR CHASSIS
-9	236	214	137		265.6	18.4	RAD. DETECTOR TUBE D
-10	234	234	126	418	259.3	7.0	TV OPTICS
-11	235	235		437	260.6	9.3	S.P.I.T.S.
-12	127	129	116	439	245.3	-18.1	MAGNETOMETER
-13	132	132	118	419	255.4	-0.1	ION CHAMBER ELECTRONICS
-14	130		117		255.2	-0.3	ION CHAMBER GM TUBE
-15	126		120		312.4	102.6	BOX 2PS3
-16	128		123		325.0	125.3	BOX 2PA2
-17	218	216	119		280.5	45.2	UPPER SUN SENSOR BAY 6
-18	217	217	135		272.3	30.5	EARTH DETECTOR BAY 6
-19	209			434	285.4	54.0	UPPER SHIELD BAY 2
-20	239	230		435	281.4	46.9	LOWER SHIELD BAY 5
-21	229	432	219		281.1	46.2	SOL. PANEL 1 INBOARD
-22	146	428	222		279.6	43.6	SOL. PANEL 1 OUTBOARD
-23	210	438	226		283.8	51.1	SOL. PANEL 3 INBOARD
-24	212	434	229		280.3	44.9	SOL. PANEL 3 OUTBOARD
-26	137	440	205		279.5	43.5	SOL. PANEL 5 OUTBOARD
-27	131	450	209		281.2	46.4	SOL. PANEL 7 INBOARD
-28	133	446	213		276.4	37.9	SOL. PANEL 7 OUTBOARD

TABLE 16

THERMAL SCALE MODEL TEMPERATURE DATA

MARS PLAYBACK S1=0.40 S2=0.44 S3=0.46
TEST 3 RDG 8 TIME2400 DATE JUNE 9 1965

ADL TH	TSM	TCM	MC3 TC	MC3 TEL	TEMPERATURE DEG K	DEG F	LOCATION
1	248	248	148		288.2	59.1	BOX 4A15
2	249	249		401	279.5	43.5	CHASSIS AT 4A15
3	250	250			278.0	40.6	BOX 4A13
4	303	303			272.8	31.4	BOX 4A17
5	305	305	146		262.0	11.9	NOZZLE
6	306	306			257.9	4.5	JET VANE RING
7	307	307		217	268.4	23.5	PROPELLANT TANK
8	309	309			245.4	-17.9	UMIBILICAL CONNECTOR
9	310	310		421	266.6	20.1	BAY 2 SHEAR PLATE
10	311	311	143		267.9	22.5	BOX 33A2
11	316	316			267.9	22.5	BOX 32A4
12	322	322			267.3	21.5	BAY 3 CHASSIS TOP
13	323	323		402	266.7	20.3	BAY 3 CHASSIS CENTER
14	324	324			265.7	18.5	BAY 3 CHASSIS BOTTOM
15	245	245		219	272.9	31.6	N2 BOTTLE TOP
16	329	329	136		282.8	49.3	BOX 6A13
17	330	330			275.9	36.9	CHASSIS AT 6A13
18	332	332			273.1	32.0	BOX 6A9
19	333	333		423	274.4	34.3	BAY 4 FLIGHT
20	336	336			283.3	50.3	BOX 2TR1
21	337	337			285.2	53.7	BOX 2RA1
22	340	340			281.1	46.2	BAY 5 CHASSIS TOP
23	341	341		404	281.3	46.7	BAY 5 CHASSIS CENTER
24	342	342			280.0	44.4	BAY 5 CHASSIS BOTTOM
25	345	345	121		294.5	70.4	BOX 2PA1
26	347	347			288.3	59.2	CHASSIS AT 2PA1
27	348	348	122		290.9	64.0	BOX 2PS1
28	349	444	202		270.9	28.0	SOLAR PANEL 5 INBOARD
29	350	350			294.8	71.0	BOX 2RE1
30	401	401			293.1	68.0	BAY 6 CHASSIS TOP
31	402	402		405	295.2	71.7	BAY 6 CHASSIS CENTER
32	403	403			291.3	64.6	BAY 6 CHASSIS BOTTOM
33	406	406	124		285.1	53.4	BOX 7A1
34	412	412	125		276.8	38.6	BOX 7A2
35	415	415			284.0	51.4	BOX 5A8
36	418	418		426	280.7	45.6	FLIGHT
37	246	246		218	267.6	22.0	N2 BOTTLE BOTTOM
38	419	419			283.3	50.3	BAY 8 DIODES UPPER
39	420	420			277.1	39.1	BAY 8 DIODES LOWER
40	422	422	129	407	294.2	69.9	BAY 8 BOOSTER UPPER
41	423	423			282.1	48.1	BAY 8 C/L TOP
42	425	425			273.3	32.3	BAY 8 C/L BOTTOM
43	426	426	127	428	278.6	41.8	BAY 8 BATTERY COVER
44	242	242			270.1	26.4	BUS TUBE BOTTOM
45	243	243			268.5	23.7	BUS TUBE TOP
46	227	227	131	410	249.5	-10.7	CANOPUS TRACKER
47	228	228		430	265.7	18.5	LOWER FRAME CANOPUS
48	139	142	140		274.1	33.7	HI GAIN ANTENNA 1/4

TABLE 16 (continued)

THERMAL SCALE MODEL TEMPERATURE DATA

MARS PLAYBACK S1=0.40 S2=0.44 S3=0.46
TEST 3 RDG 8 TIME2400 DATE JUNE 9 1965

ADL TH	TSM	TCM	MC3 TC	MC3 TEL	TEMPERATURE DEG K	DEG F	LOCATION
-1	140	140	141		274.8	34.9	HI GAIN ANTENNA CENTER
-2	145	145	133		254.9	-0.8	HI GAIN FEED
-3	147		134		265.4	18.1	SUPER STRUCTURE RING
-4	203	204	139		268.2	23.1	COS. DUST ELECTRONICS
-5	149	203	138		268.3	23.3	COS. DUST SENSOR
-6	208	208	145		266.8	20.5	BAY 2 UPPER SUN SENSOR
-7	211	211		431	268.7	24.0	BAY 2 UPPER FRAME SUN SENSOR
-8	213	213		438	259.0	6.4	RAD. DETECTOR CHASSIS
-9	236	214	137		258.5	5.6	RAD. DETECTOR TUBE D
-10	234	234	126	418	254.1	-2.4	TV OPTICS
-11	235	235		437	255.2	-0.3	S.P.I.T.S.
-12	127	129	116	439	233.9	-38.6	MAGNETOMETER
-13	132	132	118	419	248.3	-12.7	ION CHAMBER ELECTRONICS
-14	130		117		249.7	-10.3	ION CHAMBER GM TUBE
-15	126		120		309.1	96.7	BOX 2PS3
-16	128		123		321.7	119.4	BOX 2PA2
-17	218	216	119		276.0	37.0	UPPER SUN SENSOR BAY 6
-18	217	217	135		268.2	23.1	EARTH DETECTOR BAY 6
-19	209			434	279.3	43.1	UPPER SHIELD BAY 2
-20	239	230		435	276.6	38.2	LOWER SHIELD BAY 5
-21	229	432	219		276.3	37.6	SOL. PANEL 1 INBOARD
-22	146	428	222		274.8	35.0	SOL. PANEL 1 OUTBOARD
-23	210	438	226		274.9	35.0	SOL. PANEL 3 INBOARD
-24	212	434	229		272.2	30.3	SOL. PANEL 3 OUTBOARD
-26	137	440	205		269.0	24.6	SOL. PANEL 5 OUTBOARD
-27	131	450	209		272.1	30.1	SOL. PANEL 7 INBOARD
-28	133	446	213		268.5	23.6	SOL. PANEL 7 OUTBOARD

TABLE 17

THERMAL SCALE MODEL TEMPERATURE DATA

MARS PLAYBACK HI SOLAR PANEL TEMP.
TEST 4 RDG 3 TIME0130 DATE JUNE 10 1965

ADL TH	TSM	TCM	MC3 TC	MC3 TEL	TEMPERATURE DEG K	DEG F	LOCATION
1	248	248	148		289.1	60.7	BOX 4A15
2	249	249		401	280.5	45.2	CHASSIS AT 4A15
3	250	250			278.8	42.2	BOX 4A13
4	303	303			273.8	33.1	BOX 4A17
5	305	305	146		263.0	13.8	NOZZLE
6	306	306			258.8	6.2	JET VANE RING
7	307	307		217	269.5	25.3	PROPELLANT TANK
8	309	309			246.3	-16.4	UMIBILICAL CONNECTOR
9	310	310		421	268.0	22.8	BAY 2 SHEAR PLATE
10	311	311	143		269.4	25.2	BOX 33A2
11	316	316			269.3	25.0	BOX 32A4
12	322	322			268.8	24.1	BAY 3 CHASSIS TOP
13	323	323		402	268.0	22.7	BAY 3 CHASSIS CENTER
14	324	324			266.9	20.8	BAY 3 CHASSIS BOTTOM
15	245	245		219	273.9	33.3	N2 BOTTLE TOP
16	329	329	136		284.2	51.9	BOX 6A13
17	330	330			277.3	39.4	CHASSIS AT 6A13
18	332	332			274.4	34.2	BOX 6A9
19	333	333		423	275.7	36.6	BAY 4 FLIGHT
20	336	336			284.7	52.7	BOX 2TR1
21	337	337			286.3	55.7	BOX 2RA1
22	340	340			282.4	48.7	BAY 5 CHASSIS TOP
23	341	341		404	282.6	49.0	BAY 5 CHASSIS CENTER
24	342	342			281.3	46.6	BAY 5 CHASSIS BOTTOM
25	345	345	121		295.5	72.1	BOX 2PA1
26	347	347			289.2	61.0	CHASSIS AT 2PA1
27	348	348	122		292.0	65.9	BOX 2PS1
28	349	444	202		282.4	48.6	SOLAR PANEL 5 INBOARD
29	350	350			295.8	72.8	BOX 2RE1
30	401	401			294.1	69.8	BAY 6 CHASSIS TOP
31	402	402		405	296.2	73.4	BAY 6 CHASSIS CENTER
32	403	403			292.2	66.3	BAY 6 CHASSIS BOTTOM
33	406	406	124		286.1	55.3	BOX 7A1
34	412	412	125		277.8	40.3	BOX 7A2
35	415	415			285.2	53.7	BOX 5A8
36	418	418		426	281.8	47.5	FLIGHT
37	246	246		218	268.4	23.4	N2 BOTTLE BOTTOM
38	419	419			284.2	51.9	BAY 8 DIODES UPPER
39	420	420			277.9	40.6	BAY 8 DIODES LOWER
40	422	422	129	407	295.1	71.4	BAY 8 BOOSTER UPPER
41	423	423			282.9	49.4	BAY 8 C/L TOP
42	425	425			274.1	33.7	BAY 8 C/L BOTTOM
43	426	426	127	428	279.5	43.4	BAY 8 BATTERY COVER
44	242	242			270.9	28.0	BUS TUBE BOTTOM
45	243	243			269.3	25.1	BUS TUBE TOP
46	227	227	131	410	250.0	-9.7	CANOPUS TRACKER
47	228	228		430	266.4	19.8	LOWER FRAME CANOPUS
48	139	142	140		273.5	32.7	HI GAIN ANTENNA 1/4

TABLE 17 (continued)

THERMAL SCALE MODEL TEMPERATURE DATA

MARS PLAYBACK HI SOLAR PANEL TEMP.
TEST 4 RDG 3 TIME0130 DATE JUNE 10 1965

ADL TH	TSM	TCM	MC3 TC	MC3 TEL	TEMPERATURE DEG K	DEG F	LOCATION
-1	140	140	141		271.8	29.6	HI GAIN ANTENNA CENTER
-2	145	145	133		252.6	-4.9	HI GAIN FEED
-3	147		134		264.9	17.1	SUPER STRUCTURE RING
-4	203	204	139		268.6	23.7	COS. DUST ELECTRONICS
-5	149	203	138		268.6	23.8	COS. DUST SENSOR
-6	208	208	145		267.5	21.7	BAY 2 UPPER SUN SENSOR
-7	211	211		431	269.9	26.1	BAY 2 UPPER FRAME SUN SENSOR
-8	213	213		438	260.1	8.4	RAD. DETECTOR CHASSIS
-9	236	214	137		259.4	7.2	RAD. DETECTOR TUBE D
-10	234	234	126	418	254.6	-1.3	TV OPTICS
-11	235	235		437	255.8	0.7	S.P.I.T.S.
-12	127	129	116	439	234.2	-38.1	MAGNETOMETER
-13	132	132	118	419	248.5	-12.4	ION CHAMBER ELECTRONICS
-14	130		117		246.7	-15.6	ION CHAMBER GM TUBE
-15	126		120		310.0	98.4	BOX 2PS3
-16	128		123		322.6	121.1	BOX 2PA2
-17	218	216	119		276.5	38.0	UPPER SUN SENSOR BAY 6
-18	217	217	135		268.7	24.0	EARTH DETECTOR BAY 6
-19	209			434	279.4	43.2	UPPER SHIELD BAY 2
-20	239	230		435	277.7	40.2	LOWER SHIELD BAY 5
-21	229	432	219		286.0	55.1	SOL. PANEL 1 INBOARD
-22	146	428	222		284.9	53.1	SOL. PANEL 1 OUTBOARD
-23	210	438	226		285.6	54.4	SOL. PANEL 3 INBOARD
-24	212	434	229		283.0	49.7	SOL. PANEL 3 OUTBOARD
-26	137	440	205		280.5	45.2	SOL. PANEL 5 OUTBOARD
-27	131	450	209		283.2	50.2	SOL. PANEL 7 INBOARD
-28	133	446	213		279.3	43.0	SOL. PANEL 7 OUTBOARD

APPENDIX I

TSM POWER BREAKDOWN
PHASE II CONFIGURATION

BAY 1 - POWER SUBSYSTEM

D 3611-016

Identification	TSM Power (Watts)	Number of Resistors
Pyrotechnic Control (8A1/8A2)	.093	1
Inverter (4A15)	1.527	2
Battery Charger (4A13)	1.479*	2
Inverter 4A18	0	0
Pyrotechnic Control 8A1/8A2	.093	1
Power Distribution (4A11)	.299	1
Power Synchronizer (4A12)	.372	1
Inverter (4A17)	0	0
Total Power	3.864	

BAY 2 - PIPS

This Bay has no power dissipation.

*4A13 dissipates 1.479 watts at Earth Cruise Mode and 0 watt at Mars Cruise.

APPENDIX I (continued)

BAY 3 - SCIENTIFIC EQUIPMENT

D 3611-011

Identification	TSM Power (Watts)	Number of Resistors
Magnetometer Electronics (33A2)	.484	2
Magnetometer Electronics (33A3)	.246	1
Scan Electronics (31A2)	0	0
Scan Electronics (31A3)	0	0
U. V. Electronics (34A2)	0	0
T. V. Power Supply (36A6)	0	0
Analog - Digital T.V. Encoder (36A5)	0	0
Deflection and Control (36A4)	0	0
Video Channels and Computer (36A3)	0	0
Plasma Electronics 1 (32A2)	.104	1
Plasma Electronics 2 (32A3)	.153	2
Plasma Electronics 3 (32A4)	.346	1
DAS Power Supply (20A5)	.094	1
Buffer Memory (20A1)	0	0
NRT DAS Logic (20A3)	.094	1
RT DAS Logic (20A2)	0	0
RT DAS Logic (20A4)	.094	1
Cosmic Ray Telescope (21A1)	.072	1
	1.686	

APPENDIX I (continued)

BAY 4 - DATA ENCODER

D 3611-012

Identification	TSM Power(Watts)	Number of Resistors
Command Decoder and Power Supply (3A7)	.156	1
Command Decoder 2 (3A6)	.045	1
Command Detector 2 (3A2)	.117	1
Command Program Control (3A4)	.045	1
Command Detector 3 (3A3)	.117	1
Command Decoder 1 (3A5)	.045	1
Command Detector 1 (3A1)	.124	1
Decks 210, 220 (6A8)	.060	1
Decks 400, 410 (6A10)	.021	1
Decks 420, 430 (6A11)	0.0198	1
Power Supply (6A13)	1.239	3
Functional Switching (6A6)	.023	1
Event Counters (6A5)	.053	1
Modulator, Mixer, Transfer Register, Data Selector (6A2)	.091	1
PN Generators (6A1)	.091	1
Analog to Digital Converter (6A3)	.266	1
Analog to Digital Converter (6A4)	0	0
Low Level Amplifier (6A12)	.160	1
Decks 100, 110 (6A7)	.045	1
Decks 200, 300 (6A9)	.060	1
	2.7798	

BAY 5 - RECEIVER AND TAPE MACHINE

D 3611-013

Identification	TSM Power (Watts)	Number of Resistors
Tape Electronics 3 and TR (16A4)	0	0
Tape Electronics 4 (16A5)	0	0
Tape Electronics 2 (16A3)	0	0
Tape Electronics 1 (16A2)	0	0
Tape Machine (16A1)	0	0
Receiver Transformer Rectifier (2TRI)	.322	1
Receiver Subass'y. (2RA2)	.440	2
Receiver Subass'y. (2RA1)	.440	2
	1.202	

APPENDIX I (continued)

BAY 6 - RF COMMUNICATIONS

D 3611-014

Identification	TSM Power (Watts)	Number of Resistors
Control Unit Subass'y. (2CC1)	.031	2
Power Amplifiers Subass'y. (2PA1)	4.955	2
Power Amplifiers Power Sup. (2PS1)	3.716	2
Exciters Transformer Rectifier (2TR2)	.372	1
Exciters (2RE1)	1.392	4
	10.466	

APPENDIX I (continued)

BAY 7 - ATTITUDE CONTROL AND CC&S

D 3611-015

Identification	TSM Power (Watts)	Number of Resistors
Attitude Control Electronics (7A1)	0.5695	1
CC&S Transformer Rectifier (5A8)	.645	2
End Counter (5A3)	.080	1
Central Clock (5A1)	.080	1
Launch Counter (5A2)	.080	1
Maneuver Clock (5A4)	.080	1
Maneuver Duration (5A5)	.080	
Address Register and Maneuver Duration Output (5A6)	.080	1
Input Decoder (5A7)	.080	1
Gyro Control Ass'y. (7A2)	0	0
	1.7745	

APPENDIX I (continued)

BAY 8 - POWER REGULATOR ASSEMBLY

D 3611-006

Identification	TSM Power (Watts)	Number of Resistors
Maneuver Booster	0	0
Main Booster	3.328	3
Battery Diode	0	0
Solar Panel Diodes	.740	6
Electronics	1.405	7
	5.473	

APPENDIX I (continued)

TSM THERMOCOUPLE LIST

Phase II Configuration

JPL No.	Location
242	Bus tube at bottom
243	Bus tube at top
245	Bay 4 A/C nitrogen bottle, top
246	Bay 8 A/C nitrogen bottle, bottom
248	Bay 1, 4A15
249	Bay 1, chassis at 4A15
250	Bay 1, 4A13
303	Bay 1, 4A17
305	Bay 2, midcourse nozzle near throat
306	Bay 2, midcourse inside jet vane ring
307	Bay 2, propellant tank
309	Bay 2, umbilical connector
310	Bay 2, shear plate
311	Bay 3, 33A2
316	Bay 3, 32A4
322	Bay 3, chassis centerline top
323	Bay 3, chassis centerline center
324	Bay 3, chassis centerline bottom
329	Bay 4, 6A13
330	Bay 4, chassis at 6A13
332	Bay 4, 6A9
333	Bay 4, flight
336	Bay 5, 2TR1
337	Bay 5, 2RA1
340	Bay 5, chassis centerline top
341	Bay 5, chassis centerline center
342	Bay 5, chassis centerline bottom
345	Bay 6, 2PA1 case

APPENDIX I (continued)

JPL No.	Location
347	Bay 6, chassis at 2PA1
348	Bay 6, 2PS1
349	Bay 6, chassis at 2PS1
350	Bay 6, 2RE1
401	Bay 6, chassis centerline top
402	Bay 6, chassis centerline center
403	Bay 6, chassis centerline bottom
406	Bay 7, 7A1, one-third down
412	Bay 7, 7A2, gyro #2
415	Bay 7, 5A8
418	Bay 7, flight
419	Bay 8, solar panel diodes (upper, bay 7 side)
420	Bay 8, solar panel diodes (lower, bay 7 side)
422	Bay 8, main booster (upper, bay 1 side)
423	Bay 8, vertical centerline top
425	Bay 8, vertical centerline bottom
426	Bay 8, battery case
451*	Hat Center
452*	Hat Edge Bay 6
453*	Hat Edge Bay 2
454*	Flight Shield Bay 5

* ADL Numbering System--not used by JPL.

APPENDIX II

JOINT CONDUCTANCE TEST RESULTS

The following data pertains to tests made with a full-scale electronic subchassis bolted to a radiating plate and a 0.43 scale model of that system. The purpose of the tests was to measure the subchassis temperature for different bolting torques, screw materials, and conductances of a radiating plate to which the subchassis was bolted. In the tests the power dissipated in the full-scale subchassis was maintained constant at 25 watts. The power dissipated in the 0.43 scale subchassis assembly was held constant at 4.6 watts (c.f. Equation 5 which relates the power dissipation to the scaling ratio).

The primary measurement was the temperature of the subchassis. Since a constant amount of power was dissipated in the subchassis (by use of a heater) and all of the power was dissipated by the radiating plate, the average temperature of the radiating plate was a constant. The temperature differences as stated below are based on the temperature measurements of the subchassis and the average temperature of the radiating plate. An attempt was made to measure the temperatures in the radiating plate, however, the plate was not isothermal and the temperature measurements were strongly influenced by the conductance of the plate and the exact location of the thermocouples. Therefore, it was decided to use an average or reference temperature for temperature difference calculations.

The screw torques were measured with commercial torque wrenches and the absolute accuracy of the torques is subject to question. However, several tests were made to determine the reproducibility of the test

results. Between two identical thermal tests, the three screws were removed and retorqued. The differences in the measured temperatures of the subchassis were less than 2F.

The results of seven tests of the two subchassis assemblies are presented in the following table.

JPL Full-scale Subchassis (3- #6-32 pan head screws)

Power - 25 watts
Average temperature of radiating plate - 89F

Screw Torque (in-lbs)	Screw Material	Radiating Plate Material	Clearance Hole Diameter (in)	Subchassis Temperature (F)	ΔT (F)
18	S.S.	Mag.	0.166	172.5	83.5
9	S.S.	Mag.	0.166	196.3	107.3
18	Ti	Mag.	0.166	171.4	82.4
18	S.S.	Copper	0.166	130.0	41.0

0.43 Scale Subchassis (3- #4-40 pan head screws)

Power - 4.62 watts
Average temperature of radiating plate - 89F

5.5	S.S.	1018 steel	0.125	158.8	69.8
2.7	S.S.	1018 steel	0.125	177.9	88.9
5.5	S.S.	1018 steel	0.149	182.4	93.4

APPENDIX III

TSM POWER BREAKDOWN - PHASE III CONFIGURATION

BAY 1

Identification Number	Nominal TSM Power (Watts)	Number of Resistors	Volts	Resistance Identification Number	Resistance (ohms)
8A1/8A2	.093	1	25	RH5	6.8 K
4A15	2.145	2*	300	RH25	25.62K, 15.5K
4A13 (Note 1)	3.624 #	2*	300	RH25	20.0K, 5.0K
8A1/8A2	.093	1	25	RH5	6.8 K
4A11	.299	1	25	RH5	2 K
4A12 (Note 2)	.742	1	25	RH5	0.95 K
4A17	0	-	-	-	-
	6.996 Earth Cruise				
	3.372 Mars				

Note 1: 4A13 has external switching to change from 3.624 watts at Earth Cruise to 0.0 watts at Mars Cruise.

Note 2: Zero power for 4A12 in "Playback" mode.

* In series.

APPENDIX III (continued)

BAY 3

Identification Number	Nominal TSM Power (Watts)	Number of Resistors	Volts	Resistance Identification Number	Resistance (ohms)
33A2	.738	1	25	RH5	.95K
33A3	.246	1	25	RH5	2.5 K
32A2	.104	1	25	RH5	6 K
32A3	.153	1	25	RH5	4 K
32A4	.679	1	25	RH5	.95K
20A5	.094	1	25	RH5	6.8 K
20A3	.094	1	25	RH5	6.8 K
20A4	.094	1	25	RH5	6.8 K
21A1	.072	1	25	RH5	9 K
	2.274				

Note: Zero power in this bay during "playback" mode.

APPENDIX III (continued)

BAY 4

Identification Number	Nominal TSM Power (Watts)	Number of Resistors	Volts	Resistance Identification Number	Resistance (ohms)
3A7	.156	1	25	RH5	4K
3A6	.045	1	25	RH5	14K
3A2	.117	1	25	RH5	5.3K
3A4	.045	1	25	RH5	14K
3A3	.117	1	25	RH5	5.3K
3A1/3A5	0.0				
6A8/6A10	.081	2#	25	RH5/RH10	10K/30K
6A11	.0198	1	25	RH10	30K
6A13	.895	1	25	RH5	.71K
6A6	.023	1	25	RH10	27.5K
6A5	.053	1	25	RH5	12K
6A2	.091	1	25	RH5	6.8K
6A1	.091	1	25	RH5	6.8K
6A3	0.0				
6A12	.160	1	25	RH5	4K
6A7	.045	1	25	RH5	14K
6A9	.060	1	25	RH5	10K
	1.998				

* In Series

\# In parallel

BAY 5

Identification Number	Nominal TSM Power (Watts)	Number of Resistors	Volts	Resistance Identification Number	Resistance (ohms)
2TR1	.322	1	25	RH5	2K
2RA2*	.625	2#	25	RH5	1.25K, 5.0K
2RA1	.440	2*	25	RH5	0.71, 0.71
	1.387				
Playback Mode					
16A4	.760	2#	25	RH5	0.95K, 6.0K

* In series.
\# In parallel.

APPENDIX III (continued)

BAY 6

Identification Number	Nominal TSM Power (Watts)	Number of Resistors	Volts	Resistance Identification Number	Resistance (ohms)
2CC1	.573	2#	25	RH5	10K, 1.25K
2PA1	4.250	2*	300	RH25	9.0K, 12.1K
2PS2 (2PS1)	1.109	3*	300	RH25	(2)36.0K,9.25K
2TR2	.372	1	25	RH5	1.6K
2RE1	1.392	4*	300	RH25	15.5K
2PS3	1.812	2#	25	RH5	0.48K,1.25K
2PA2	6.841	2*	300	RH25	8.52K,5.0K

TOTALS

Cavity	7.698
TWT	10.992

	TWT Mode	Cavity Amp. Mode
2PA1	0	
2PS2	0	
2PS3	1.812	
2PA2	6.841	

* In series.

\# In parallel.

APPENDIX III (continued)

BAY 7

Identification Number	Nominal TSM Power (Watts)	Number of Resistors	Volts	Resistance Identification Number	Resistance (ohms)
7A1	.569	2#	25	RH5	9.0K, 1.25K
5A8	.645	2*	25	RH5	.48K
5A3	.080	1	25	RH5	8K
5A1	.080	1	25	RH5	8K
5A2	.080	1	25	RH5	8K
5A4	.080	1	25	RH5	8K
5A5	.080	1	25	RH5	8K
5A6	.080	1	25	RH5	8K
5A7	.080	1	25	RH5	8K
7A2	0	-	-	-	-
	1.7749				

* In series

\# In parallel

APPENDIX III (continued)

BAY 8

Identification Number	Nominal TSM Power (Watts)	Number of Resistors	Volts	Resistance Identification Number	Resistance (ohms)
Main Booster	3.328	3*	300	RH25	9K
Solar Panel Diodes	.740	6*	300	RH25	20K
Electronics	1.405	7*	300	RH25	25.62K
				RH25	8.52K
	5.473			RH25	5.0K

EXTERNAL EXPERIMENTS

Magnetometer	0.185	1	25	RH5	4.0K
Ion Chamber	0.092	1	25	RH5	6.8K
Canopus	0.277	2*	25	RH5	0.48K, 1.75K
Cosmic Dust	0.030	2*	25	RH5	10K, 10K
Trapped Rad.	0.080	1	25	RH5	8.0K
Hi-gain Feed	0.107	1	25	RH5	6.0K

Note: All external experiments have zero power in playback mode, except the Canopus, and Hi-gain feed.

*In series

APPENDIX IV

CALCULATION OF ANTENNA HEAT LOSS

We consider the antenna to be shaded from sunlight and joined to the spacecraft bus without any thermal contact resistance. If the antenna tube is assumed to be infinitely long, the heat loss from the spacecraft bus which is maintained at a temperature T is given by the expression

$$q^2 = 2/5\ k\ A\ p\ \epsilon\ \sigma\ T^5$$

where

- q - heat loss
- k - thermal conductivity
- A - crossectional area of tube
- p - perimeter
- ϵ - surface emittance
- T - spacecraft bus temperature

The prototype antenna tube has the following characteristics

- k = 1.55 watts/cm-K (6061 Al)
- A = 1.96 cm^2
- p = 30.9 cm
- ϵ = 0.03 (assumed value for polished aluminum)
- T = 300K

The calculated heat loss is 3.94 watts. The heat loss is actually expected to be lower than this figure due to the thermal contact resistance at the joint between the antenna and spacecraft and the fact that the tube is infinitely long.

The antenna used in the TSM was constructed of aluminum and it was a 1.75 inch OD tube with a wall thickness of 0.020 inches. The maximum heat leak for this configuration is calculated to be 1.44 watts.

For perfect thermal scaling, the ratio of heat leaks would be proportional to the square of the scaling ratio or 0.73 watts for the 0.43 scale model. The resultant error in the average bus temperature of the scale model is estimated to be less than 1F (c.f. the results of Test 1 and 2 of Phase II where the influence of internal power on the average temperature is approximately 0.5F per watt of internal power).

APPENDIX V

TEMPERATURE CONTROL SURFACES SCIENCE AND APPENDAGES

	Component	Description
1.	Omni Ground Plane	Laminar x-500 green paint on top and sides.
2.	Omni Antenna Mast	Polished aluminum exterior; buffed aluminum interior.
3.	Magnetometer Sensor	Polished aluminum chassis; vacuum deposited aluminum Helmholz coil cover.
4.	Ion Chamber	Polished metal except black oxide on ion ball and G-M tube. PV-100 white paint pattern on G-M tube.
5.	High Gain Antenna	Concave face and potted edges are Laminar x-500 green paint.
6.	Ion Chamber Thermal Shield	Laminar x-500 green paint on top and sides.
7.	High Gain Feed	PV-100 white paint pattern and polished aluminum.
8.	Solar Panel Structure	Laminar x-500 black paint.
9.	Solar Panel Boost Dampers	PV-100 white paint on cylindrical body of dampers.
10.	Omni Mast Long Damper	PV-100 white paint on cylindrical body of damper.
11.	Omni Mast Short Damper	Outer tube is black anodize.
12.	High Gain Support Structure	Polished aluminum and gold plate.
13.	MIT Plasma Probe	Unpolished gold plate on body. PV-100 white paint on top.
14.	Cosmic Dust Detector	Clear Laminar x-500 on bottom and sides of electronics. Vacuum deposited aluminum detector plate with aluminum-silicone paint pattern.

	Component	Description
15.	Sun Sensors	Cat-a-Lac black paint pattern and polished aluminum.
16.	Sun Gate	As machined aluminum.
17.	Earth Detector	Polished aluminum body. Black anodized cavity.
18.	Canopus Tracker	Polished aluminum.
19.	Sun Sensor Pedestals	Cat-a-Lac white paint on outboard surface. Polished gold plate exterior elsewhere. Cat-a-Lac black paint inside.
20.	Science Cover	Polished aluminum.
21.	High Gain Feed Support Truss	As received plastic.
22.	TV Camera	Polished gold plate and polished aluminum.
23.	Science Platform Inertial-Thermal Simulator (SPITS)	Polished aluminum.
24.	Mars Gate	Polished aluminum.
25.	Planetary Sensor	Polished gold plate and polished aluminum.
26.	Planet Scan Platform	Polished aluminum and Cat-a-Lac black paint.
27.	Planet Science Mounting	
28.	Octagon Science Installation	
29.	Science Installation 26A1 and 33A1	
30.	Trapped Radiation Detector	Polished gold plate, Cat-a-Lac white paint, and ARF-2 white paint.
31.	Separation Initiated	Polished aluminum.
32.	Pyro Arming Switch	Polished aluminum.
33.	Cosmic Ray Telescope	ARF-2 white paint on radiator.

APPENDIX VI

ERROR ANALYSIS - SUNLIT APPENDAGES

The magnetometer and ion chamber were thermally isolated from the low-gain antenna and their temperatures were primarily determined by internal power dissipation, the amount of sunlight absorbed, and their effective radiating area.

The general form of the heat balance equation for a radiatively coupled component with internal power is

$$\sigma T^4 = a S + b$$

where

T - average temperature of the body

S - solar intensity

and a and b are constants.

The constant "a" is of the form

$$a = f(\alpha_o, \epsilon_o, \mu, A_p, A)$$

where

α_o - solar absorptance

ϵ_o - emittance

μ - shielding factor of insulation

A_p - projected area

A - total area

and the constant "b" is of the form

$$b = f(P, \mu, A)$$

where

P - internal power dissipation.

By using the measured temperatures of the Mariner IV at the Earth and Mars Cruise conditions, the constants can be evaluated.

The equations are

$$\sigma T_m^4 = 0.1764S + 0.0075$$

$$\sigma T_i^4 = 0.2457S + 0.0061$$

where

T_m - magnetometer temperature

T_i - ion chamber temperature

From these equations, we can evaluate the uncertainty in the temperatures for a given uncertainty interval in either of the constants. The results are tabulated below

	Uncertainty in Temperature (F)	
	Magnetometer	Ion Chamber
$\frac{\Delta a}{a} = \pm 5\%$	$\pm$ 4F	$\pm$ 5F
$\frac{\Delta b}{b} = \pm 5\%$	$\pm$ 1.5F	$\pm$ 1.3F

The results show that a 5 percent error in scaling the surface finishes or shielding, etc., will introduce an error of approximately 5F in the temperatures of the ion chamber and magnetometer.

We can also differentiate these equations to find the influence of an uncertainty in solar intensity on the average temperatures. We have evaluated these expressions at the Mars Playback intensity and find

$$\left(\frac{\partial T}{\partial S}\right)_m = 742 \text{ K cm}^2/\text{watt}$$

$$\left(\frac{\partial T}{\partial S}\right)_i = 749 \text{ K cm}^2/\text{watt}$$

At the Mars Playback intensity the uncertainty in temperature is approximately 4F for a 5 percent change in solar intensity. The conclusion is that a "perfectly" scaled model of either the ion chamber or magnetometer would be subject to an error in temperature of $\pm$ 4F in a test chamber where the solar intensity was controlled to $\pm$ 5%.

APPENDIX VII
DISCUSSION OF CANOPUS TRACKER TESTS

The following data was obtained in the tests of the Canopus tracker made within a cold-wall vacuum bell jar. The tracker was bolted to a heated plate whose temperature was regulated to simulate the temperature boundary condition at the spacecraft frame. The following table summarizes the data. The bolt torque is measured in inch pounds, the temperatures in Fahrenheit. The Canopus temperature is T_c, the frame or lower ring temperature is T_f, and the ΔT is the temperature difference across the bolted joint. For reference, the data obtained from Mariner IV and the solar simulation tests of the TSM are also presented.

Test	Bolt Torque	T_f	T_c	ΔT	
1	5	34	5	29	Original Test Condition
2	5	58	24	34	Increased Frame Temperature
3	15	58	32	26	Increased Bolt Torque
4	15	58	31	27	Installed Baffles
5	15	58	56	2	Added Super-insulation
Mariner IV		58	55	3	
TSM Test	5	34.4	1.3	33	

The results show that the addition of two layers of super-insulation in Test 5 reduced the ΔT across the joint and the temperature of the Canopus tracker was increased to approximately the correct value.

If it is assumed that the power dissipated by the Canopus tracker arises from the internal dissipation and the heat flowing through the joint, the following equation can be used to describe the average temperature of the tracker.

$$\overline{\epsilon A}\ \sigma\ T^4 = C\ (T_f - T) + p$$

where

$\overline{\epsilon A}$ - effective radiating area (cm^2)

C - joint conductance (watts/K)

T_f - frame temperature

p - internal power

The numerical values of $\overline{\epsilon A}$ and C can be determined from experimental data obtained in two independent tests.

The following table summarizes the results of the evaluations.

	C	$\overline{\epsilon A}$
TSM (Solar Simulation Test)	0.073	66.2
TSM Test 3	0.126	66.2
TSM Test 5	0.126	10.8
Mariner IV Prototype*	0.023	9.4

Using the Mariner IV values of joint conductance and effective radiating area, we find that the rate of heat flow through the joint is less than one-third of the internal power dissipation. Therefore, the temperature of the tracker is mainly determined by the internal power and the effective radiating area, and errors in modeling the joint conductance are not as important as errors in modeling the effective area for radiation.

---

* The data for the Mariner IV was scaled by the square of the geometric scaling ratio.

The data clearly show that the radiating area of the original TSM design was in error by a factor of six. Adding the super-insulation reduced the effective area to approximately the correct value.

Two factors could have influenced the errors made in the effective area of the tracker. First, in small scale, the area of the gaps between the thermal shields becomes a larger percentage of the total area and these gaps have an effective emittance of nearly unity. Second, there may have been temperature gradients in the shield used on the prototype and the presence of temperature gradients decreases the effective radiating area because of the "fin effect." The conductive paths in the thermal shield of the TSM Canopus tracker were not scaled and, therefore, it would be possible to dissipate more power at a given internal temperature. Third, there could be a difference between the emittance of the prototype and model thermal shield. We expect this to be a remote possibility as both shields were made from polished aluminum and a factor of six in the emittance is unlikely.

On the basis of these limited test results we conclude that an error in modeling the effective radiating area of the TSM Canopus tracker led to a significant error in its temperature. Further tests will be required to determine whether an uncertainty in the emittance of the shield, the presence of a temperature gradient in the shield, or non-scaled gaps in the shield produced the errors.

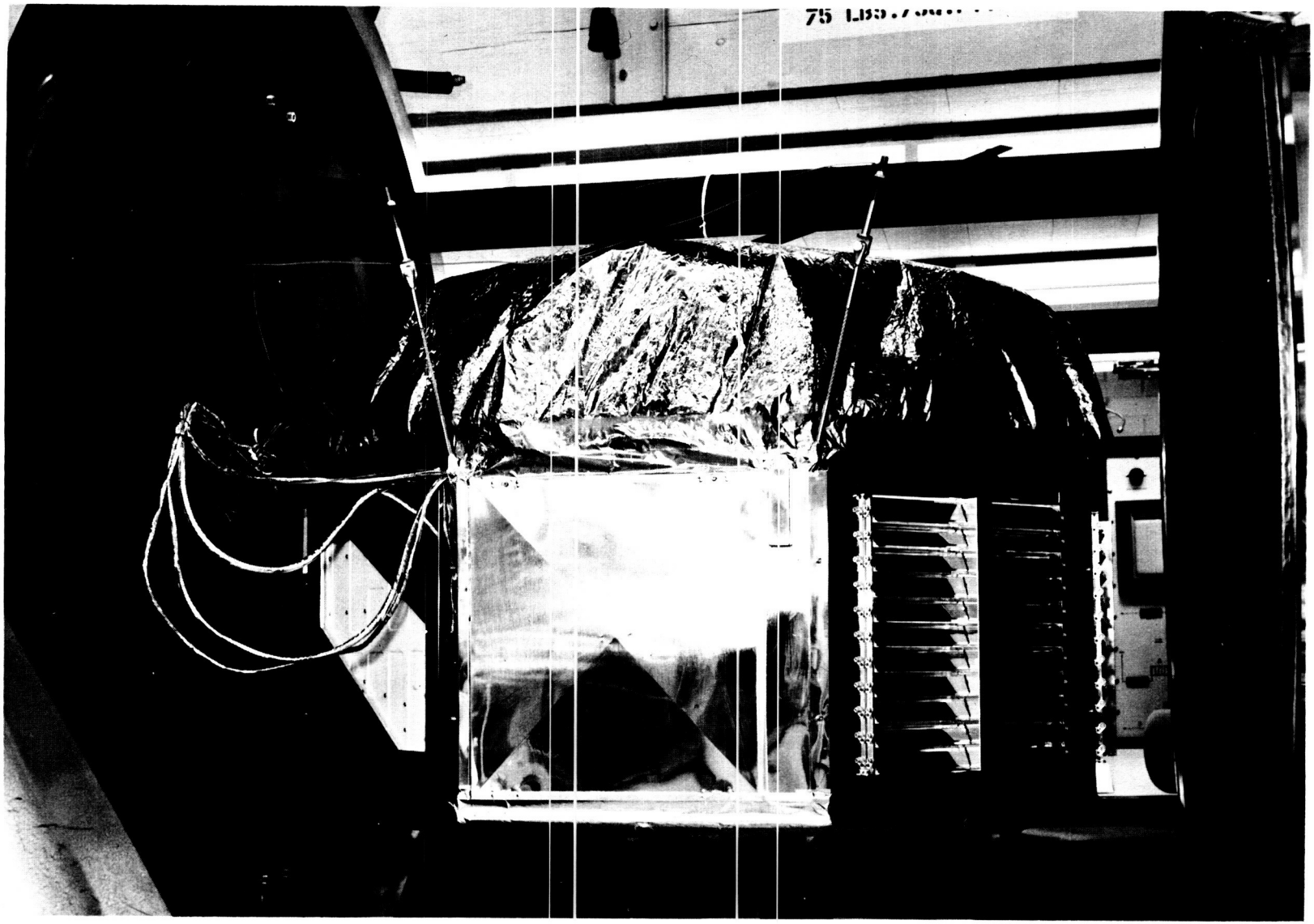

FIGURE 1 TEMPERATURE CONTROL MODEL - PHASE II CONFIGURATION

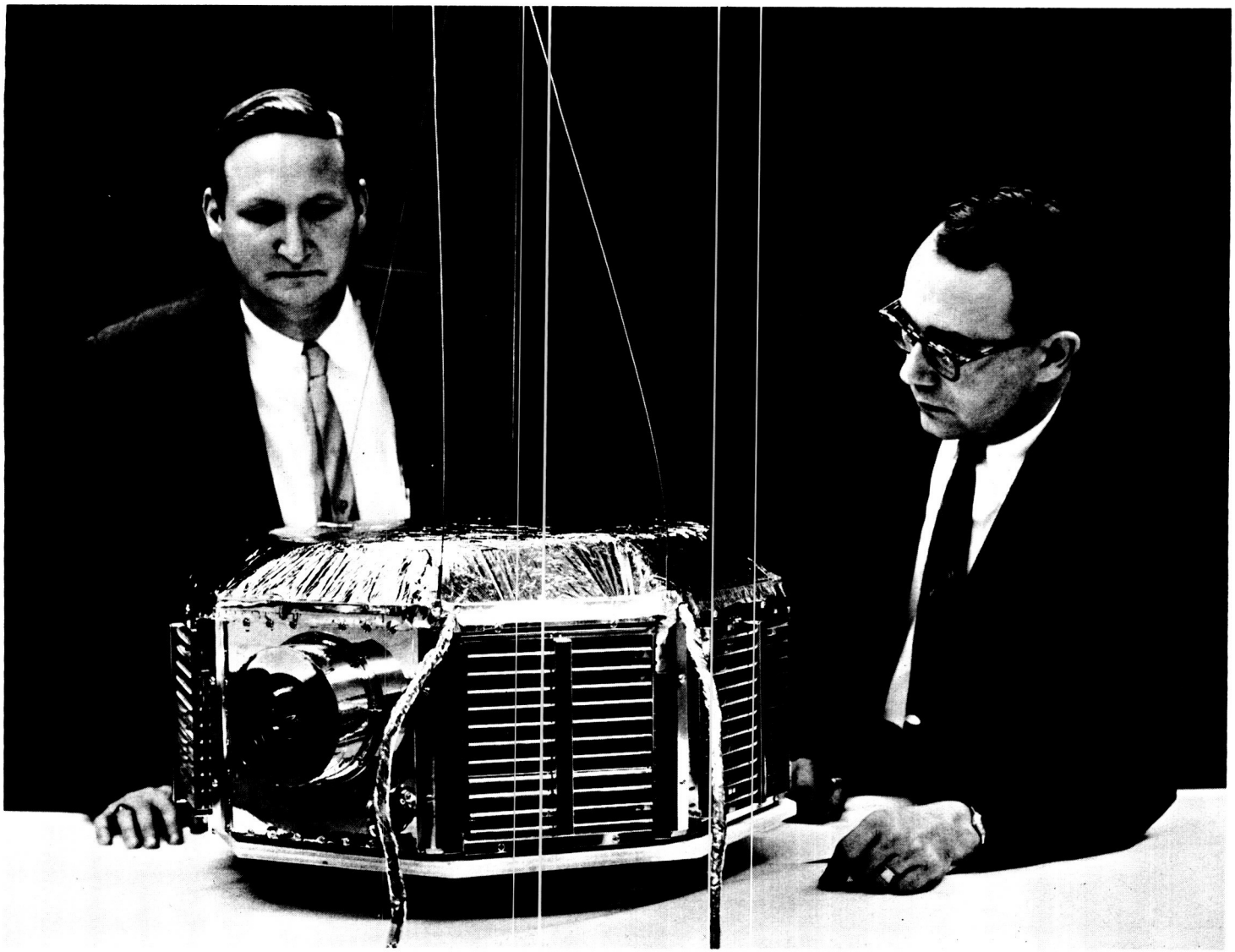

FIGURE 2 THERMAL SCALE MODEL
PHASE II CONFIGURATION

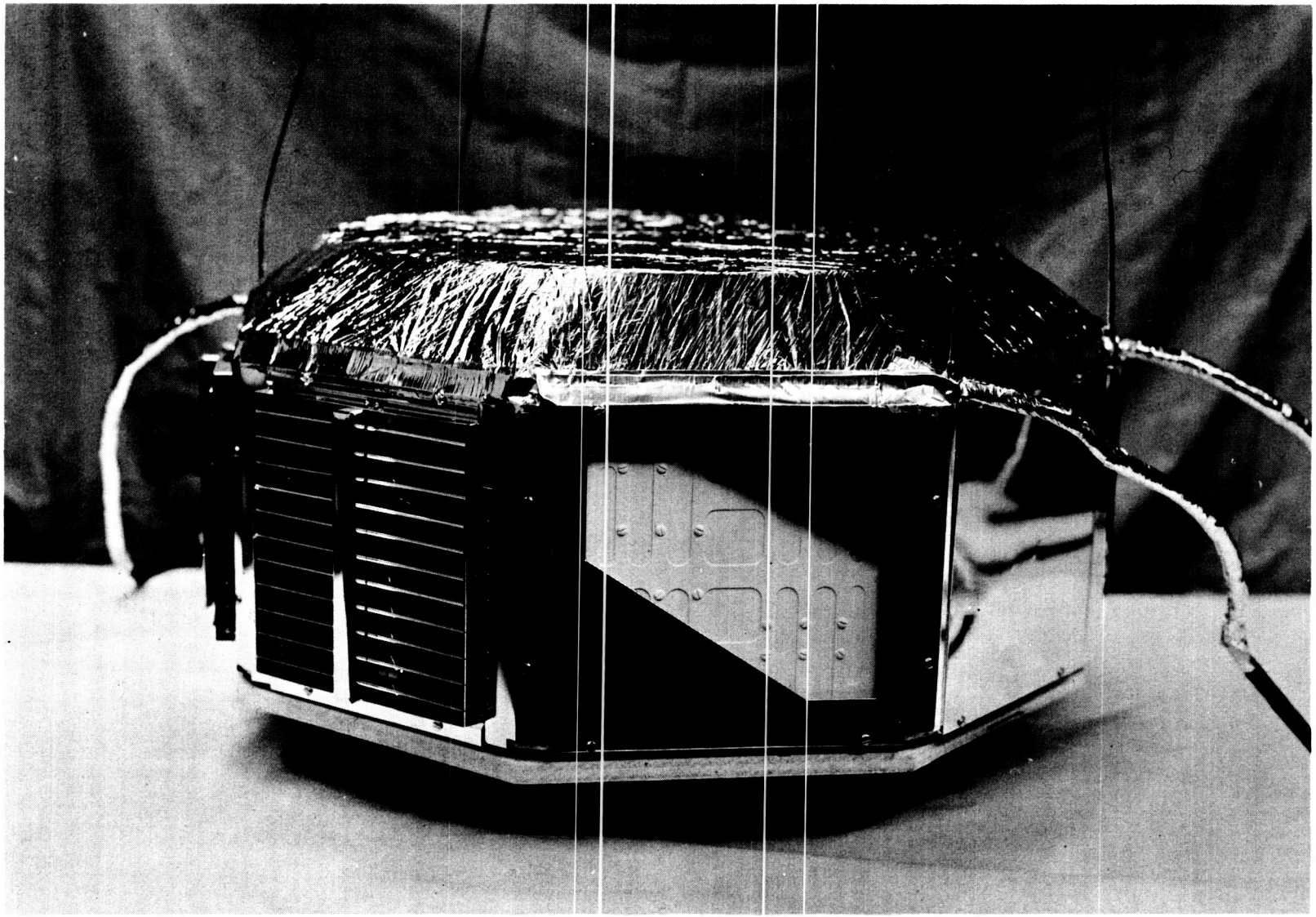

FIGURE 3 THERMAL SCALE MODEL (BAYS 5, 6, 7)

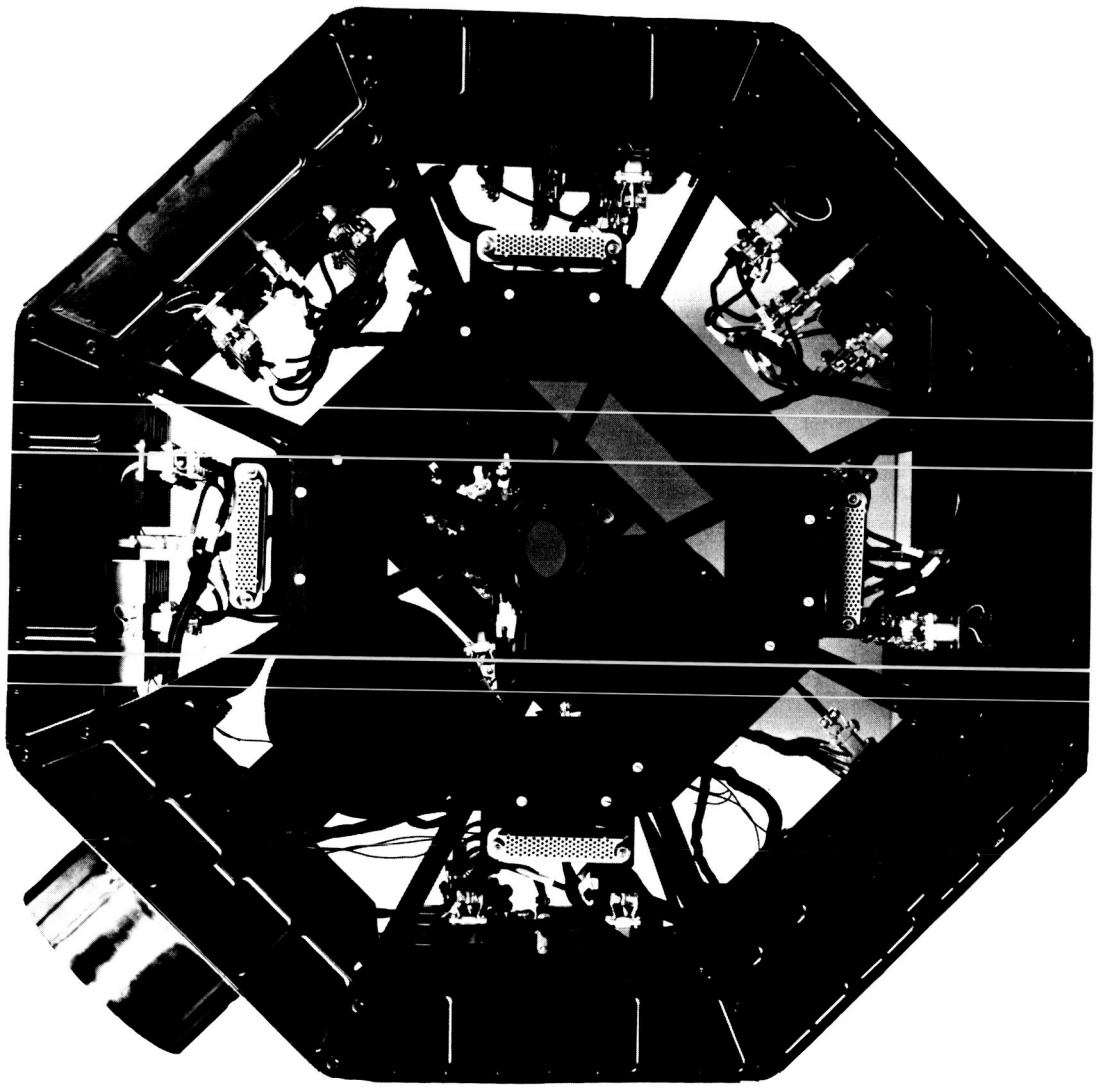

FIGURE 4 TOP VIEW - TSM BUS

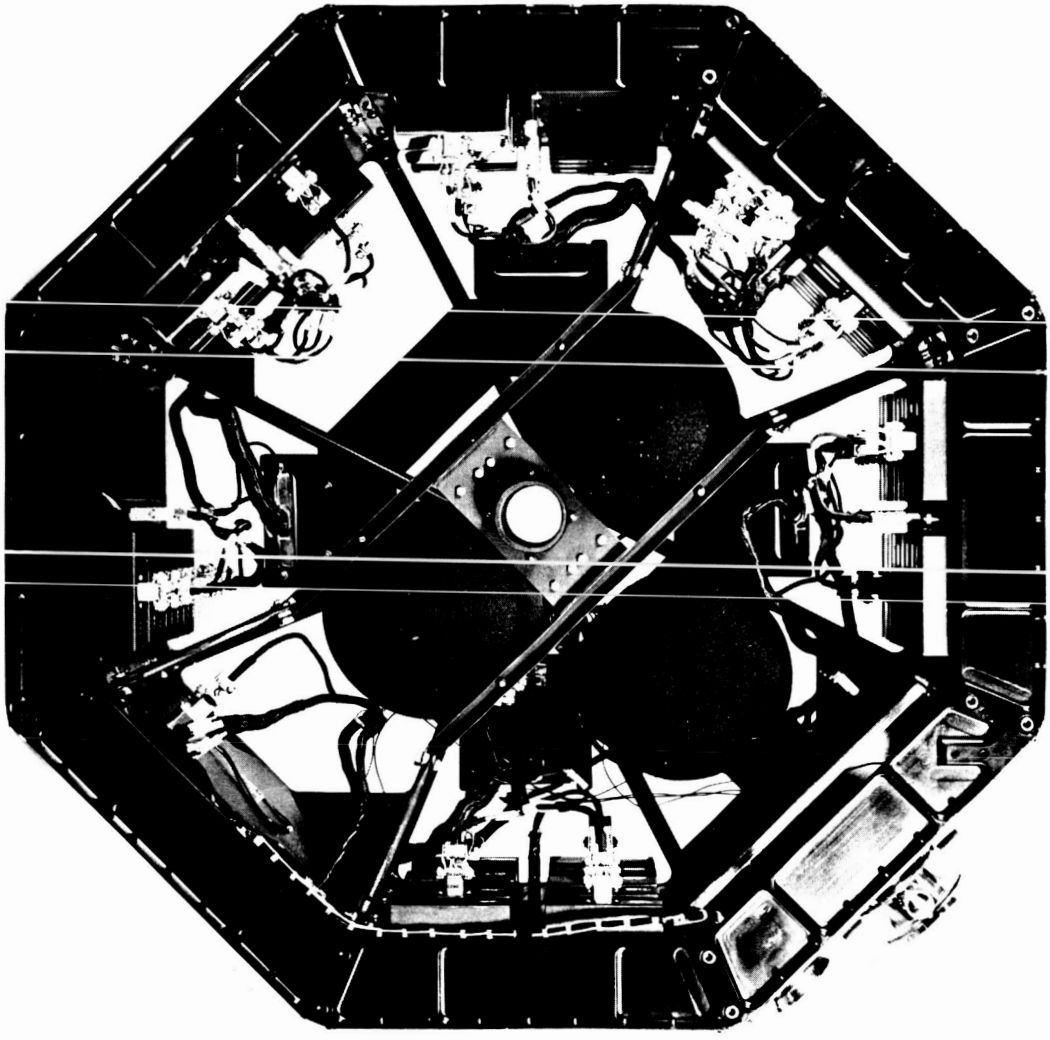

FIGURE 5 BOTTOM VIEW - TSM BUS

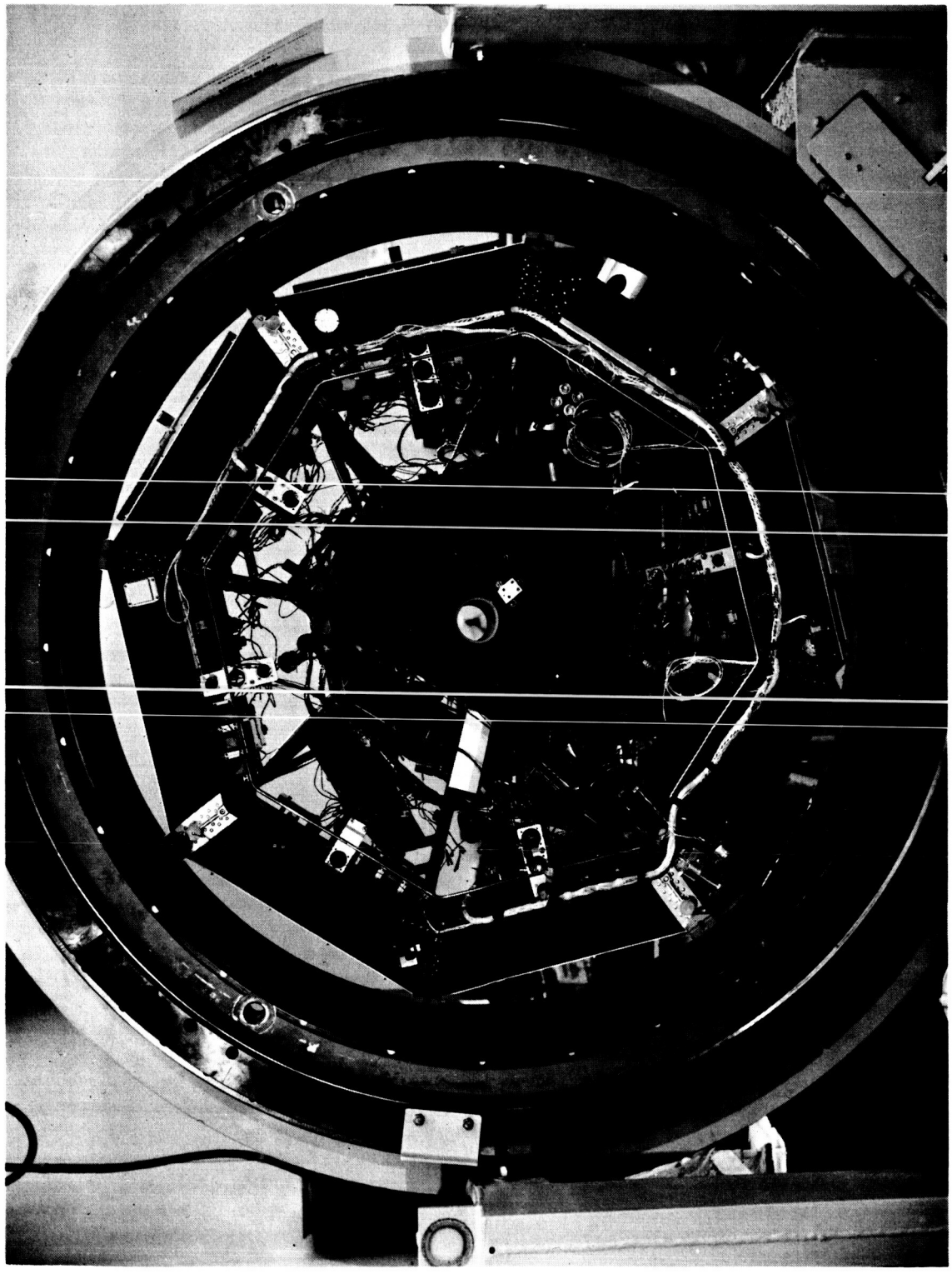

FIGURE 6 BOTTOM VIEW - TCM BUS

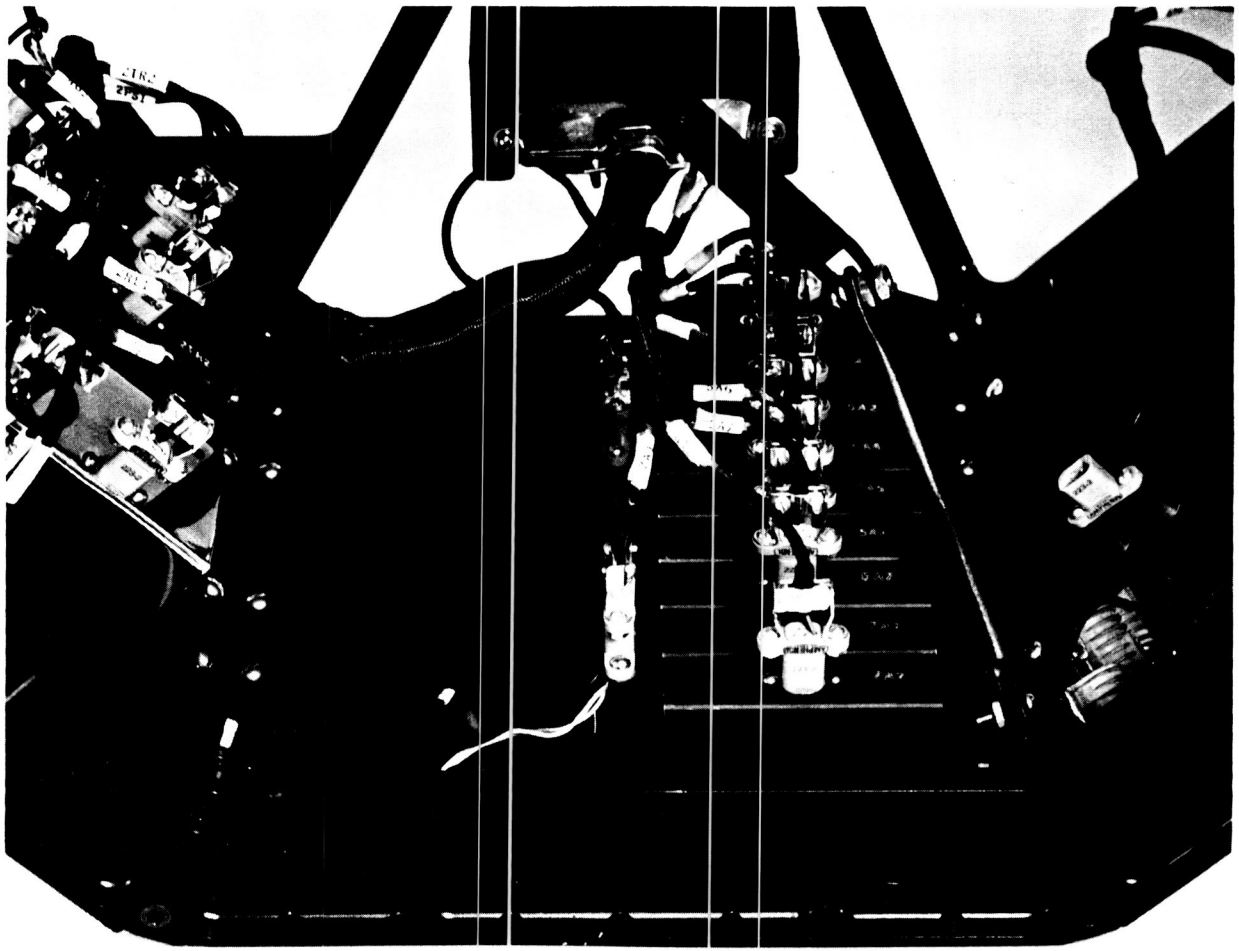

FIGURE 7 INTERIOR VIEW - TSM

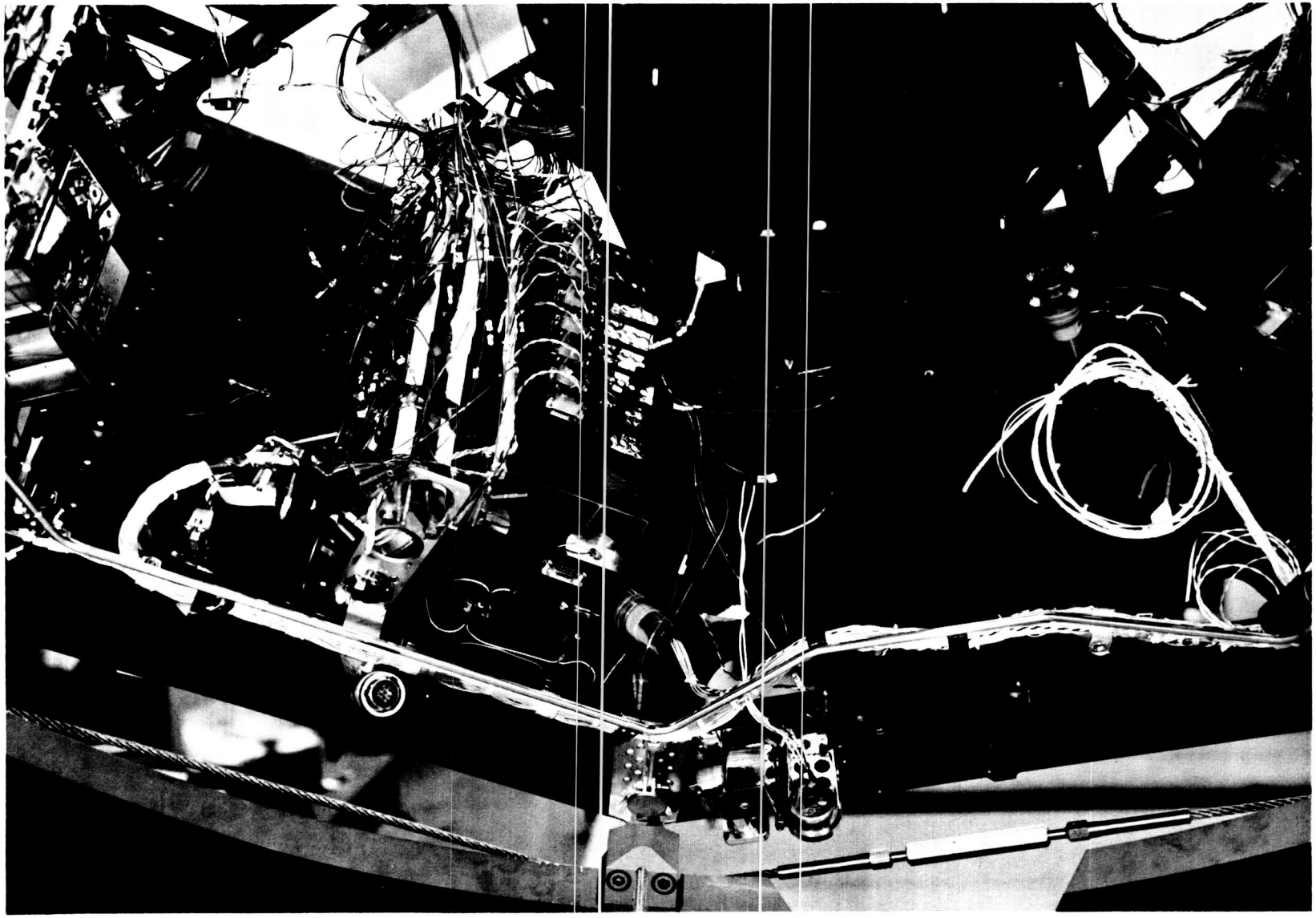

FIGURE 8 INTERIOR VIEW - TCM

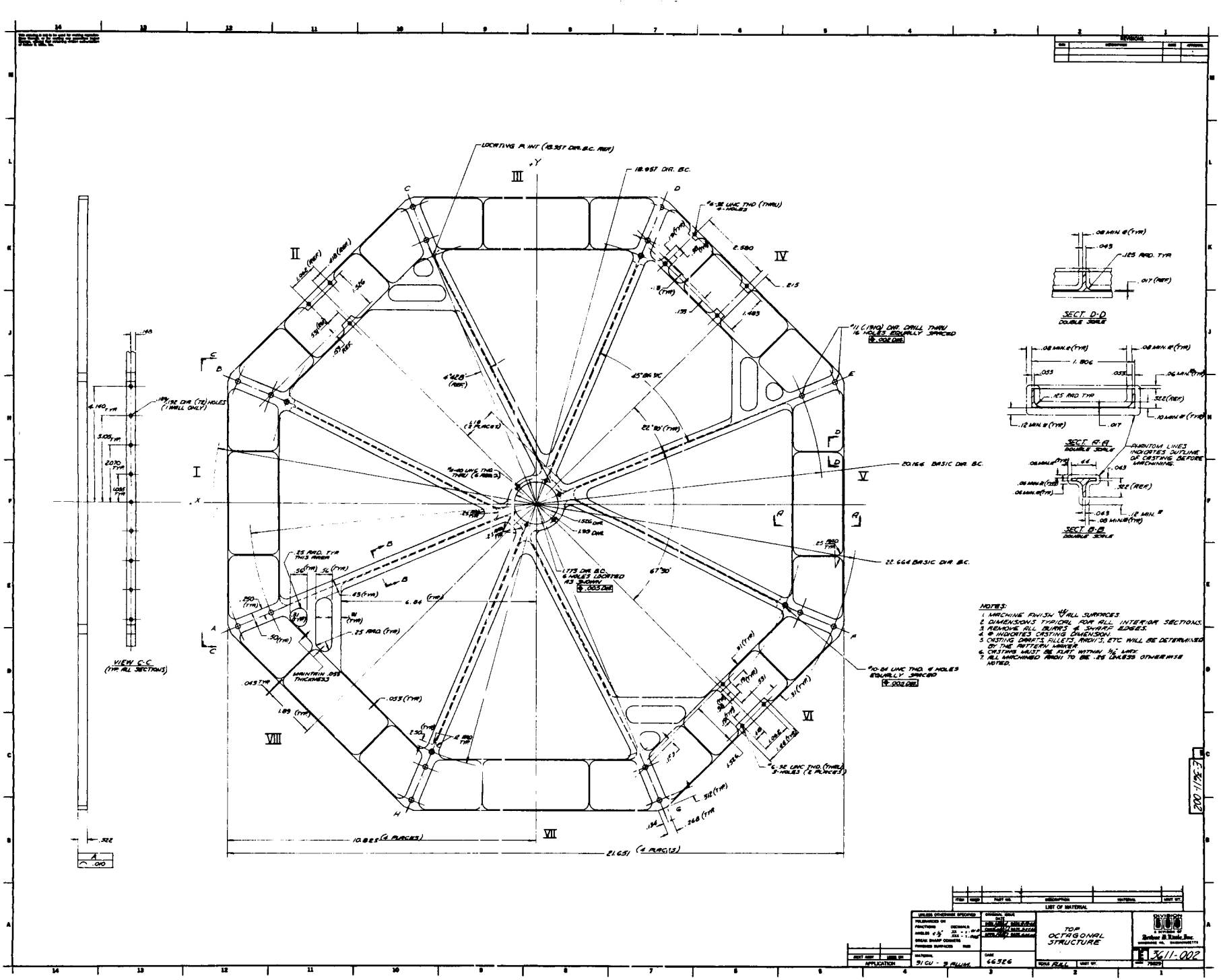

FIGURE 9 TOP OCTAGONAL FRAME

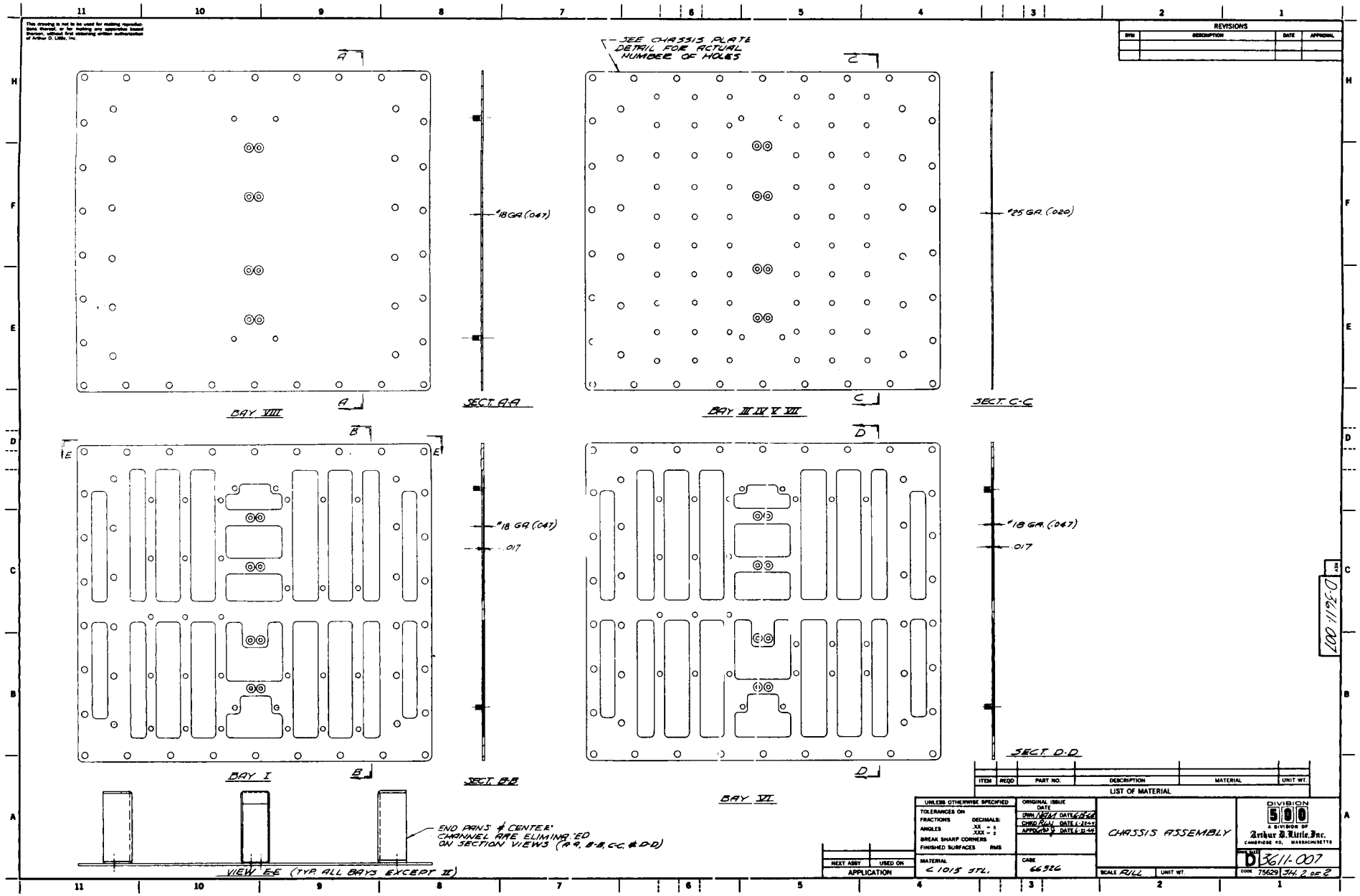

FIGURE 10 CHASSIS ASSEMBLY

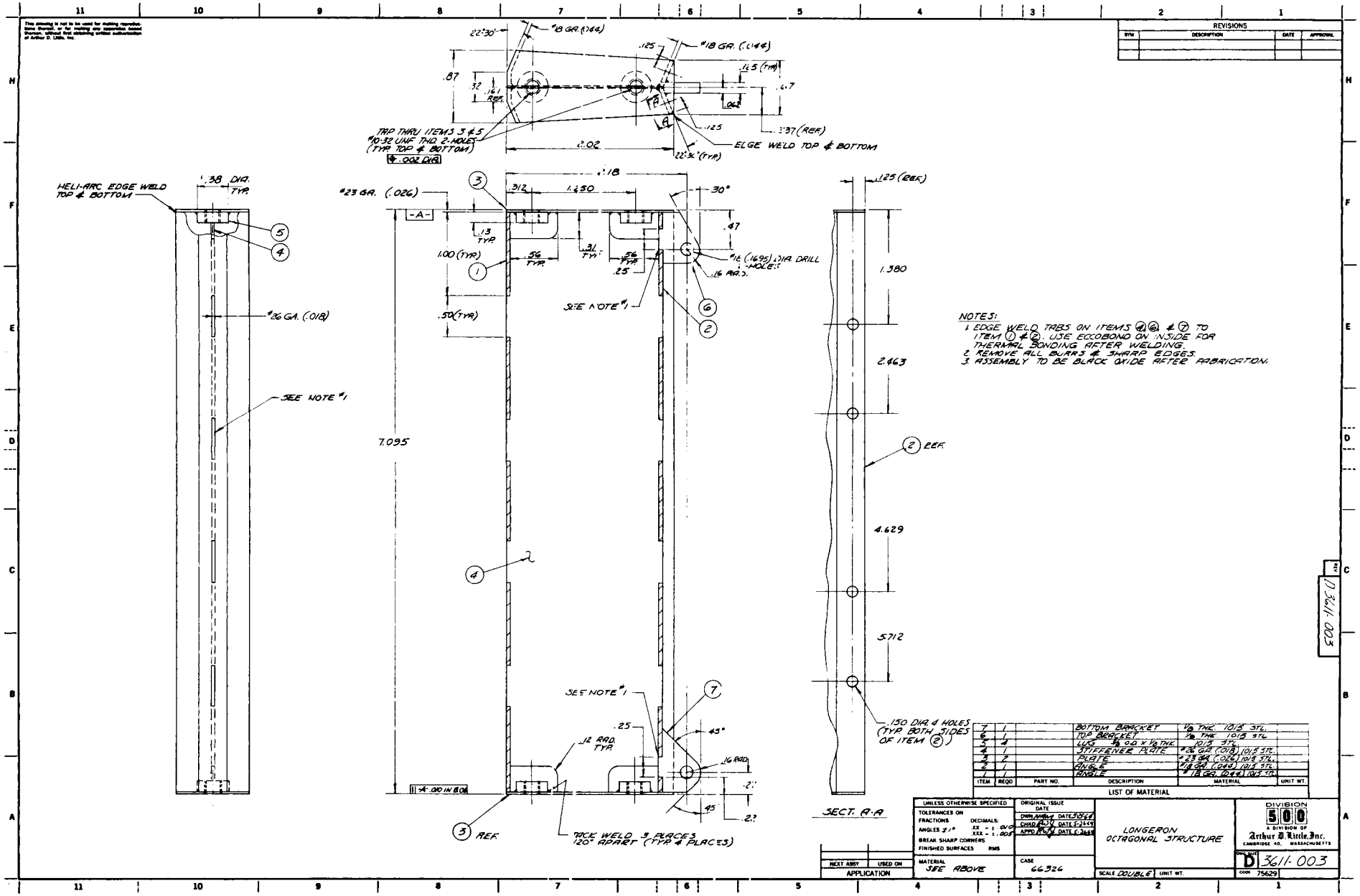

FIGURE 11 LONGERON

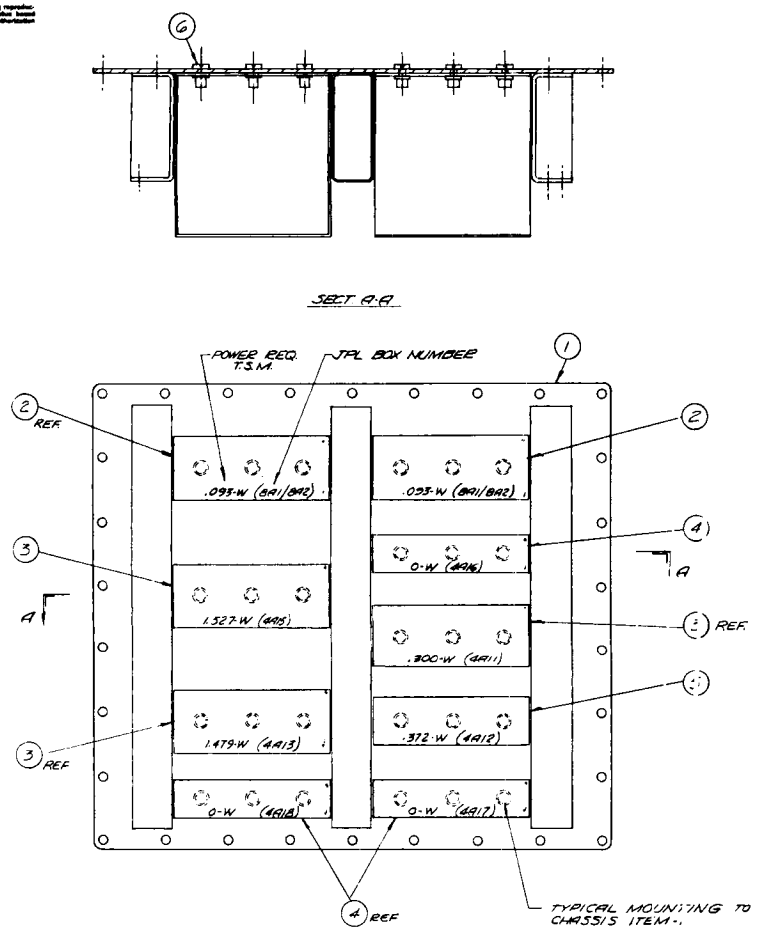

REVISIONS

SYM	DESCRIPTION	DATE	APPROVAL
A	GENERAL REVISION	8-4-64	[illegible]

ITEM	REQD	PART NO.	DESCRIPTION	MATERIAL	UNIT WT.
6	27		AN 40 MACH SCR	#4-40 x 5/16 LG STL	
5	1	C-3611-005-2	POWER MODULE #1		
4	3	B-3611-010-1	POWER MODULE #2		
3	3	C-3611-005-1	POWER MODULE #1		
2	2	B-3611-010-3	POWER MODULE #2		
1	1	D-3611-007	CHASSIS ASSEM.	BAY I	

LIST OF MATERIAL

UNLESS OTHERWISE SPECIFIED
TOLERANCES ON FRACTIONS DECIMALS: XX ± .1, XXX ± .1
ANGLES
BREAK SHARP CORNERS
FINISHED SURFACES Rms
MATERIAL
NEXT ASSY. USED ON
APPLICATION

ORIGINAL ISSUE DATE
DWN [illegible] DATE 6-12-64
CHKD [illegible] DATE 6-12-64
APPD [illegible] DATE 6-12-64
CASE 66326

PACKAGING ASSEMBLY BAY I
SCALE FULL UNIT WT.

DIVISION 500 A DIVISION OF Arthur D. Little, Inc. CAMBRIDGE 40, MASSACHUSETTS
SIZE D 3611-016
CODE 75629

D-3611-016

FIGURE 12 PACKAGING ASSEMBLY BAY I

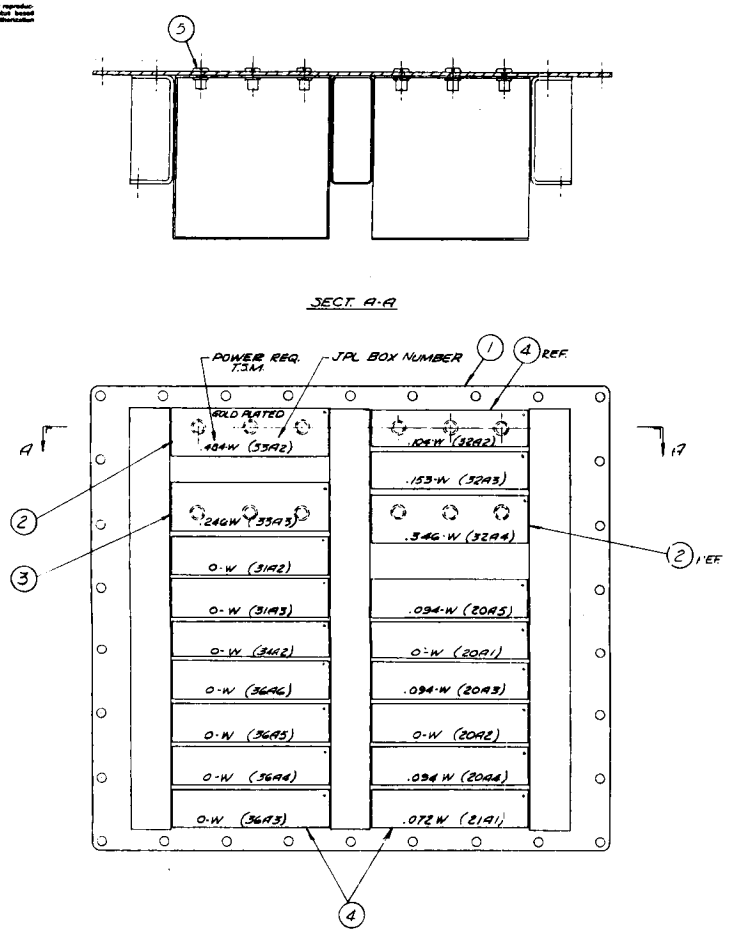

REVISIONS			
SYM	DESCRIPTION	DATE	APPROVAL
A	GENERAL REVISION	8-6-64	[illegible]

ITEM	REQD	PART NO.	DESCRIPTION	MATERIAL	UNIT WT.
5	54		PAN HD. MACH. SCR. #4-40 x 5/16 LG. STL.		
4	15	D-3611-010-1	POWER MODULE #2		
3	1	C-3611-005-4	POWER MODULE #1		
2	2	C-3611-005-3	POWER MODULE #1		
1	1	D-3611-007	CHASSIS ASSEM.	BAY III	

LIST OF MATERIAL

UNLESS OTHERWISE SPECIFIED
TOLERANCES ON FRACTIONS DECIMALS: ANGLES .XX ± .1, .XXX ± .1
BREAK SHARP CORNERS
FINISHED SURFACES RMS
MATERIAL

ORIGINAL ISSUE DATE
DWN W.B.M. DATE 6-5-64
CHKD [illegible] DATE 6-24-64
APPD R.W.S. DATE 6-24-64
CASE 66326

NEXT ASSY | USED ON
APPLICATION

PACKAGING ASSEMBLY BAY III

SCALE FULL UNIT WT.

DIVISION 500
A DIVISION OF Arthur D. Little, Inc.
CAMBRIDGE 40, MASSACHUSETTS

Dwg. Size D 3611-011
CODE 75629

REV. A D 3611-011

FIGURE 13 PACKAGING ASSEMBLY BAY III

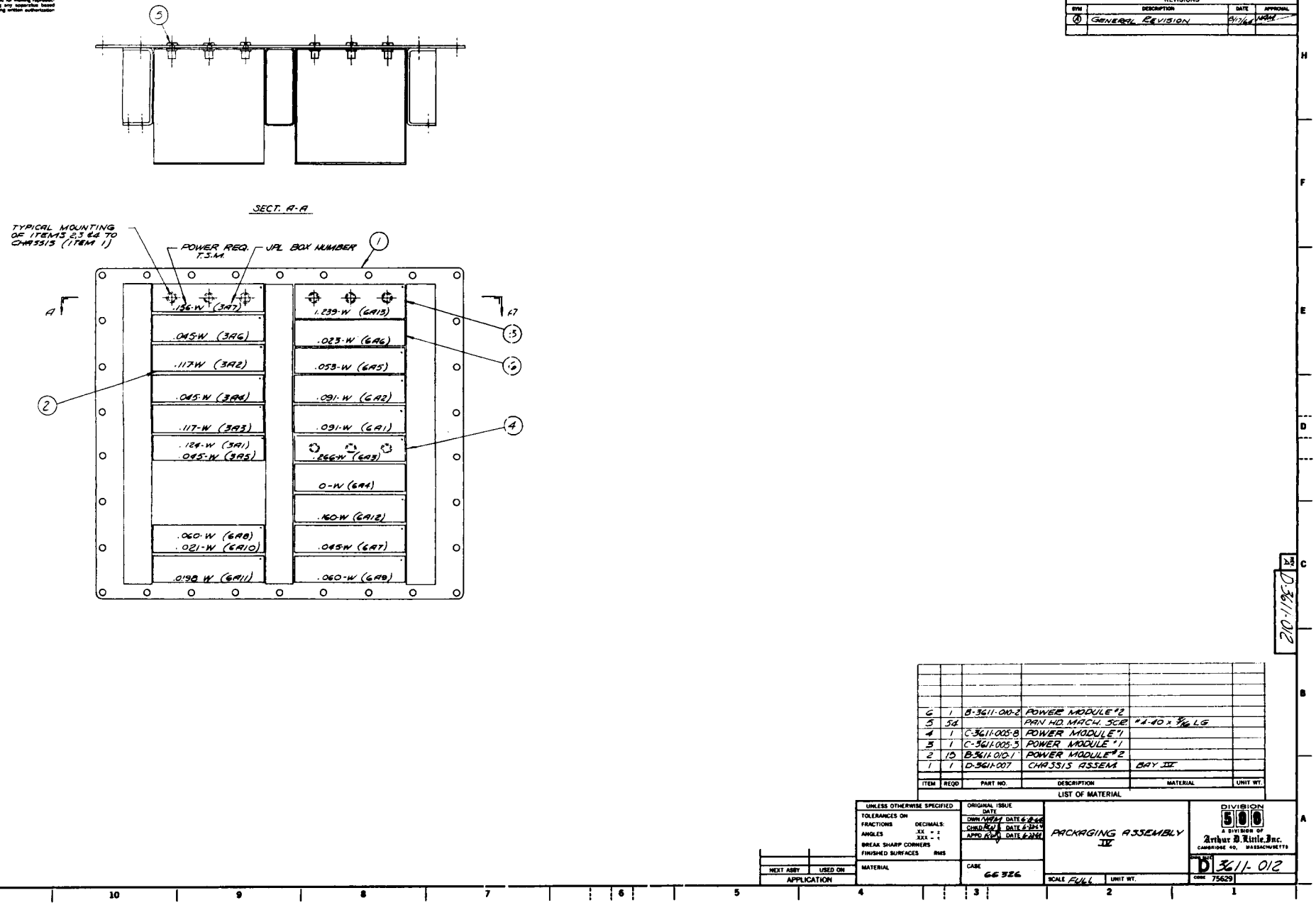

SYM	REVISIONS DESCRIPTION	DATE	APPROVAL
A	GENERAL REVISION	6/17/64	

ITEM	REQD	PART NO.	DESCRIPTION	MATERIAL	UNIT WT.
6	1	B-3611-010-2	POWER MODULE #2		
5	54		PAN HD. MACH. SCR.	#4-40 x 3/16 LG	
4	1	C-3611-005-8	POWER MODULE #1		
3	1	C-3611-005-3	POWER MODULE #1		
2	15	B-3611-010-1	POWER MODULE #2		
1	1	D-3611-007	CHASSIS ASSEM.	BAY IV	

LIST OF MATERIAL

UNLESS OTHERWISE SPECIFIED
TOLERANCES ON FRACTIONS DECIMALS: XX = ± ANGLES XXX = ±
BREAK SHARP CORNERS
FINISHED SURFACES rms
MATERIAL

ORIGINAL ISSUE DATE
DWN DATE 6-8-64
CHKD DATE 6-24-64
APPD DATE 6-24-64

CAGE 66326

NEXT ASSY | USED ON
APPLICATION

PACKAGING ASSEMBLY IV

SCALE FULL | UNIT WT.

DIVISION 500
A DIVISION OF Arthur D. Little, Inc.
CAMBRIDGE 40, MASSACHUSETTS

SIZE D | 3611-012
CODE 75629

D-3611-012

FIGURE 14 PACKAGING ASSEMBLY BAY IV

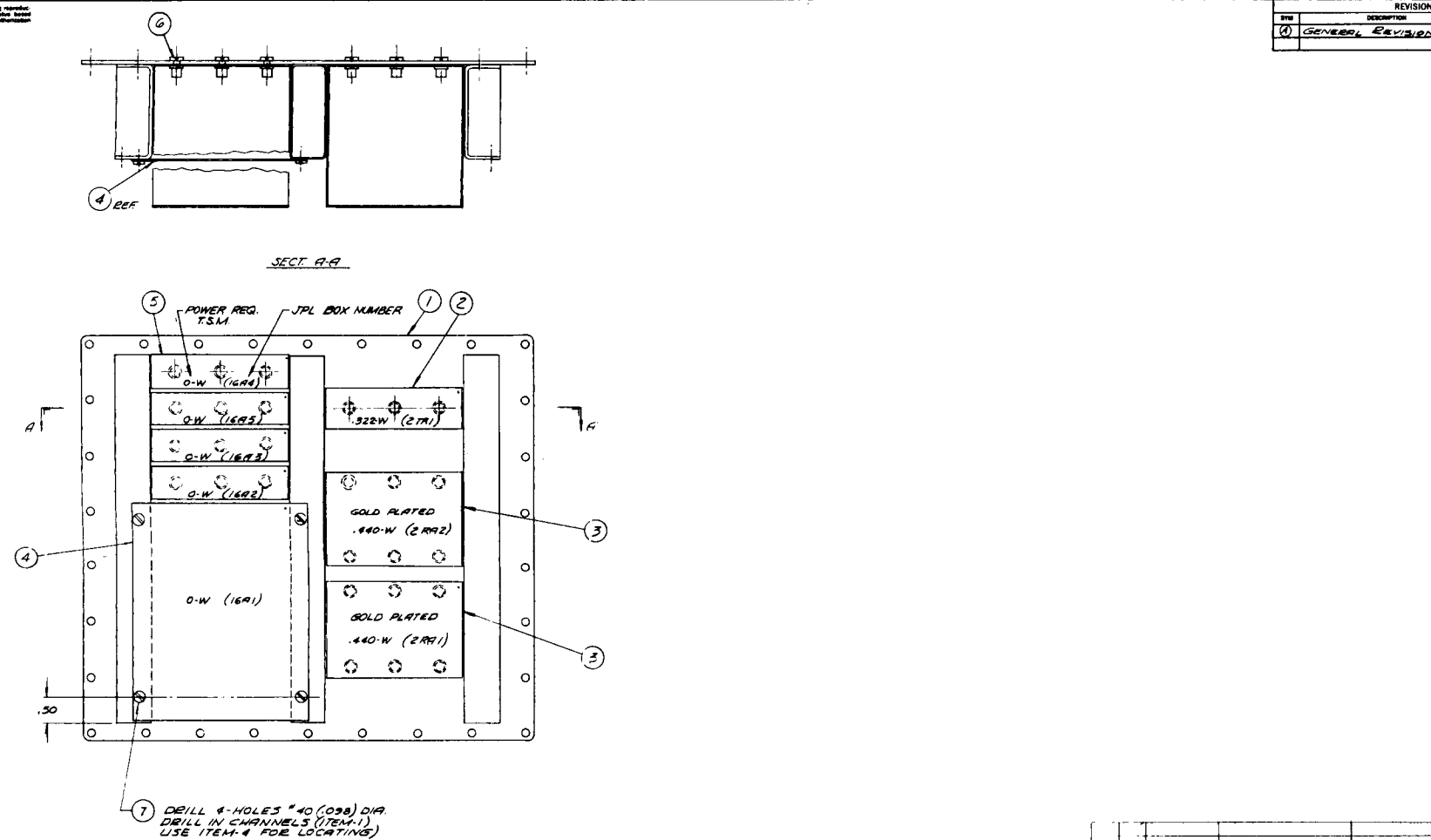

REVISIONS			
SYM	DESCRIPTION	DATE	APPROVAL
A	GENERAL REVISION	8-17-67	

ITEM	REQD	PART NO.	DESCRIPTION	MATERIAL	UNIT WT.
7	4		TAPPING SCR PAN HD.	#4 x 3/8 LG. STL	
6	27		PAN HD. MACH. SCR	#4-40 x 7/16 LG. STL	
5	4	D-3611-010.1	POWER MODULE #2		
4	1	B-3611-017	POWER MODULE #3		
3	2	C-3611-005.3	POWER MODULE #1		
2	1	C-3611-005.2	POWER MODULE #1		
1	1	D-3611-007	CHASSIS ASSEM.	BAY V	

LIST OF MATERIAL

UNLESS OTHERWISE SPECIFIED
TOLERANCES ON FRACTIONS DECIMALS: .XX ± .1, .XXX ± .1
ANGLES ±
BREAK SHARP CORNERS
FINISHED SURFACES RMS
MATERIAL

ORIGINAL ISSUE DATE
DWN APPD DATE 6-22-67
CHKD APPD DATE 6-22-67
APPD DATE 6-22-67

CASE 66326

NEXT ASSY | USED ON
APPLICATION

PACKAGING ASSEMBLY BAY V

SCALE FULL | UNIT WT.

DIVISION 500
A DIVISION OF Arthur D. Little, Inc.
CAMBRIDGE 40, MASSACHUSETTS
SIZE D | 3611-013
CODE 75629

D3611-013

FIGURE 15 PACKAGING ASSEMBLY BAY V

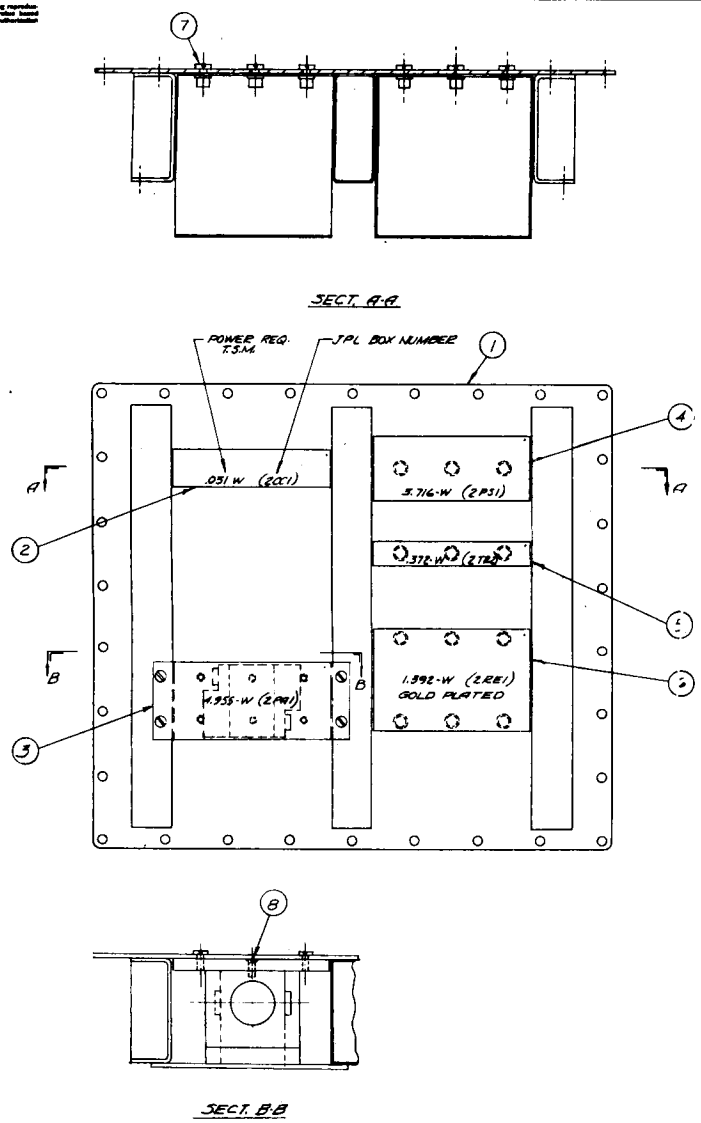

REVISIONS

SYM	DESCRIPTION	DATE	APPROVAL
(4)	GENERAL REVISION	3-17-64	

ITEM	REQD	PART NO.	DESCRIPTION	MATERIAL	UNIT WT.
8	2		FLAT HD. MACH. SCR. #4-40 x 5/16 LG. STL.		
7	19		PAN HD. MACH. SCR. #4-40 x 5/16 LG. STL.		
6	1	C-3611-005-7	POWER MODULE #1		
5	1	C-3611-005-6	POWER MODULE #1		
4	1	C-3611-005-1	POWER MODULE #1		
3	1	C-3611-023	POWER MODULE #6		
2	1	B-3611-010-1	POWER MODULE #2		
1	1	D-3611-007	CHASSIS ASSEM.	BAY VI	

LIST OF MATERIAL

UNLESS OTHERWISE SPECIFIED
TOLERANCES ON FRACTIONS DECIMALS: ANGLES XX ± 1, XXX ± .1
BREAK SHARP CORNERS
FINISHED SURFACES RMS
MATERIAL

ORIGINAL ISSUE DATE
DWN ARTM DATE 6-3-61
CHKD AJL DATE 6-29-61
APPD RSU DATE 6-29-61

CASE 66926

PACKAGING ASSEMBLY BAY VI

SCALE FULL UNIT WT.

DIVISION 500 A DIVISION OF Arthur D. Little, Inc. CAMBRIDGE 40, MASSACHUSETTS

SIZE D 3611-014 CODE 75629

NEXT ASSY USED ON APPLICATION

D-3611-014

FIGURE 16 PACKAGING ASSEMBLY BAY VI

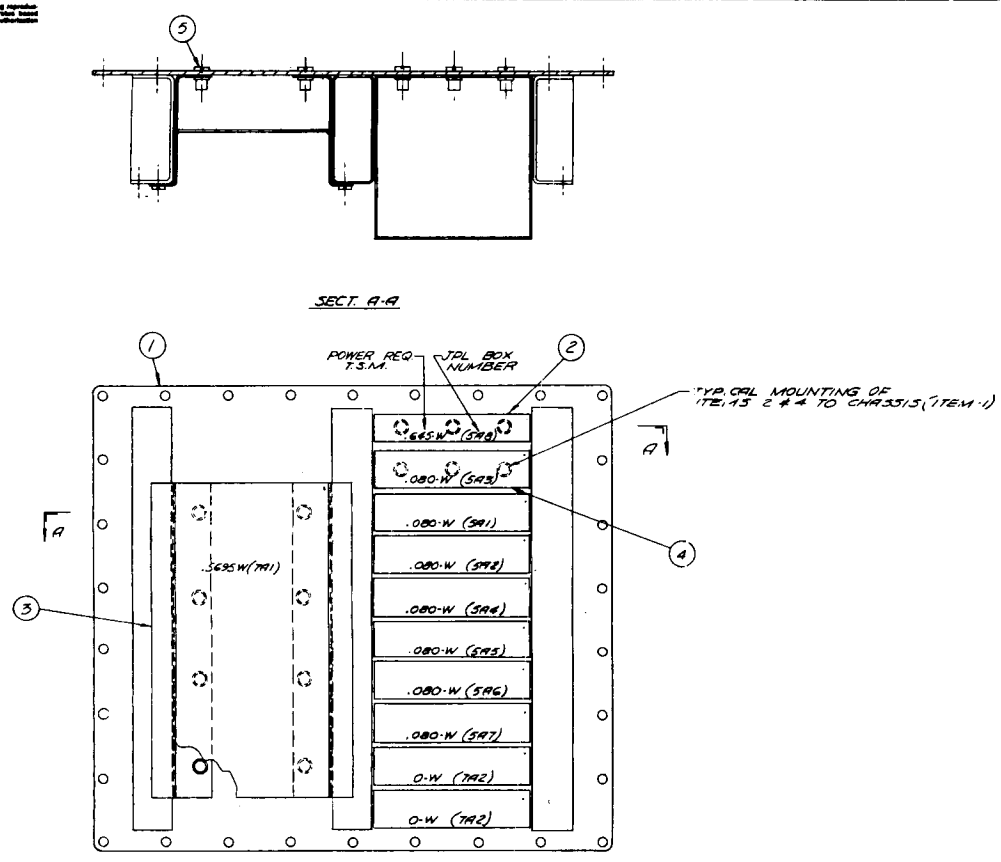

REVISIONS

SYM	DESCRIPTION	DATE	APPROVAL
A	GENERAL REVISION	5-17-66	

ITEM	REQD	PART NO.	DESCRIPTION	MATERIAL	UNIT WT.
5	38		PAN HD. MACH. SCR. #4-40 x 3/16 LG.		
4	3	B-3611-010-1	POWER MODULE #2		
3	1	B-3611-019	POWER MODULE #3		
2	1	C-3611-005-6	POWER MODULE #1		
1	1	D-3611-007	CHASSIS ASSEM.	BAY III	

LIST OF MATERIAL

UNLESS OTHERWISE SPECIFIED	ORIGINAL ISSUE DATE	PACKAGING ASSEMBLY BAY III	DIVISION 500 A DIVISION OF Arthur D. Little, Inc. CAMBRIDGE 40, MASSACHUSETTS
TOLERANCES ON FRACTIONS DECIMALS: XX ± XXX ± ANGLES BREAK SHARP CORNERS FINISHED SURFACES RMS	DWN MAH DATE 5-17-66 CHKD DATE 5-21-66 APPD DATE 5-31-66		SIZE D 3611-015 CODE 75629
NEXT ASSY USED ON APPLICATION	MATERIAL	CASE 66526	SCALE FULL UNIT WT.

D-3611-015

FIGURE 17 PACKAGING ASSEMBLY BAY VII

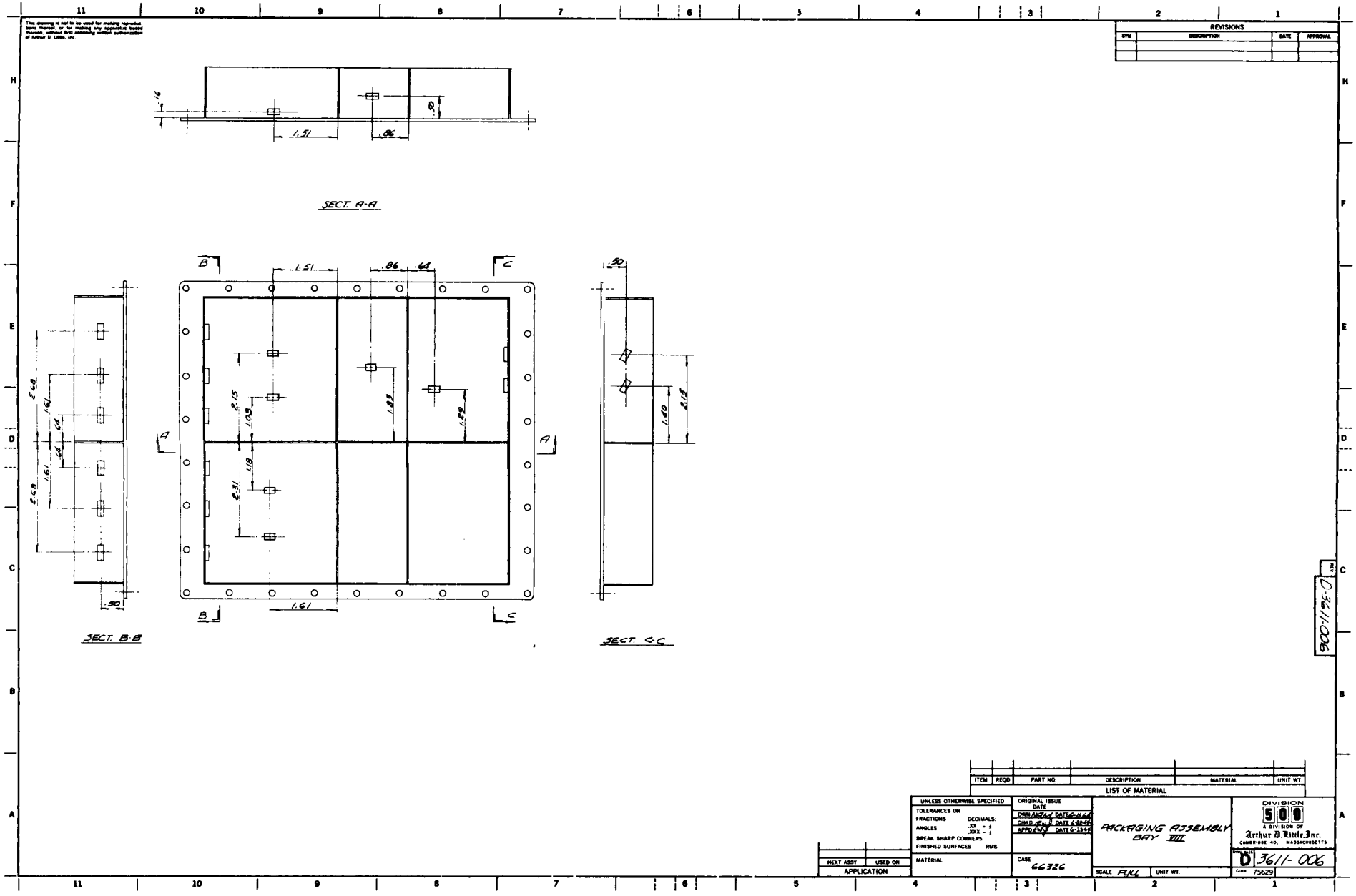

FIGURE 18 PACKAGING ASSEMBLY BAY VIII

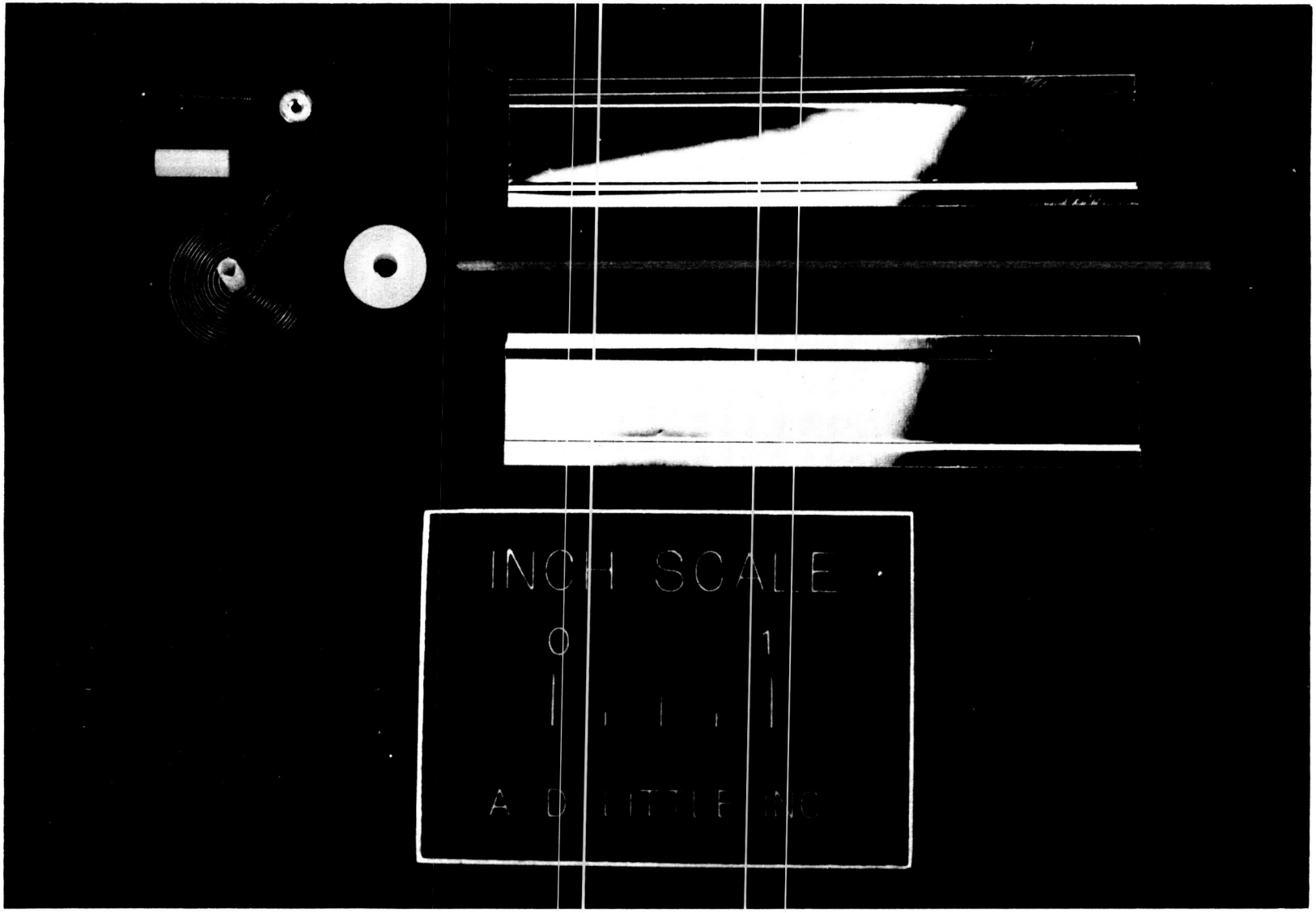

FIGURE 19 THERMAL CONTROL LOUVER BLADE ASSEMBLY

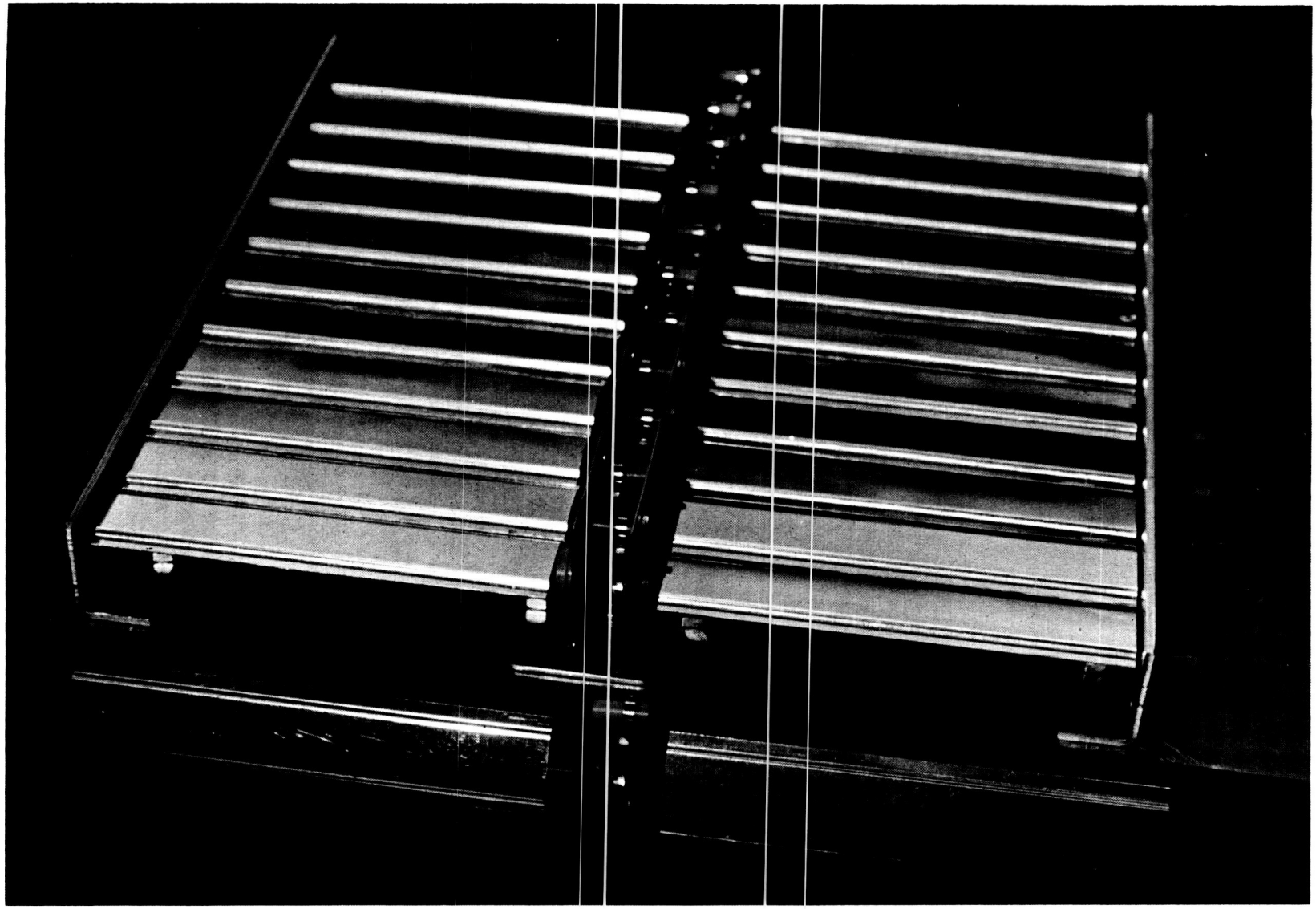

FIGURE 20 THERMAL CONTROL LOUVER ASSEMBLY

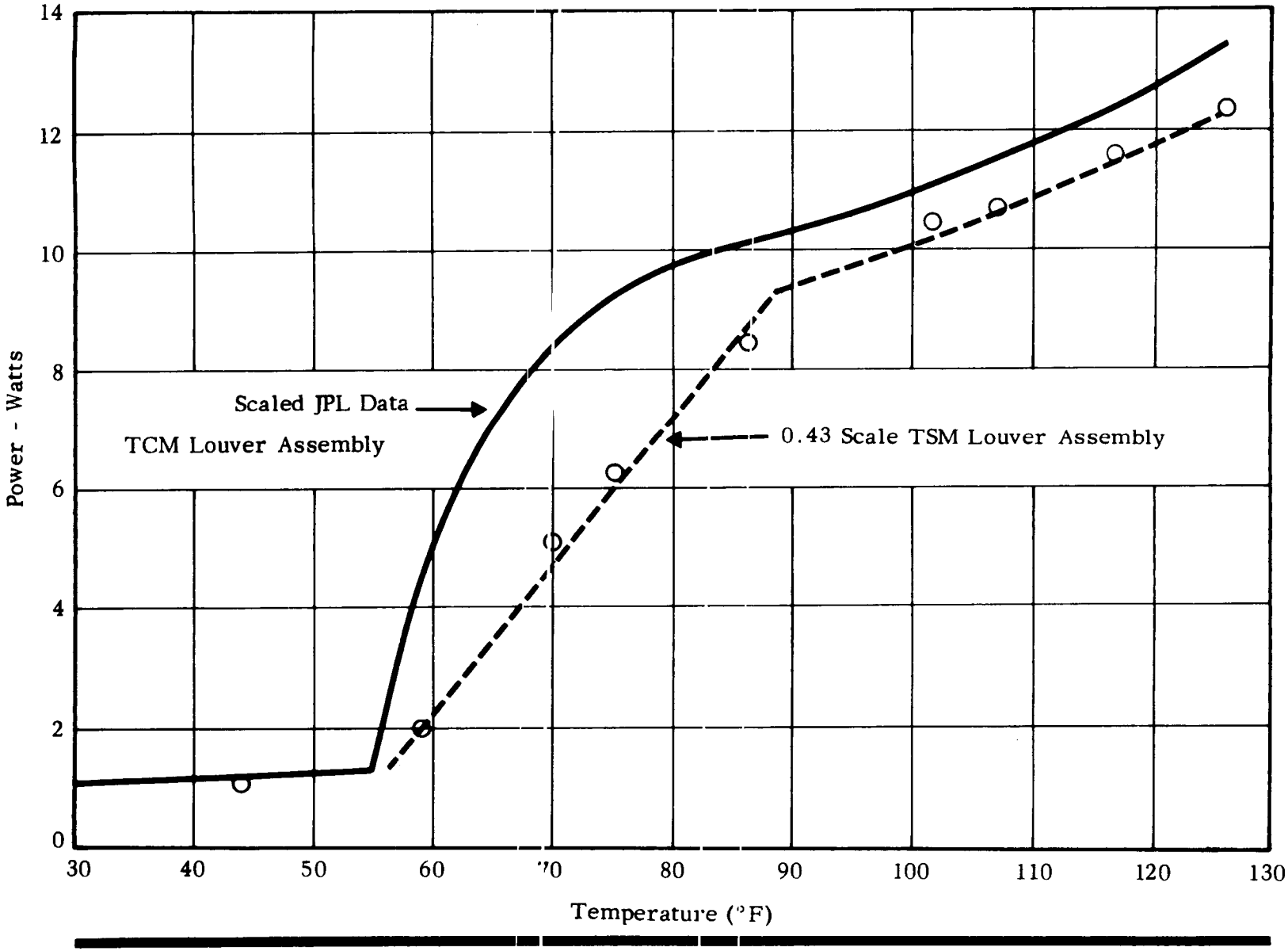

FIGURE 21 THERMAL CONTROL LOUVER PERFORMANCE

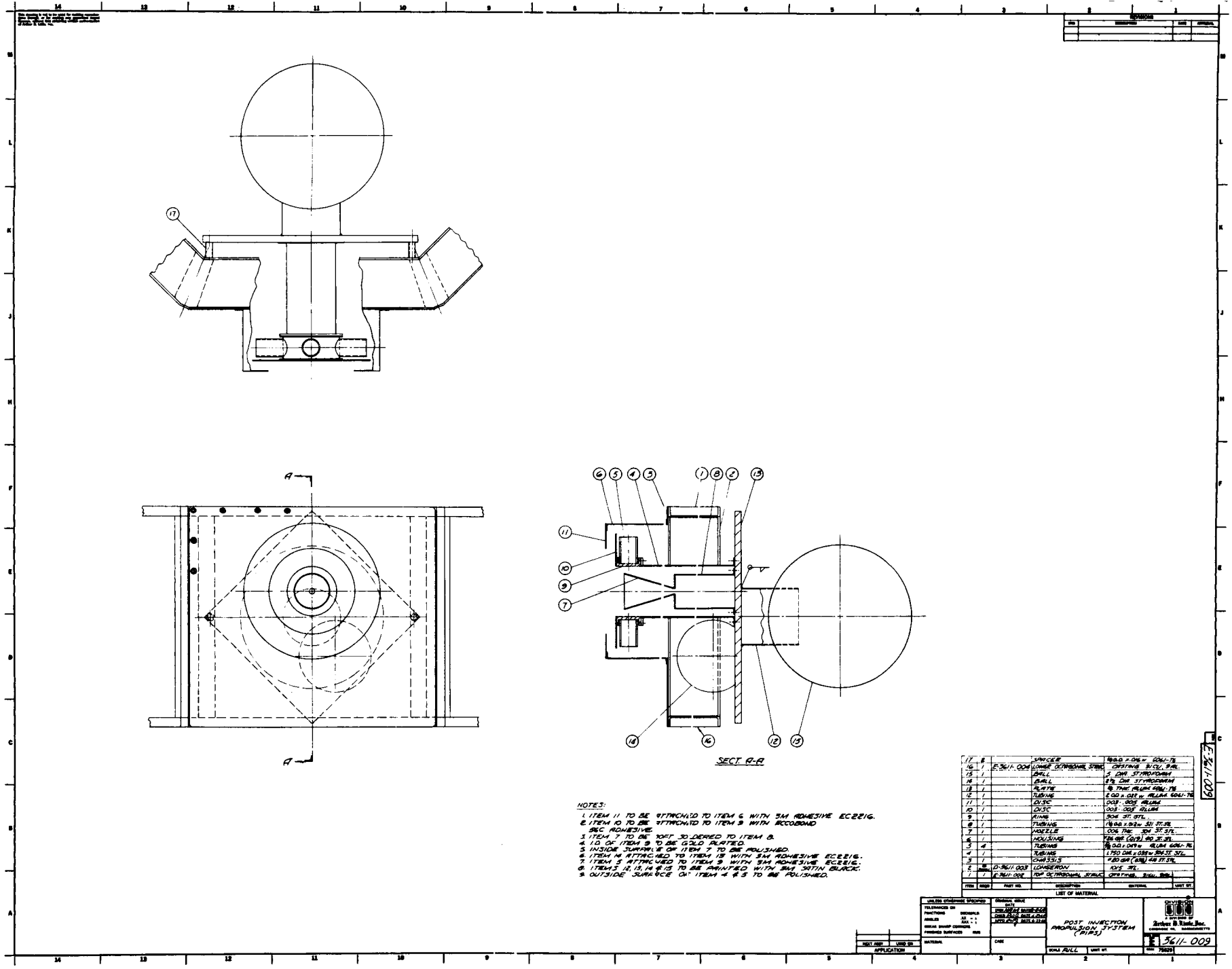

FIGURE 22 POST INJECTION PROPULSION SYSTEM

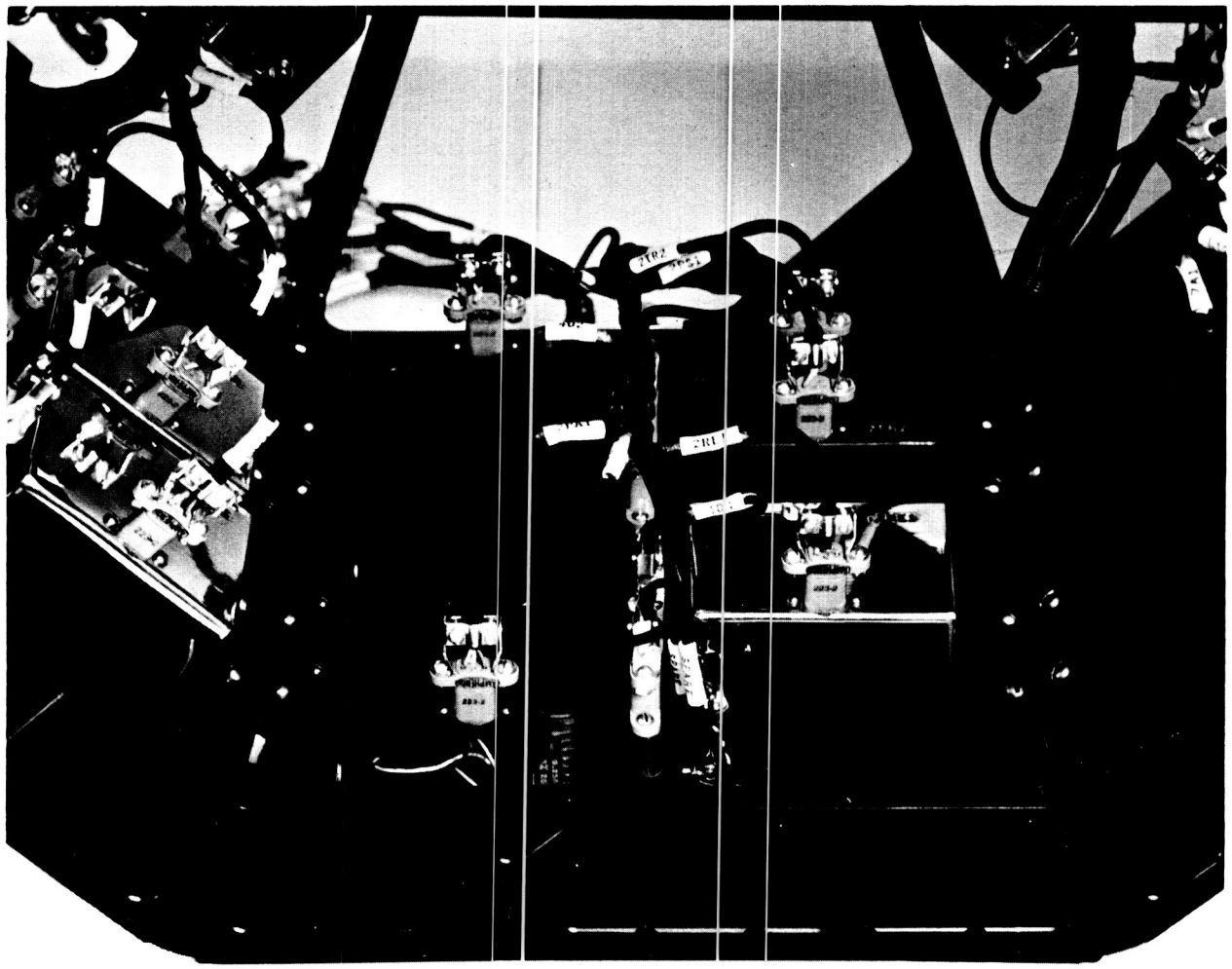

FIGURE 23 BAY 6 CONFIGURATION - TEST 3

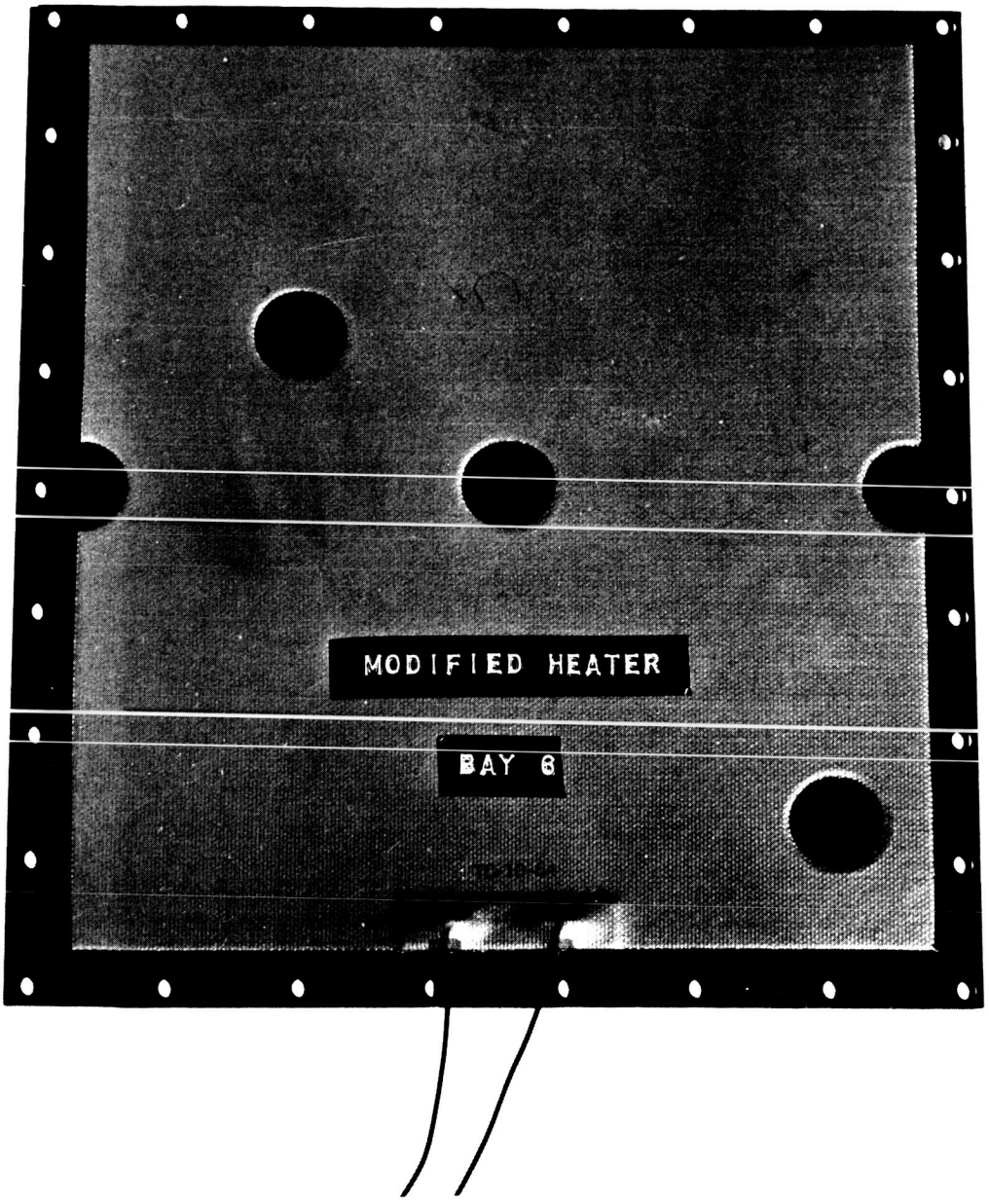

FIGURE 24 MODIFIED BAY 6 CONFIGURATION - TEST 4

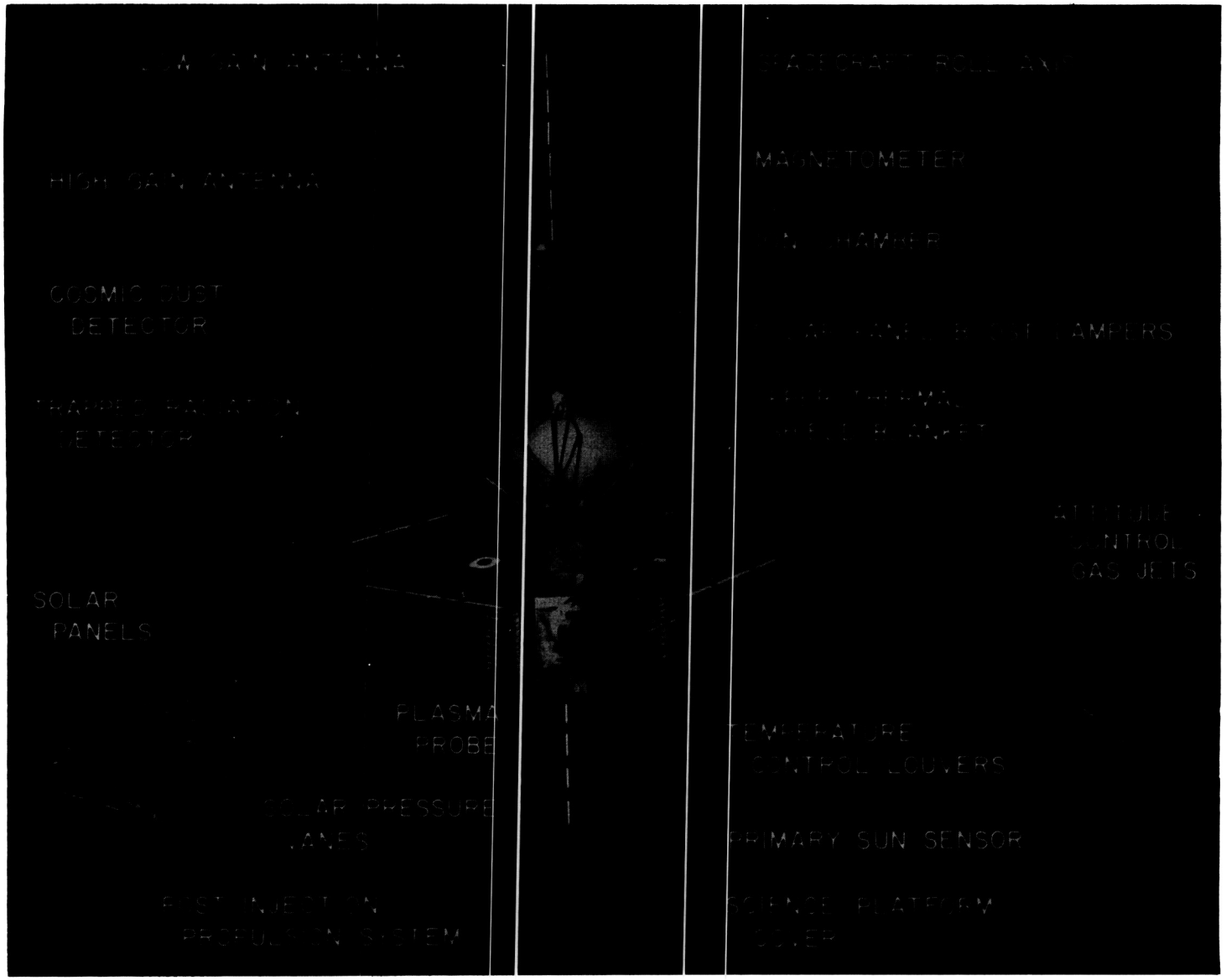

FIGURE 25 CONFIGURATION - MARINER IV SPACECRAFT

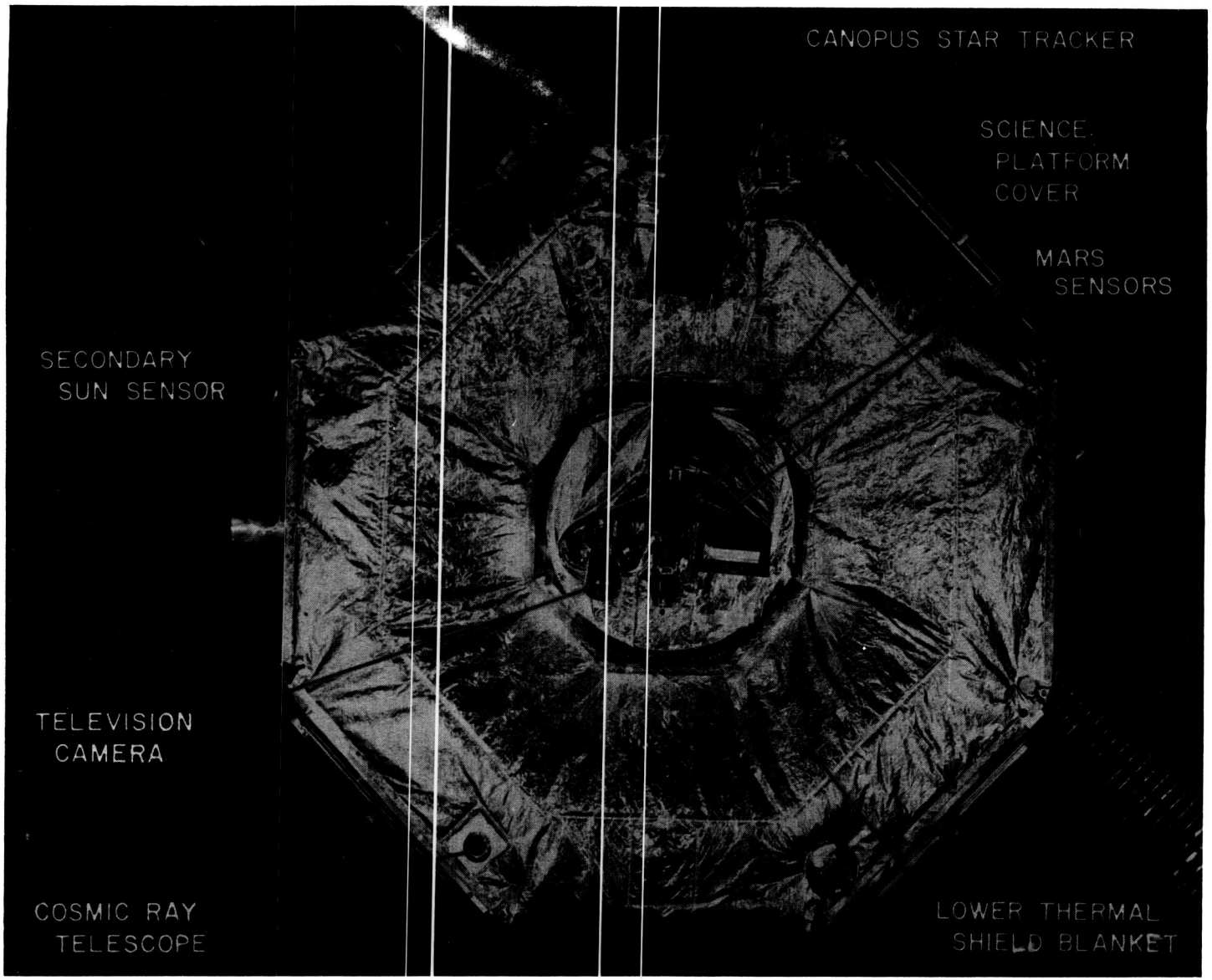

FIGURE 26 BOTTOM VIEW - MARINER IV SPACECRAFT

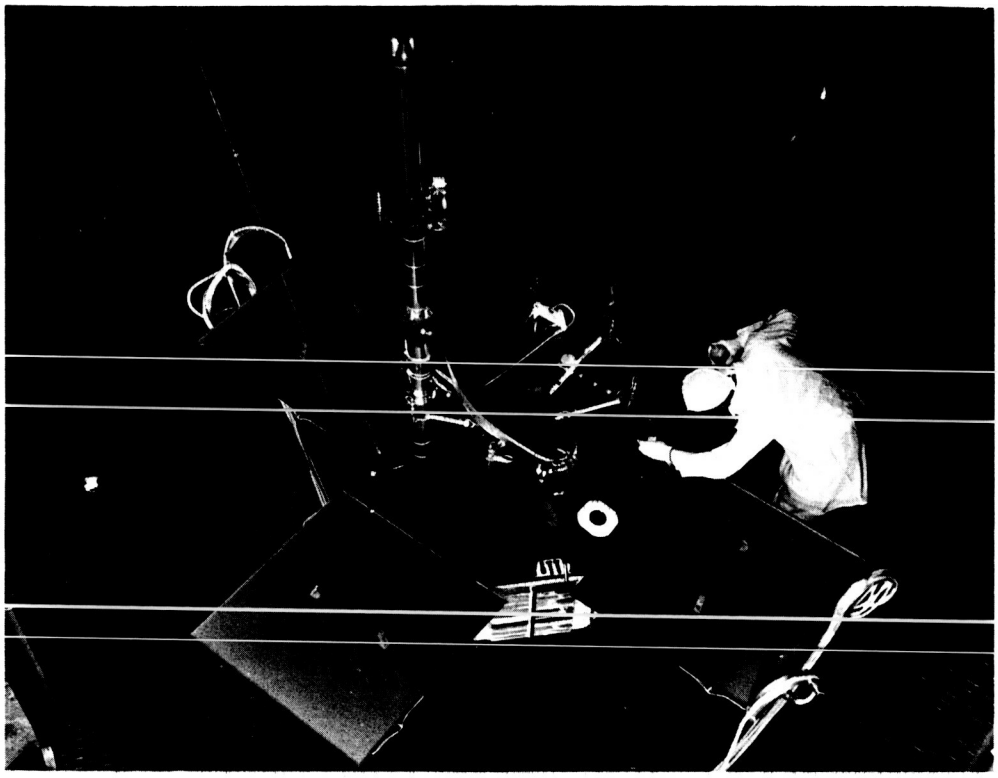

FIGURE 27 MARINER MARS 64 TEMPERATURE CONTROL MODEL

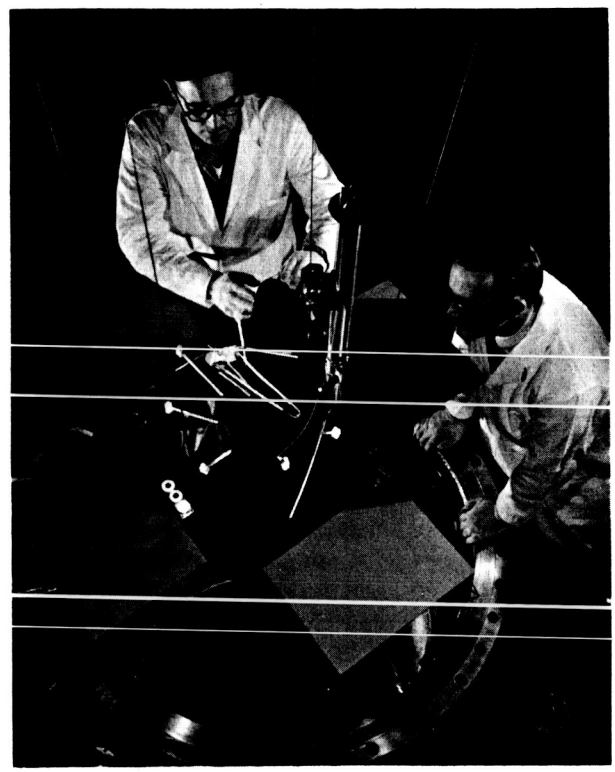

FIGURE 28 THERMAL SCALE MODEL - TOP VIEW

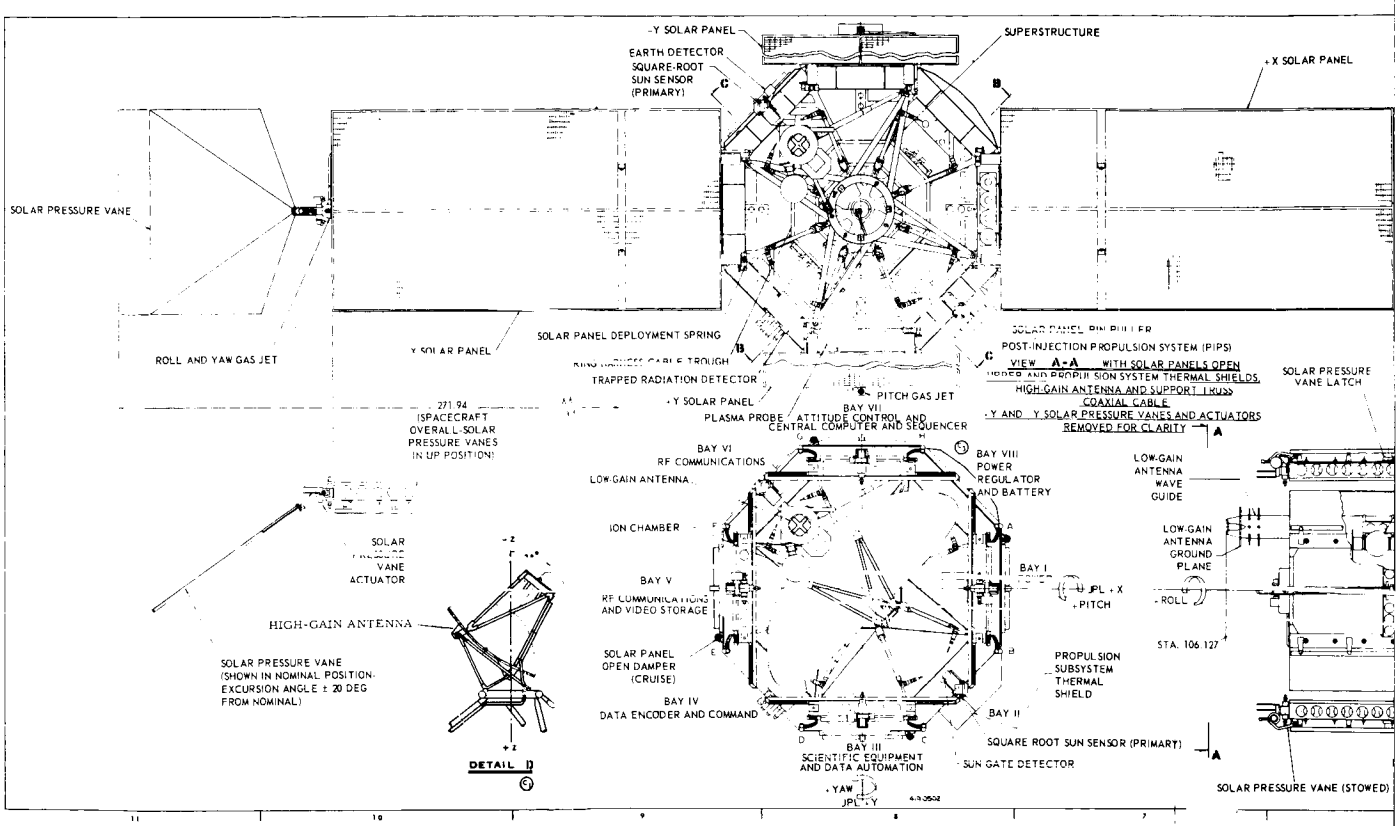

FIGURE 29 CONFIGURATION, MARINER-C S

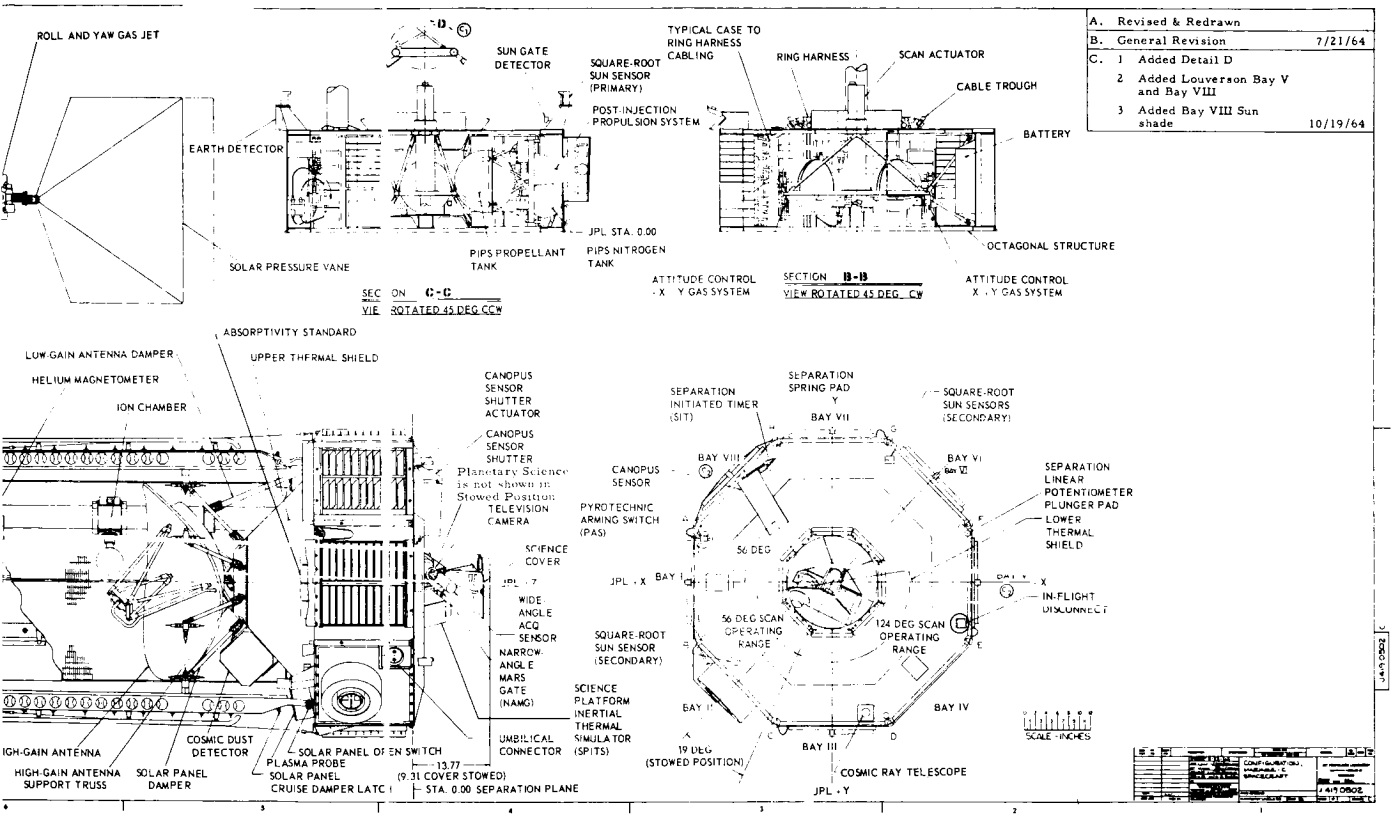

PACECRAFT AS OF 10-16-64

FIGURE 30 THERMAL SCALE MODEL

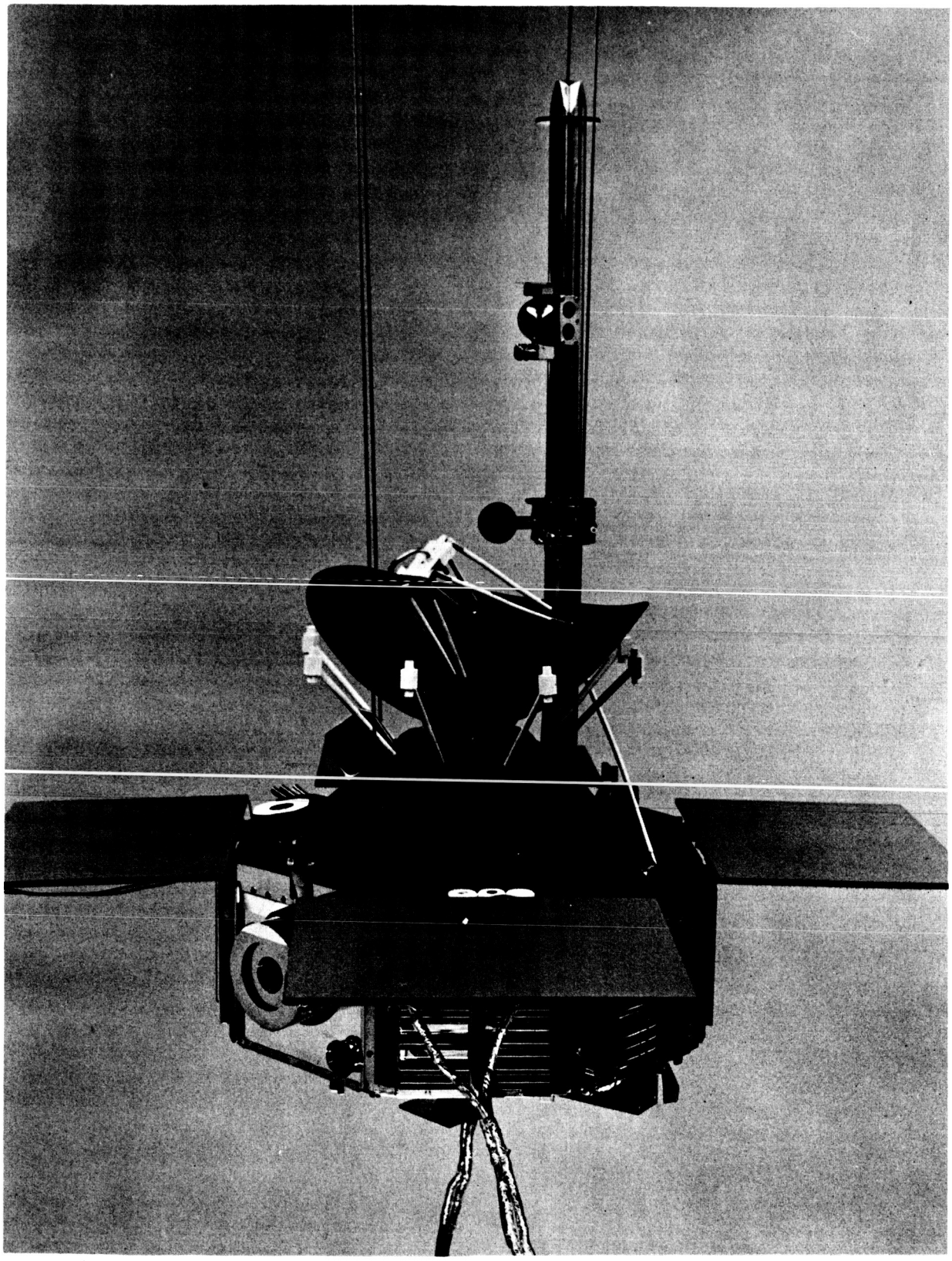

FIGURE 31 THERMAL SCALE MODEL

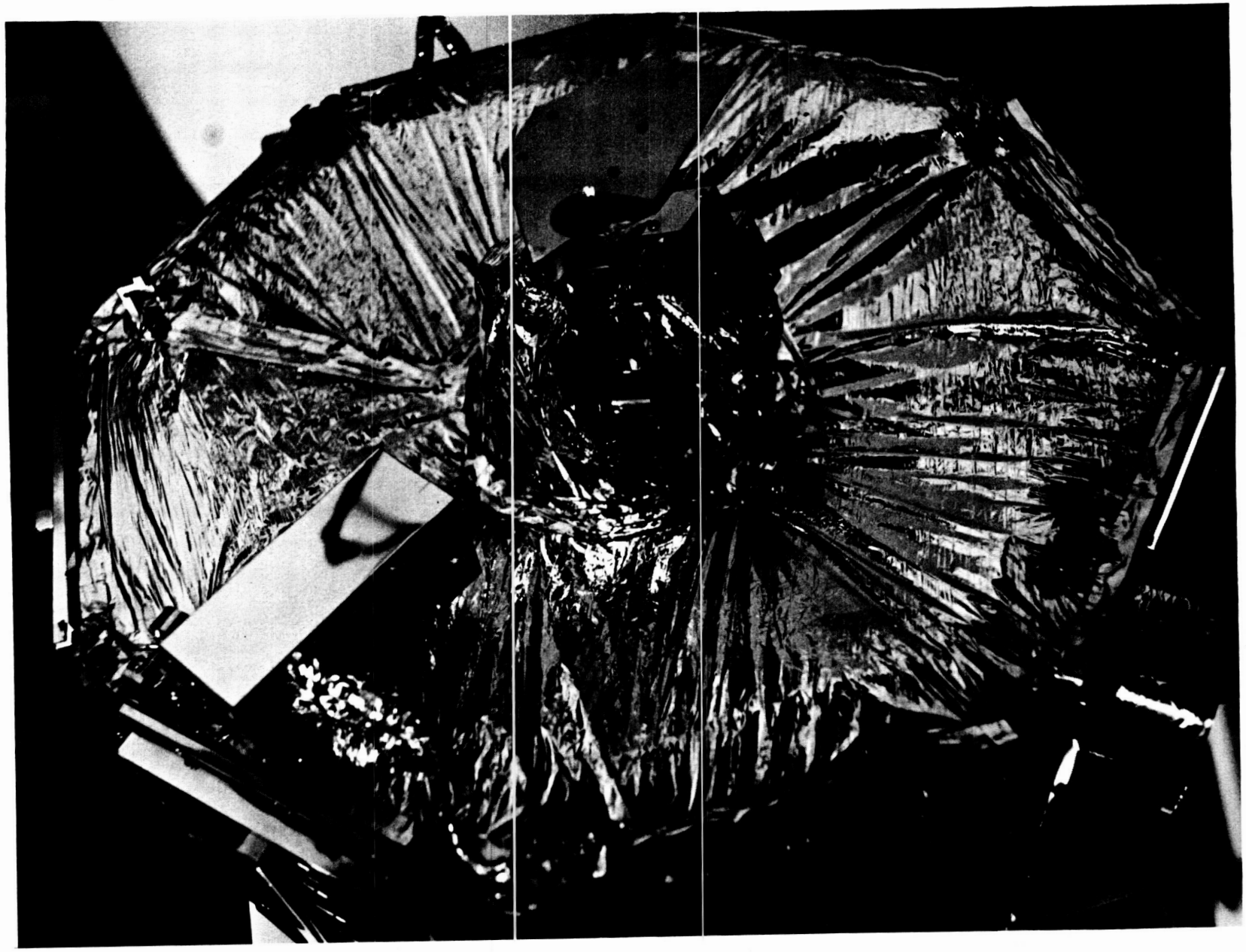

FIGURE 32 THERMAL SCALE MODEL - BOTTOM VIEW

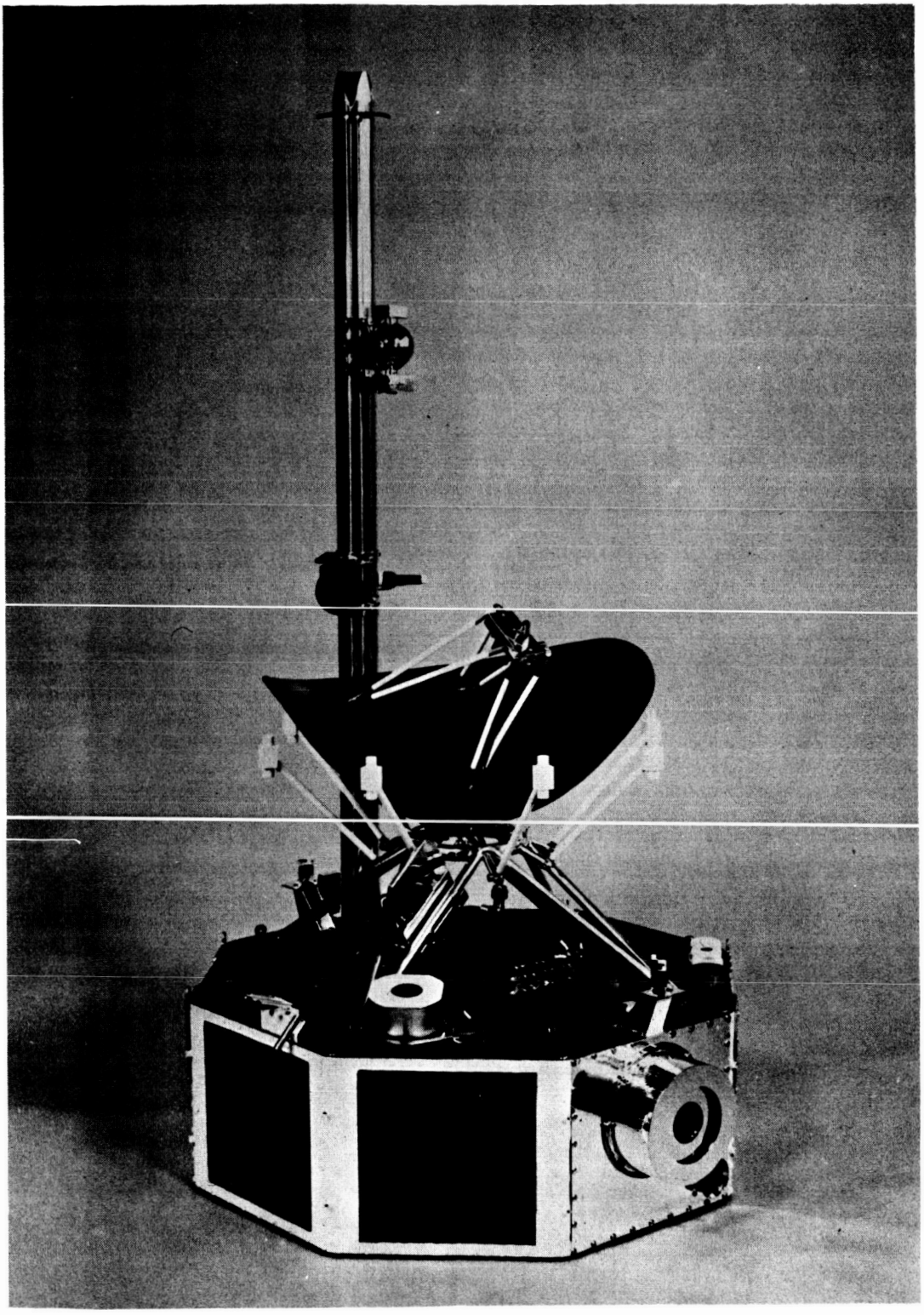

FIGURE 33 THERMAL SCALE MODEL - LOUVERS AND UPPER SHIELD REMOVED

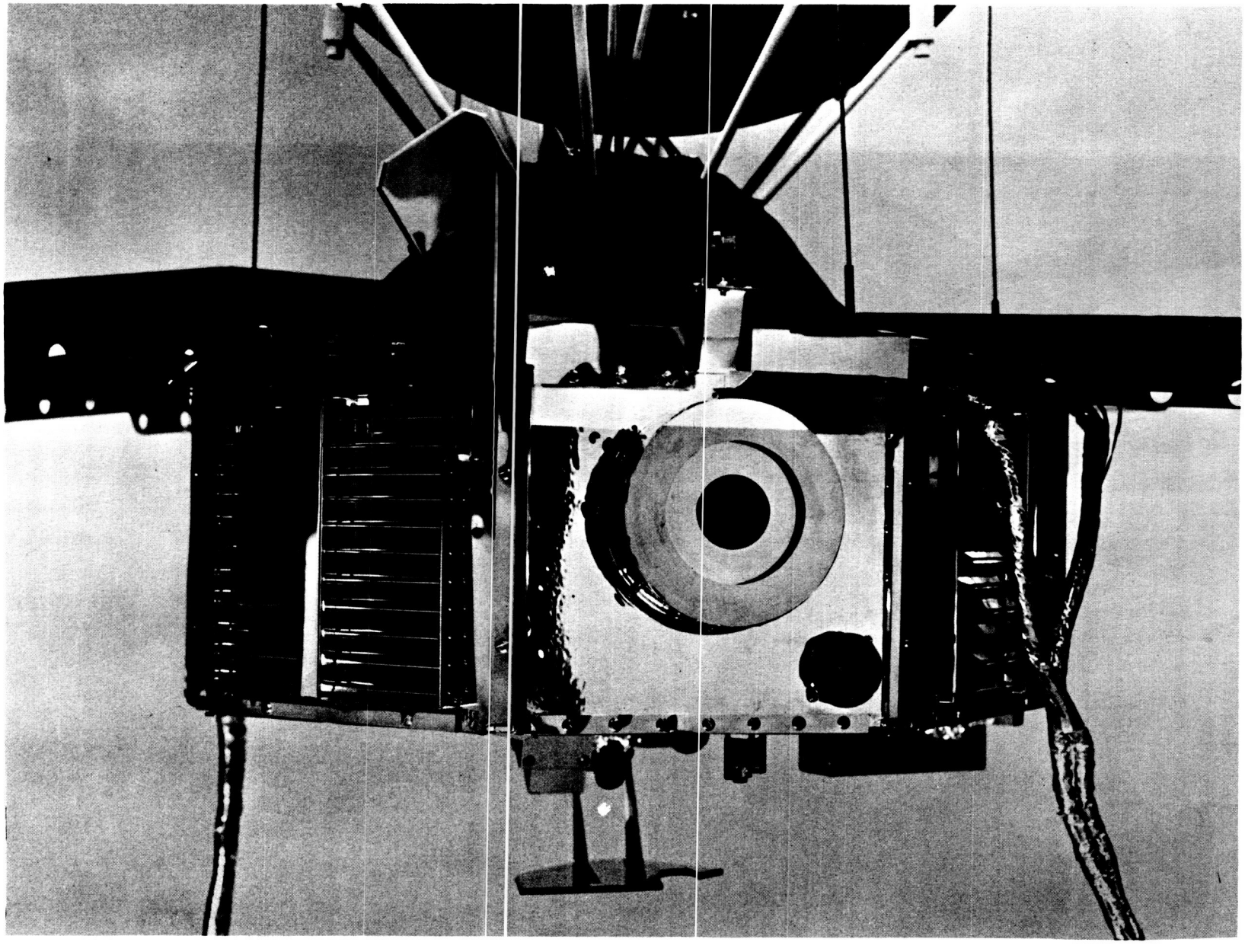

FIGURE 34 THERMAL SCALE MODEL - BAYS 1, 2, 3

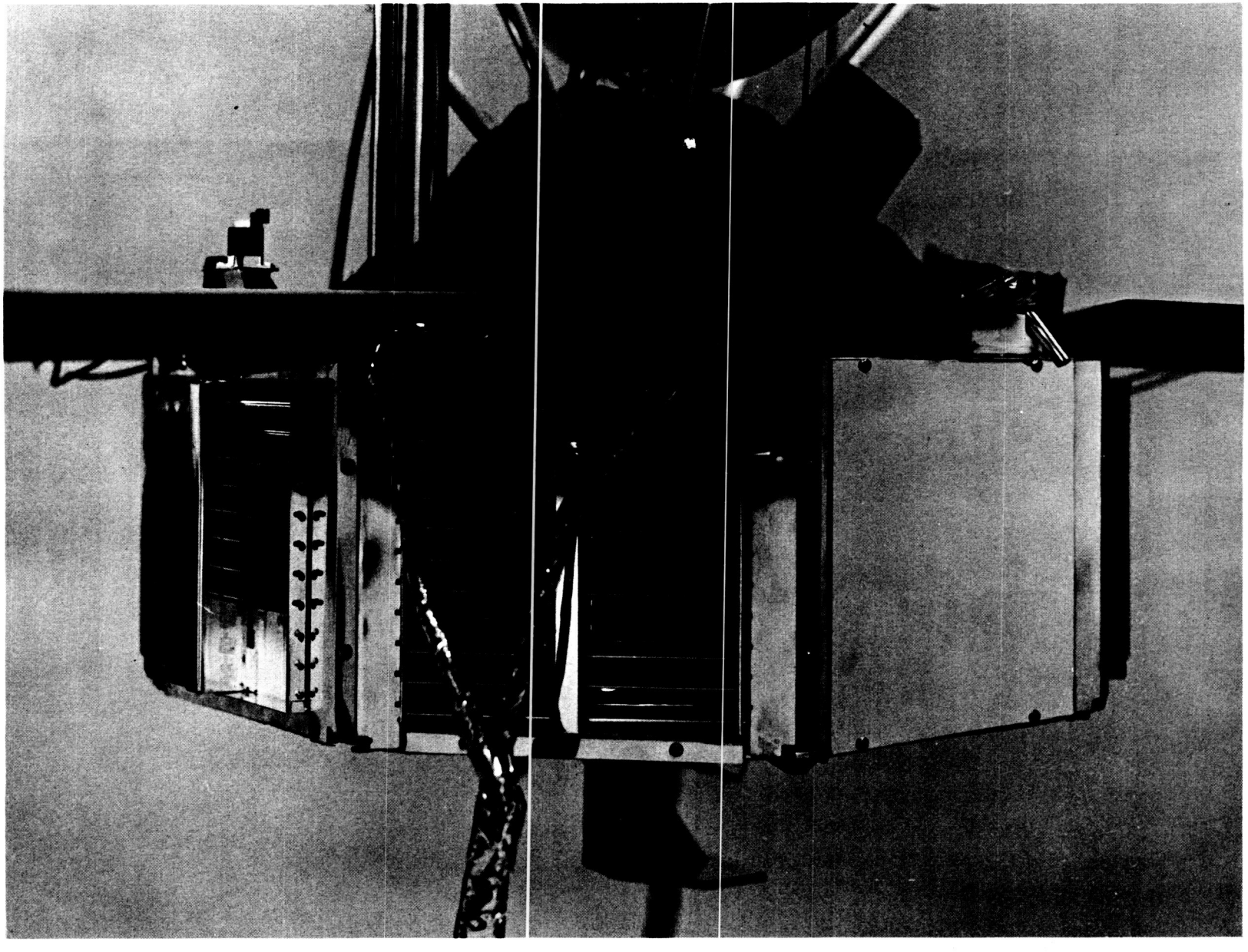

FIGURE 35 THERMAL SCALE MODEL - BAYS 4, 5, 6

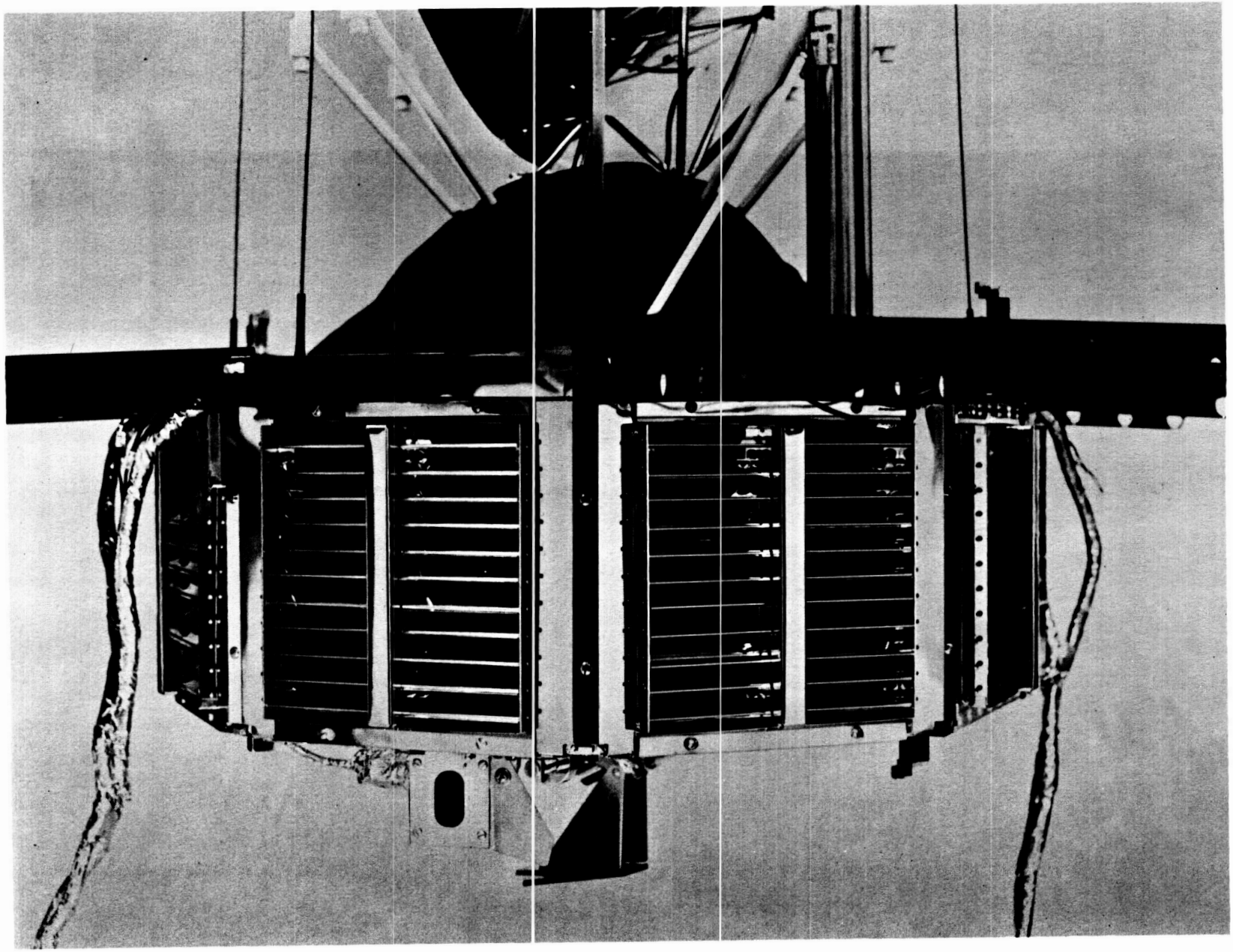

FIGURE 36 THERMAL SCALE MODEL - BAYS 7, 8

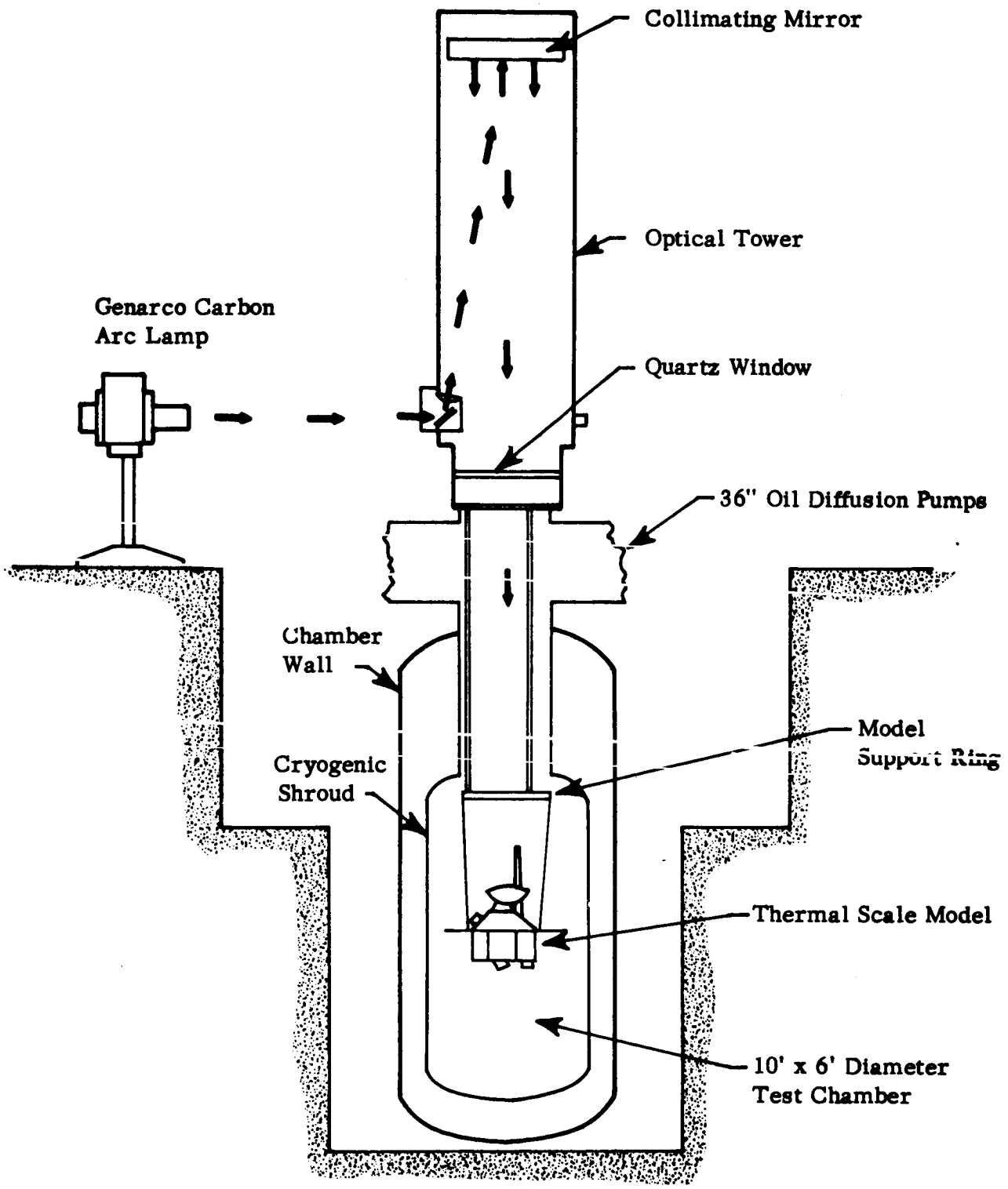

FIGURE 37 SCHEMATIC OF NASA LEWIS SPACE SIMULATOR

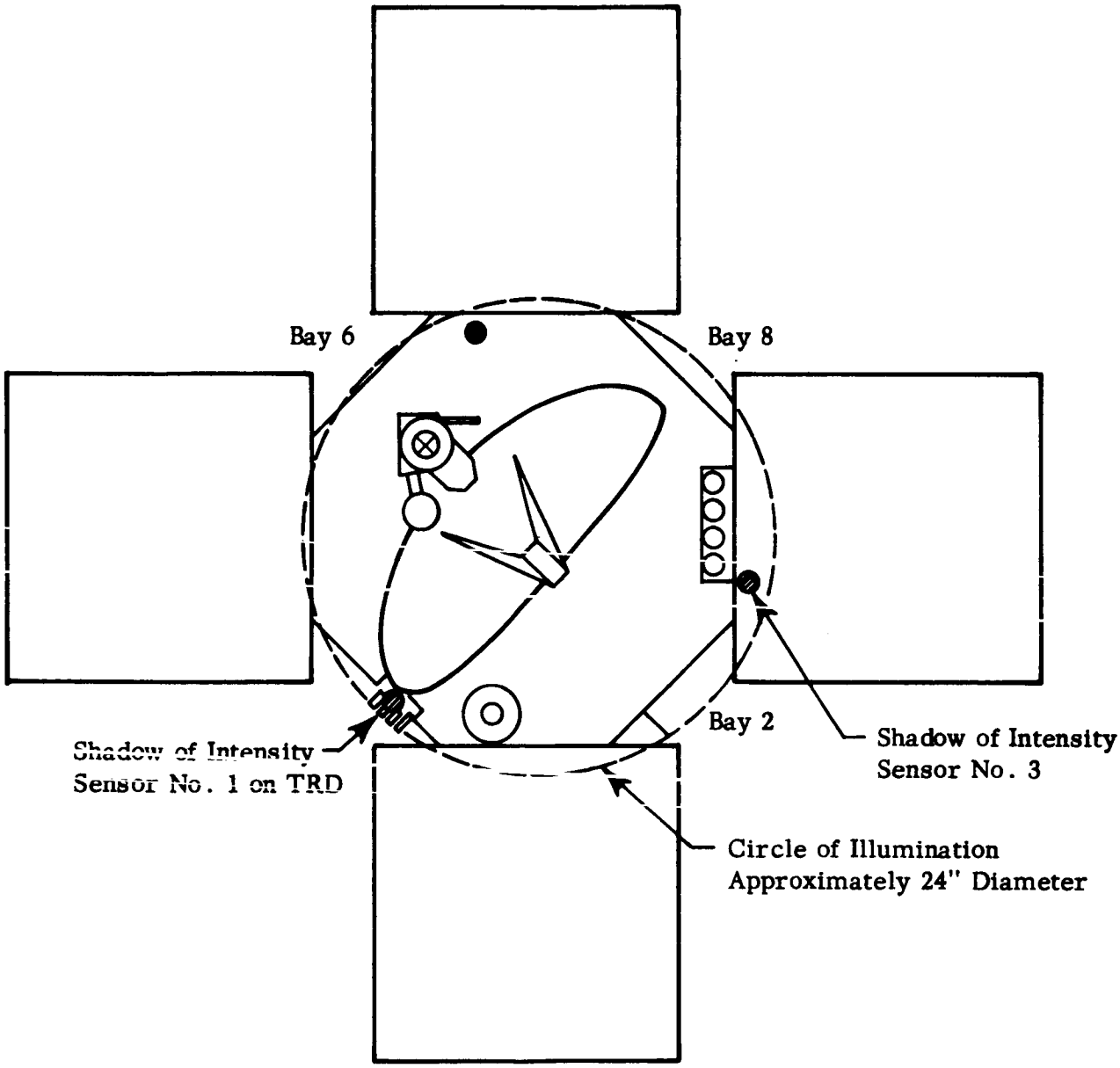

FIGURE 38 SOLAR ILLUMINATION PATTERN

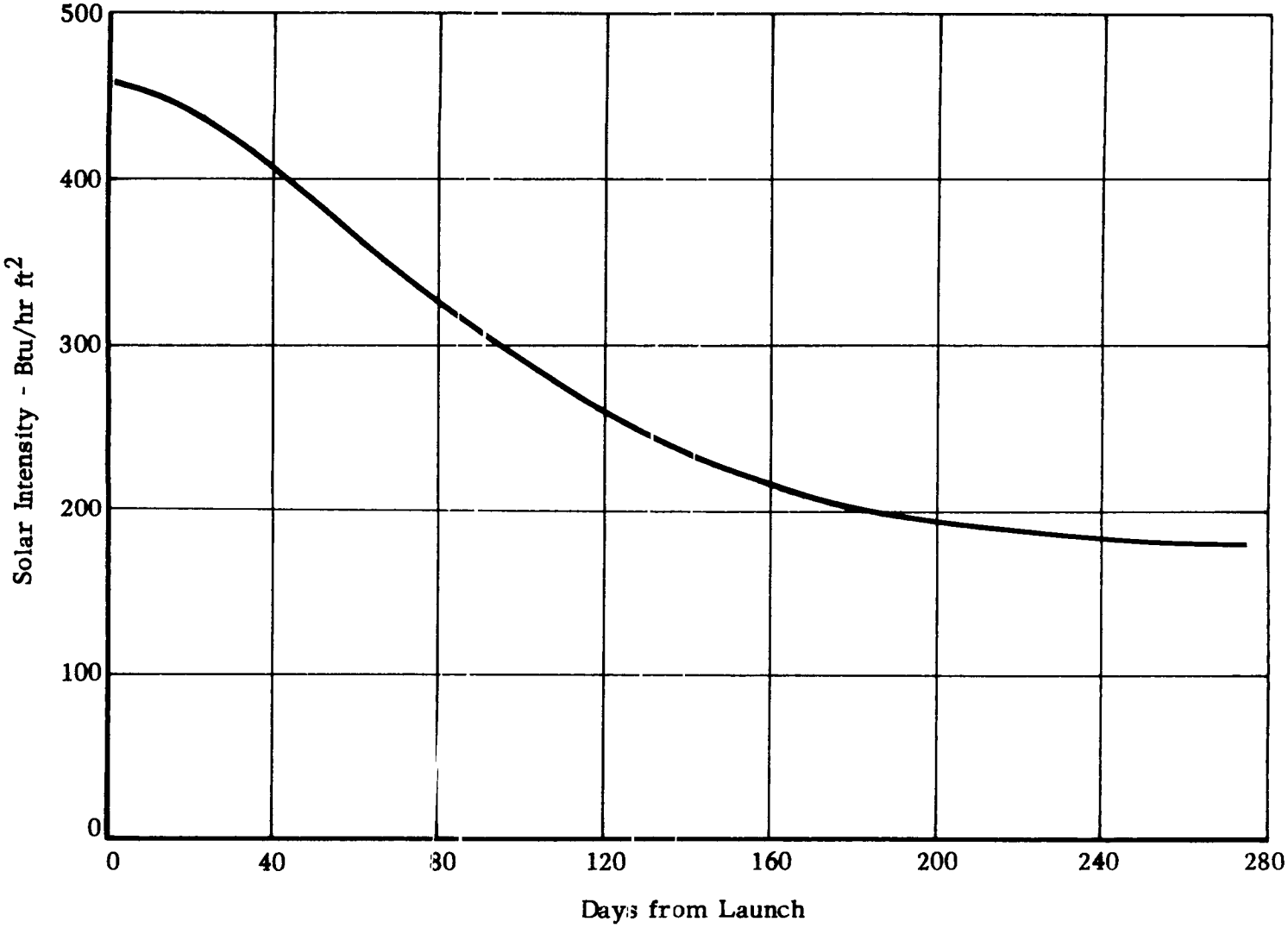

FIGURE 39 SOLAR INTENSITY VARIATION

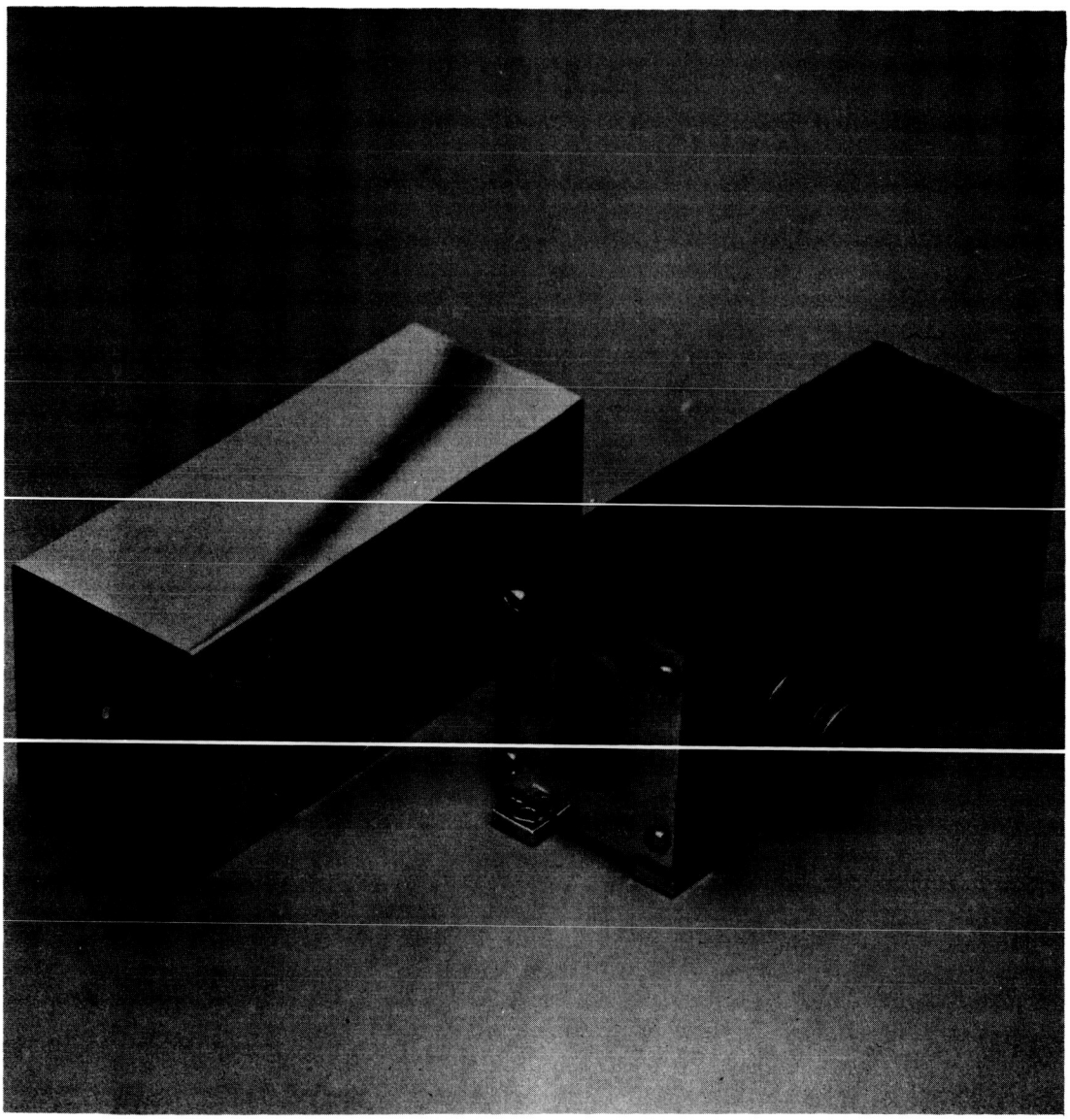

FIGURE 40 TSM CANOPUS TRACKER